AD-A146 271 THERMOMECHANICAL CRACKING DUE TO MOVING FRICTION LOADS (U) NEW MEXICO UNIV ALBUQUERQUE BUREAU OF ENGINEERING RESEARCH F D JU ET AL. MAY 84 ME-125(84)ONR-233-2 1/2

UNCLASSIFIED N00014-83-K-0304 F/G 12/1 NL

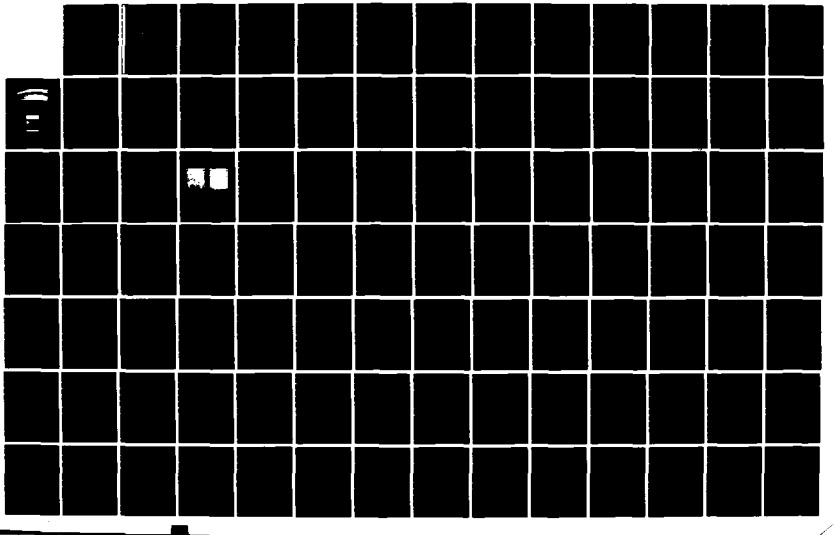

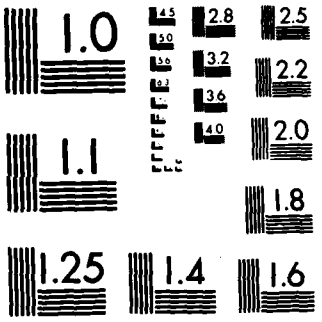

(12)

THE UNIVERSITY OF NEW MEXICO
COLLEGE OF ENGINEERING

BUREAU OF ENGINEERING RESEARCH

THERMOMECHANICAL CRACKING DUE TO MOVING FRICTION LOADS

BY

FREDERICK D. JU AND JOHN H. HUANG

REPORT NO. ME-125(84) ONR-233-2

WORK PERFORMED UNDER CONTRACT NO. ONR-N00014-83-K-0304

MAY 1984

Final Report

on

Thermomechanical Cracking Due to Moving Frictional Loads

by

Frederick D. Ju and John H. Huang

Department of Mechanical Engineering
The University of New Mexico
Albuquerque, New Mexico 87131

Report No. ME-125(84) ONR-233-2
Work Performed Under Contract No. ONR-N00014-83-K-0304

May 1984

ABSTRACT

The heat checking phenomenon in mechanical seals resulting from the passage of asperities traversing at a high speed over the surface of a seal ring is solved with a thermomechanical model of a semi-infinite medium subjected to frictional heating over a moving contact zone. The traverse speed is considered to be the same as the rubbing speed for the current problem. The two-dimensional theory depicts essentially a single moving line contact with uniform or parabolic pressure distribution over the narrow width. For the actual asperity, single or periodic, the contact area is best described by a "spot" that may be approximated with a circular or a rectangular geometry. For such a configuration, a three-dimensional theory is developed. In the present analysis the general solutions are obtained for arbitrary distribution of contact loads. Numerical solutions are given for both uniform and non-uniform pressure distributions. The roles of material properties and operating variables are expressed in terms of dimensionless parameters. The double Fourier transform and the Green's function methods are used throughout the analysis. Numerical schemes for the corresponding analytic solutions of integral form are developed.

For a constant traversing speed of 15 m/s (600 ips) and a Coulomb coefficient of 0.5, the two-dimensional theory for a single moving asperity concludes that the crack could initiate at a normal average pressure of 482 MPa (70,000 psi) for the case of a parabolic pressure distribution over the narrow width of 1 mm (0.04 in.). The three-dimensional theory for a single moving asperity with a circular contact

area of radius 0.25 mm (0.01 in.) yields a critical average pressure of 196 MPa (28,400 psi) at the fracture threshold.

The investigations show that the distribution of the pressure over the contact zone is more of a deciding factor than the shape of the contact area. In addition, heat checking from cyclic asperity excitation is worse than that from a single asperity excitation. However, all results predict a below-the-surface crack initiation. Typically, for an asperity with the half-width, or radius, of the contact area equal to 0.5 mm (0.02 in.), the critical location for crack initiation is 0.05 mm (0.002 in.) below the surface. The result in a sense justifies the use of linear thermoelastic theory, since at this depth the material considered remains in an elastic state.

The cumulative effect is demonstrated with a sequence of three asperities spaced apart by a distance of $\lambda' = 12$ (12 times the asperity characteristic dimension a). As compared with 196 MPa (28,400 psi) for a single moving asperity, the critical average pressure becomes 88 MPa (12,700 psi) which is much lower. Consequently, the possibility of initiating cracks is higher when periodic moving asperities can occur in the contact zone than when only a single asperity can occur.

TABLE OF CONTENTS

		Page
LIST OF FIGURES		vi
NOMENCLATURE		ix
1.0	INTRODUCTION AND LITERATURE SURVEY	1
1.1	Purpose of the Investigation	1
1.2	General Background	1
1.3	Related Investigation in Progress	5
1.4	Mathematical Models and Analytical Approach	8
1.5	The Uncoupled, Quasi-Static Thermoelastic Theory	11
1.6	The Brittle Fracture Criteria	14
2.0	A TWO-DIMENSIONAL MODEL OF A SINGLE MOVING ASPERITY	22
2.1	Mathematical Model	22
2.2	Mechanical Stress Field	25
2.3	Temperature Field	32
2.4	Thermal Stress Field	34
2.5	Numerical Results	40
3.0	A THREE-DIMENSIONAL MODEL OF A SINGLE MOVING ASPERITY	46
3.1	Mathematical Model	46
3.2	Mechanical Stress Field	49
3.3	Temperature Field	56
3.4	Thermal Stress Field	62
3.5	Numerical Results	70
3.5.1	Rectangular Contact Area with Uniform Pressure (Case 1)	71
3.5.2	Disk Contact Area with Uniform Pressure (Case 2)	81
3.5.3	Disk Contact Area with Paraboloidal Distribution of Pressure (Case 3)	87
4.0	A THREE-DIMENSIONAL MODEL OF PERIODIC MOVING ASPERITIES	104
4.1	Mathematical Model	104
4.2	Mechanical Stress Field	106
4.3	Temperature Field	108
4.4	Thermal Stress Field	115
4.5	Numerical Results	122
4.5.1	Rectangular Contact Area with Uniform Pressure (Case 1)	122
4.5.2	Disk Contact Area with Uniform Pressure (Case 2)	128
4.5.3	Disk Contact Area with Paraboloidal Distribution of Pressure (Case 3)	132

TABLE OF CONTENTS (continued)

Page

5.0 DISCUSSIONS AND CONCLUSIONS 144

5.1 Asperity-Size, Shape of Contact Area, Load Distribution. .144
5.2 Comparison of Two- and Three-Dimensional Analyses. 149
5.3 Cumulative Effects of Periodic Loads 157
5.4 Justifications and Recommendations 161

APPENDIX I - METHODS OF INTEGRAL TRANSFORM AND GREEN'S FUNCTIONS . .164

APPENDIX II - NUMERICAL INTEGRATION. 169

SELECTED REFERENCES. 176

LIST OF FIGURES

Figure		Page
1.1	Radial hairline cracks on the metallic ring after running against a carbon ring at a high peripheral speed	2
1.2	Thermal cracks on the brake shoe.	2
1.3	Mechanical face seal.	4
1.4	Geometry of the hot spot moving on the metallic mating seal.	9
1.5	Griffith model of microcrack.	15
1.6	Brittle fracture under biaxial stress	18
1.7	Brittle fracture solid representing the states of tri-axial stress for brittle fracture	18
1.8	(a) Specimen with a number of randomly oriented cracks, and (b) the failure pattern under overall axial compression.	19
1.9	The three modes of cracking	21
1.10	Crack in an infinite plate.	21
2.1	Two-dimensional asperity.	23
2.2	Plane model of the half-space problem for a plane moving load (P_1 and P_2 denote the uniform and parabolic pressure distributions, respectively).	24
2.3	Unit normal load on a two-dimensional half-plane.	26
2.4	Unit tangent load on a two-dimensional half-plane	26
2.5	Mechanical stresses due to combined pressure and friction	41
2.6	Temperatures due to friction.	42
2.7	Thermostresses due to friction	43
2.8	Principal stress fields	44
2.9	Principal stress fields for different half widths (ℓ_1 = 0.25 mm (0.01 in.), ℓ_2 = 0.5 mm (0.02 in.))	46

LIST OF FIGURES (continued)

Figure		Page
3.1	Moving asperities	48
3.2	Maximum mechanical principal stresses in the surface layer (Case 1)	91
3.3	Maximum mechanical principal stresses in the surface layer (Case 2)	92
3.4	Maximum mechanical principal stresses in the surface layer (Case 3)	93
3.5	Temperature field in the surface layer (Case 1)	94
3.6	Temperature field in the surface layer (Case 2)	95
3.7	Temperature field in the surface layer (Case 3)	96
3.8	Maximum thermal principal stresses (Case 1)	97
3.9	Maximum thermal principal stresses (Case 2)	98
3.10	Maximum thermal principal stresses (Case 3)	99
3.11	Maximum combined thermomechanical principal stress field (Case 1)	100
3.12	Maximum combined thermomechanical principal stress field (Case 2)	101
3.13	Maximum combined thermomechanical principal stress field (Case 3)	102
4.1	Three-dimensional model of N periodic moving aperities	105
4.2	Maximum mechanical principal stress fields from periodic excitation	138
4.3	Temperature fields in the surface layer from periodic excitation	139
4.4	Temperature fields from periodic excitation	140
4.5	Maximum thermal principal stress fields from periodic excitation	142
4.6	Maximum combined thermomechanical principal stress fields from periodic excitation	143

LIST OF FIGURES (continued)

Figure		Page
5.1	Maximum mechanical thermomechanical principal stress fields from periodic excitation	145
5.2	Temperature fields for three cases.	146
5.3	Maximum thermal principal stress fields for three cases	147
5.4	Maximum combined thermomechanical principal stress fields for three cases.	148
5.5	Temperature fields from different asperity sizes.	150
5.6	Maximum combined thermomechanical principal stress fields from different asperity sizes.	151
5.7	Temperature field at ζ = 10 for Case 1, t = 10.	154
5.8	Temperature field at ζ = 10 for Case 1, t = 10.	155
5.9	Stresses from two- and three-dimensional analyses for Case 1.	156
5.10	Temperature fields due to different number of moving asperities.	159
5.11	Maximum combined thermomechanical principal stress fields due to different number of moving asperities	160

NOMENCLATURE

a	Asperity characteristic dimension, the half width of the rectangular contact area in the direction of traverse or radius of the circular contact area
b	Half length of the rectangular contact area perpendicular to the direction of traverse
c	Specific heat
D	Differential operator with respect to x_3
k	Thermal conductivity
M_1	Dilatational speed ratio $[= V(\rho/(\lambda + 2\mu))^{1/2}]$
M_2	Shear speed ratio $[= V(\rho/\mu)^{1/2}]$
p	Load distribution
P_o	Average pressure over the contact area
q_o	Heat flux through the contact area
R_i	Traction over the contact area
t	Aspect ratio (b/a) or time coordinate
T	Temperature field
$\{u_i\}$, $\underset{\sim}{u}$	Displacement field
V	Traverse speed of asperity ($-x_1$ direction)
$\{x_i\}$	Coordinates fixed to the moving asperity
$\bar{(\ )}$	Fourier transform of a variable
∂_i	Partial derivative with respect to x_i coordinate
α	Coefficient of thermal expansion
δ_{ij}	Kronecker delta
ϕ	Dimensionless temperature field $(= Tk/q_o a)$

κ	Thermal diffusivity
P_e	Péclet number (= Va/κ)
λ	Lamé coefficient
μ	Lamé coefficient, modulus of rigidity
μ_f	Coulomb coefficient of friction
ρ	Mass density
σ_{ij}	Stress field
σ_{ij}^M	Mechanical stress field
σ_{ij}^T	Thermal stress field
$\{\xi,\eta,\zeta\}$	Dimensionless coordinates (= x_i/a)
τ	Period of asperity occurrence
λ'	Spacing of periodic asperities (= $V\tau/a$)
N	Number of moving asperities
B_j	Asperity contact regions, j = 1,2,...,N
σ_I	Maximum combined thermomechanical principal stress
σ_I^M	Maximum mechanical principal stress
σ_I^T	Maximum thermal principal stress

CHAPTER 1

INTRODUCTION AND LITERATURE SURVEY

1.1 Purpose of the Investigation

The investigation uses several mathematical models to study the possibility of fracture initiation by dry friction and the configuration of fracture. The general study of friction cracking has a special application in marine seals. The purpose of this study is to extend our understanding of the problem by looking into the thermomechanical state of stress in a mechanical part resulting from the traversing of a single asperity or periodic asperities over its surface. The understanding of such a failure process could be used to improve the design of devices such as marine seals by alleviating the problem of friction cracking.

1.2 General Background

When two bodies are in high speed sliding contact under heavy loads, the localized contact area is much smaller than the design sliding surface. The resulting pressure in the area can be higher than the design pressure by an order of magnitude. Localized hot spots may occur as a result of excessive frictional heating near the contact surfaces. Because of a combination of thermal heating and the mechanical load, the material may crack in the neighborhood of the contact zone. This phenomenon is called "heat checking" or "thermocracking". It commonly occurs in mechanical seals and brakes as shown in Figures 1.1 and 1.2. In general numerous radial cracks can be observed perpendicular

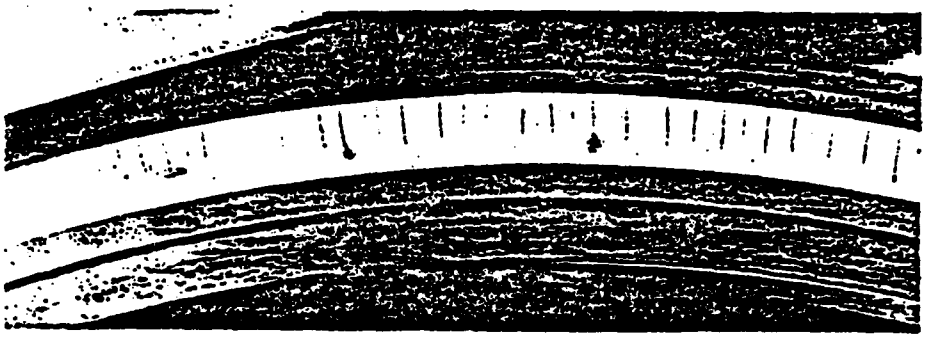

Figure 1.1. Radial hairline cracks on the metallic ring after running against a carbon ring at a high peripheral speed.

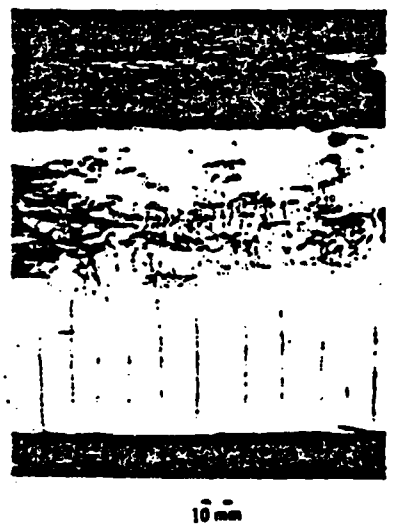

Figure 1.2. Thermal cracks on the brake shoe.

to the sliding direction and almost periodically separated along the circumference. While extensive analysis of thermoelastic effects in brakes has been studied [1-5][1], the bulk of which is in the railroad industry, much intensive study of the effects is needed in mechanical seals. Of concern here will be the face seals located along the propeller shaft in submarines to prevent leakage of sea water through the shaft tunnel. Figure 1.3 illustrates one assembly of such a device, in which the seal consists essentially of two annular rings, one of which is fixed to the shaft tunnel housing, another is mounted on and rotates with the shaft. The mating surfaces of the rings therefore are pressed against each other under spring pressure and rub at a high speed. The design nominal pressure between the seal rings depends on the type of vessel and the location of the seal. For instance, a low pressure of about 100 kPa (14.5 psi) is sufficient for most surface vessels; for submarines, the pressure required could increase by orders of magnitude. Had the pressure been evenly distributed according to design, the service life of the face seals would no longer be a serious problem even at a high rubbing speed. However, it is well known that the actual contact area may only be a small fraction of the nominal area at the design interface. In other words, a low nominal design pressure may very well result in a very high interfacial pressure, thus a very high dry frictional force in the actual contact area. The high friction would cause locally an extremely high temperature, called

---

[1]Numbers in brackets denote references.

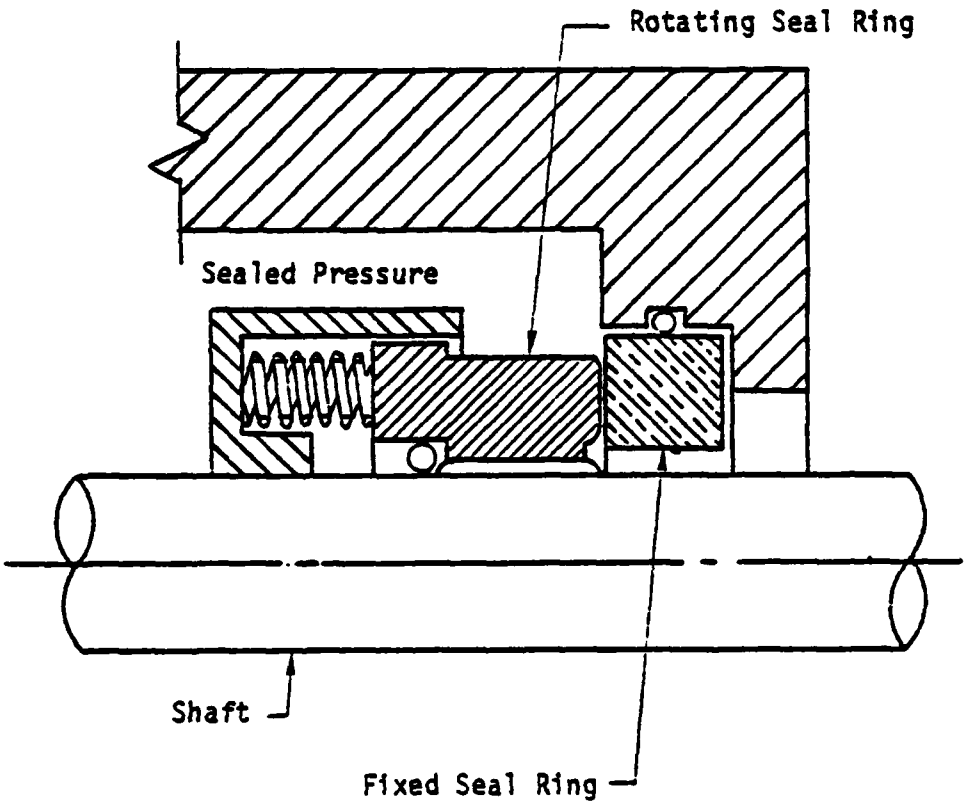

Figure 1.3. Mechanical face seal.

"flash temperature" by Archard [6]. The local contact area is also called the "red banding" or "hot spot" [7], which has been experimentally demonstrated. In severe cases the temperature can be extremely high, leading to cracking of the surface [8]. If we use the figure of 10^{-3} as area ratio (contact area/nominal area)--Burton [9] considered 10^{-4} as a possible area ratio--a low design pressure of 240 kPa (35 psi) could result in a 240 MPa (35,000 psi) local pressure in the contact zone, a pressure well within the range of fracture initiation with unfavorable Coulomb coefficients.

The cause of the localization of the contact area, which is in the province of thermoelastic instability (TEI), will not be considered; nor will the metallurgical change in the surface layer. It will suffice to assume that the localization of contact area is due to some form of asperities, which may be fixed to any of the mating surfaces or may precess with respect to both. The present work treats the thermomechanical stress state in the part that mates with the one containing the asperity and the possibility of heat checking therein. The specific investigation will consider the asperity or asperities being on the carbon-graphite, which moves relatively on the face seal of Stellite III. The failure due to heat checking is on the face seal which prior to the onset of failure is assumed to have no other defect on its contacting surface.

1.3 Related Investigation in Progress

The failure records have shown that the performance life of devices with pressurized moving contact surfaces becomes drastically

reduced whenever the parameters such as the load, sliding speed, or the temperature field attain certain range of values. There has been increased emphasis on finding a solution of failure control, experimentally and analytically, of this physical problem in recent years. A general survey of the problem of cracking through the development of a frictional hot spot was discussed by Burton [7]. A series of experiments carried out by Sibley and Allen [10] showed photographic evidence of systematically moving hot patches in the contact zone. Based on the results in the recent literature [11-15], it can be assumed that TEI precedes thermocracking and that contact is localized at several hot patches. Considerable evidence was also shown by Kennedy [16] to support this crucial assumption. In his experiment, using the carbon ring against a metallic mating ring made from 440 C stainless steel, beryllium copper or 52100 bearing steel under both dry and liquid lubricated conditions, the existence of distinct spot asperities on the metallic ring was observed. It was found that the spots at least in dry operation tend to remain stationary with respect to the metallic mating ring of the seal, whether that ring be stationary or rotating. However, other investigations have shown hot patches moving relative to the mating ring and stationary on the primary ring [12,13]. In addition, Burton [14] reported that for an aluminum ring sliding on a glass disk, the hot spot precessed at a much lower speed than the rubbing speed. The uncertainty of this observed discrepancy on the speed of the moving asperities remains, but there is no doubt about the existence of the moving asperities due to TEI on mechanical face seals through the effort of all the researchers in this field. Therefore, several

analytical studies of the failure due to the existence of the moving asperities, which are characterized by high normal and frictional loads and the resulting thermal heating on the contact surface of the sliding mechanical parts, have been in progress.

When the thermal effect is neglected, the study is isothermal. Various analyses of stresses and displacements induced in an elastic half plane by a concentrated line load moving at a constant speed along its surface have been developed [17-19]. Eason [21] dealt with several types of moving surface forces and procured the solution of the mechanical stress and displacement field in a semi-infinite solid. Surface displacement and temperature field of a convective elastic half space under an arbitrarily distributed fast-moving line heat source were obtained, using integral transform methods, by Ling and Mow [20]. The problem of thermal stresses [22] and temperature distribution [23] was examined. A finite element analysis was recently developed by Kennedy [24] for studying surface temperatures resulting from frictional heating in sliding systems. He also applied finite element techniques to study the stresses in the mechanical face seal [25] and showed that the dominant stresses in the seal components are thermal stresses. Marscher [26,27] analyzed the thermomechanical stress state in the part that contains the asperity. A two-dimensional repeated loading phenomenon was first studied for stability of contacting surfaces by Burton, et al. [28,29]. The surface stress component (parallel to the surface) resulting from a periodic row of moving patches, with width 2ℓ each, and a spacing of $2m$ was investigated by Tseng and Burton [30], who restricted the analysis to the two-dimensional plane stress case. They

concluded from the computed results that the tensile stress would appear instantaneously with each passage of the heat source.

1.4 Mathematical Model and Analytical Approach

According to the results of the experiment by Kennedy, et al. [16], the width of the moving asperity was about 0.1 to 1 mm (0.004 to 0.04 in.); while the diameter of a typical marine shaft seal could be 50 cm (19.7 in.) or more. Because of this size difference between the contact area and the seal, as shown in Figure 1.4, the mathematical model is represented by a half-space subjected to fast-moving loads of a constant velocity (V). The loads come from a combination of thermal and traction contributions. Fast moving refers to the case wherein $V \gg \kappa/a$, where κ and a are defined as the thermal diffusivity and the half width of the asperity. The investigation starts with the study of a model with a moving line asperity. For such an asperity a two-dimensional analysis is adequate to develop the thermomechanical solutions. In order to better model the contact area and periodic excitation of asperities in practice, the research adopts eventually a more realistic three-dimensional analysis. Since it has been observed that the lubricated film is continually being broken by small patches of solid-to-solid contact during seal operation [16], we may as well assume that the working seals are in dry contact representing the worst operating condition. In addition, for the worst case, the mating seal that contains the asperity is regarded as an insulator. The analyses are based on the general theory of a continuum. The relative speed of contact surfaces is assumed to be large enough to result in a high

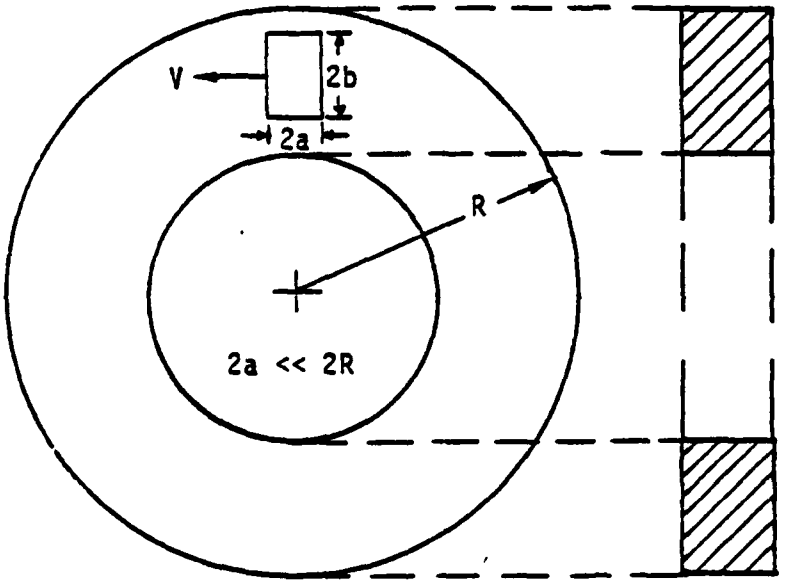

Figure 1.4. Geometry of the hot spot moving on the metallic mating seal.

Péclet number (Va/κ). But it is much smaller than the Rayleigh wave, which for a steel based seal material is approximately 2800 m/s (11×10^4 ips), and justifies the use of the quasi-static theory. Furthermore, since such loading also results in a low dilatation rate, the uncoupled thermal stress theory is then applicable. From observations of failed specimens near the surface, it is reasonable to postulate that the plastic deformation and rupture at the surface are at the granular or even the subgranular level. The base solid material subjected to the asperity friction is essentially elastic. Consequently, the linear theory of thermoelasticity holds. The principal advantage of using the linear theory is the application of the superposition principle, enabling a delineation in the stress field to one from the mechanical load of the moving pressure and friction and another from the moving heat input, a result of the irrecoverable frictional work. The combined effects will then determine the possibility of fracture initiation using the tensile fracture criterion. In two-dimensional analysis, the Green's function approach is used; while in three-dimensional analysis, the analytical solutions of the mechanical and the thermal stress fields are solved by means of double Fourier transform. The temperature field is obtained by both the integral transform and Green's function methods. Numerical results of the corresponding integral solutions are represented in graphs. Schematic geometries and detailed analyses are given in the following chapters.

Two-dimensional and three-dimensional models are examined in Chapters 2 and 3, respectively. The former demonstrates a simpler means of formulation; while the latter gives a better description of

the physical problem. Both models deal with a single moving asperity. In Chapter 4, a three-dimensional model of periodic moving asperities is investigated further. The formulation leads to a general solution which can be used to justify the results from Chapters 1 and 2. Detailed discussions and conclusions are given in Chapter 5 and the related mathematical background is given in the appendices.

1.5 The Uncoupled, Quasi-Static Thermoelastic Theory

The analysis is restricted to the dynamic and coupled theory of an isotropic linear thermoelastic solid, which can be found in most thermoelasticity textbooks [31-36]. In vector form, the displacement formulation in the absence of body forces and the Duhamel heat equation [37] with no internal heat generation are

$$\mu\nabla^2\underset{\sim}{u} + (\lambda + \mu)\ \text{grad div}\ \underset{\sim}{u} - (3\lambda + 2\mu)\ \alpha\ \text{grad}\ T = \rho\ddot{\underset{\sim}{u}}\ , \tag{1.1}$$

$$k\nabla^2 T = \rho c\dot{T}\left[1 + \frac{(3\lambda + 2\mu)\ \alpha^2\ T_o}{\rho c}\frac{\dot{\varepsilon}_{kk}}{\alpha\dot{T}}\right] \tag{1.2}$$

where T_o is the temperature of the solid in the unstressed state, $\dot{\varepsilon}_{kk}$ is the dilatation rate and $\dot{T}$ is the temperature rate. Equations (1.1) and (1.2) are simplified by deleting the inertia term, $\rho\ddot{\underset{\sim}{u}}$ for the quasi-static case and of the mechanical coupling term,

$$\frac{(3\lambda + 2\mu)\ \alpha^2\ T_o}{\rho c}\frac{\dot{\varepsilon}_{kk}}{\alpha\dot{T}}$$

for the uncoupled theory. Thus the governing equations for the uncoupled, quasi-static thermoelastic theory are

$$\mu\nabla^2\underset{\sim}{u} + (\lambda + \mu)\ \text{grad div}\ \underset{\sim}{u} = (3\lambda + 2\mu)\ \alpha\ \text{grad}\ T\ , \qquad (1.3)$$

$$\nabla^2 T = \frac{1}{\kappa}\dot{T}\ . \qquad (1.4)$$

A short discussion follows to justify the use of the quasi-static uncoupled theory. The mechanical coupling term is considered first. It can be shown that for steel it is approximately

$$k\nabla^2 T = \rho c\dot{T}\left[1 + 10^{-5}\ T_o\ \frac{\dot{\varepsilon}_{kk}}{\alpha\dot{T}}\right]$$

where T is absolute temperature measured in Rankines. For aluminum, it becomes

$$k\nabla^2 T = \rho c\dot{T}\left[1 + 1.8 \times 10^{-5}\ T_o\ \frac{\dot{\varepsilon}_{kk}}{\alpha\dot{T}}\right].$$

If SI units are used, i.e., the temperature is measured in degrees Kelvin, the coefficients, 10^{-5} for steel and 1.8×10^{-5} for aluminum should be replaced by 1.8×10^{-5} and 3.24×10^{-5}, respectively. It is argued that, for most cases of a high thermal load, $\dot{\varepsilon}_{kk}/\alpha\dot{T}$ should be of the order, O(1), so that the coupling term is negligible except for conditions in which the temperature distributions have sharp variations or discontinuities in their time histories, which often occurs during the propagation of thermoelastic waves in the aftermath of thermal shocks. The similar argument is also made by Boley and Weiner [38] who rewrote Equation (1.2) as

$$k\nabla^2 T = \rho c \dot{T} \left[1 + \delta \left(\frac{\lambda + 2\mu}{3\lambda + 2\mu} \right) \frac{\dot{\varepsilon}_{kk}}{\alpha \dot{T}} \right]$$

where δ is defined by

$$\delta = \frac{(3\lambda + 2\mu)^2 \alpha^2 T_o}{(\lambda + 2\mu) \rho c}$$

which has the values 0.029 and 0.014 for aluminum and steel at T_o = 660°R (corresponding to 367 K), respectively. Further, they showed that for both cases the coupling is small if

$$\frac{\dot{\varepsilon}_{kk}}{3 \alpha \dot{T}} << 20 \ .$$

They therefore concluded that the possibility of omitting the coupling terms depends not only on the fact that the inequality $\delta << 1$ must hold (as it does for most metals), but also on the fact that strain rates must be of the same order of magnitude as temperature rates times the coefficient of thermal expansion.

The dynamic effect can be a result from either a dynamic loading state or a non-steady thermal state in which the time rate of temperature change could keep up with the stress waves in the material. It was stated by Duhamel [39] that the inertia term can be disregarded if the time rate of change of temperature is slow enough. Parkus [40] showed that the significant effect from inertia term can arise only when there is an instantaneous change in the surface temperature or in the temperature of the surrounding medium. In fact, the dynamic effect is greatly reduced if the temperature change occurs in a very short, but finite, interval of time. This was confirmed by Danilovskaya

[41-42], who studied the dynamic effect due to a thermal shock on the surface of a half-space in detail and demonstrated that the maximum dynamic stress is reduced to 86 percent even for the extremely short duration of heating of 10^{-12} seconds. In general, under usual conditions of heat exchange, the rate of temperature change is small in comparison with the speed of sound in the material. Thus, at any instant, the thermal stress state can be determined by the instantaneous values of the temperature field. Consequently, there is no need to consider the inertia force corresponding to the motion of the particles during the varying thermal expansion, i.e., the inertia term $\rho\ddot{\underset{\sim}{u}}$ in Equation (1.1) can be omitted.

1.6 The Brittle Fracture Criteria

Metals can be generally divided into two categories: (1) ductile metals, in which marked plastic deformation commences at a fairly definite stress and which exhibits considerable ultimate elongation prior to fracture; and (2) brittle metals, for which plastic deformation is not clearly evident at fracture. Since the heat checking phenomenon as evidenced in Stellite III and in ceramic materials [43] is associated with very little plastic flow, the brittle fracture criterion is ascertained. Based on the hypothesis enunciated by Griffith [44] in 1921, the weakening of the material is attributed to the growth of minute cracks resulting from an induced stress field. He [45] derived the criterion for failure under a biaxial principal stress field σ_1 and σ_3 at an arbitrary orientation β with respect to the axis σ_1 as seen in Figure 1.5, and studied in detail the variation of the

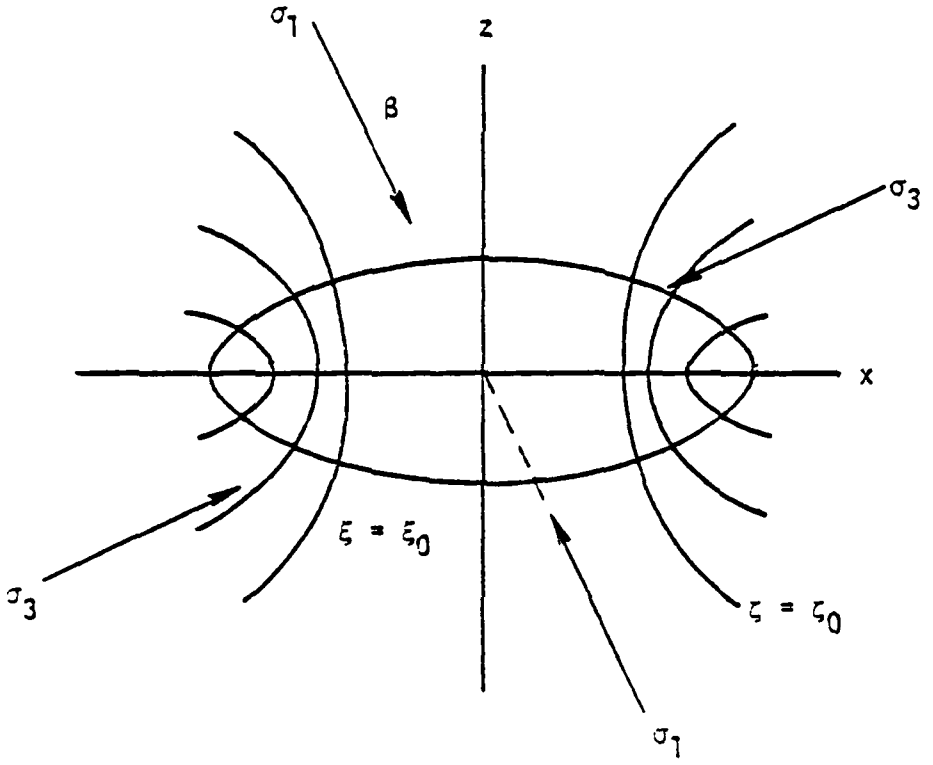

Figure 1.5. Griffith model of microcrack.

peripheral stress $\sigma_{\zeta\zeta}$ on the surface of a flat elliptical crack ($\xi = \xi_0$). He postulated that fracture would result when the maximum peripheral stress reaches a characteristic value of the material. His theory modified by McClintock and Walsh [72], who took into account the fact that cracks may be expected to close under sufficiently high compressive stresses, is stated as follows. As the normal stress σ_n acting across the face of a pre-existing crack causes the crack to close, i.e., when

$$\sigma_n = \frac{1}{2}[(\sigma_1 + \sigma_3) + (\sigma_1 - \sigma_3)\cos 2\theta] < 0$$

or

$$\sigma_1[(\mu_f^2 + 1)^{1/2} + \mu_f] + \sigma_3[(\mu_f^2 + 1)^{1/2} - \mu_f] < 0 ,$$

then a compressive fracture [72] will occur when

$$\sigma_c = \sigma_3 - \sigma_1\left[\frac{(\mu_f^2 + 1)^{1/2} + \mu_f}{(\mu_f^2 + 1)^{1/2} - \mu_f}\right]$$

where σ_c is the uniaxial compressive strength of the material, μ_f is the surface coefficient of friction and θ, which is equal to 0.5 $\tan^{-1}(1/\mu_f)$ and measured from the minor principal stress σ_3 axis, is the orientation of the crack at which fracture initiation will commence. If $\mu_f \to 0$, $\theta \to \pi/4$; if $\mu_f \to \infty$, $\theta \to 0$. Thus the direction of fracture is always inclined at an acute angle to the direction of the axis of the largest principal compressive stress.

When σ_n causes the crack to open, i.e., as $\sigma_n > 0$, tension cracking occurs. For the case that

$$-3\ \sigma_u \leq \sigma_3 \leq \sigma_1$$

fracture initiation occurs when $\sigma_1 = \sigma_u$ where σ_u is the uniaxial tensile strength of the material. For this condition of tensile failure, the crack begins to extend in its own plane in a direction perpendicular to that of the major principal stress σ_1. While for the case that

$$\sigma_3 < -3\ \sigma_u\ ,$$

failure takes place if

$$(\sigma_1 - \sigma_3)^2 + 8\ \sigma_u(\sigma_1 + \sigma_3) = 0\ ,$$

and the crack runs towards the σ_3 axis as in compressive fracture. The corresponding fracture locus, as shown in Figure 1.6, is well illustrated by McClintock [46]. He also extended the criterion to the three-dimensional case (see Figure 1.7).

Concerning the crack propagation direction under uniaxial compression of plates of brittle materials, both analytical and experimental results from Nemat-Nasser, et al. [73] provide good correlation with the Griffith's theory. It was shown that, for the wide range of pre-existing crack orientation, the out-of-plane crack extension initiates at an angle close to 72° from the direction of the pre-existing crack, and then curves into a position almost parallel to the maximum axial compressive stress as shown in Figure 1.8.

Within the framework of the linear elastic fracture mechanics (LEFM), three modes of cracking as in Figure 1.9 are often referred.

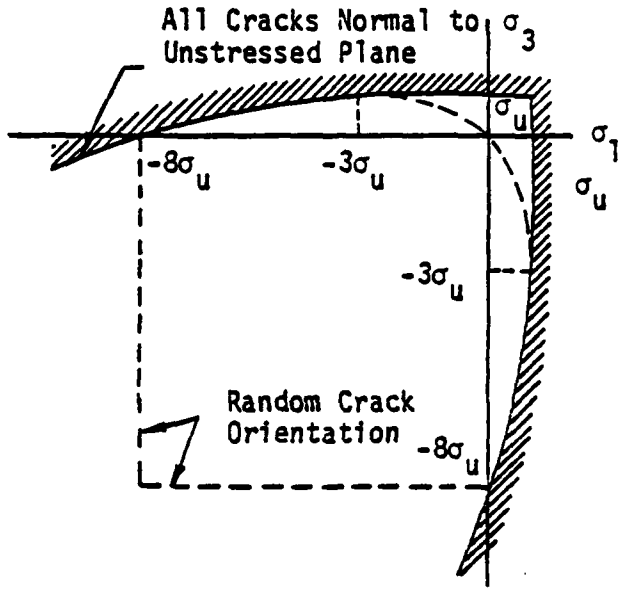

Figure 1.6. Brittle fracture under biaxial stress.

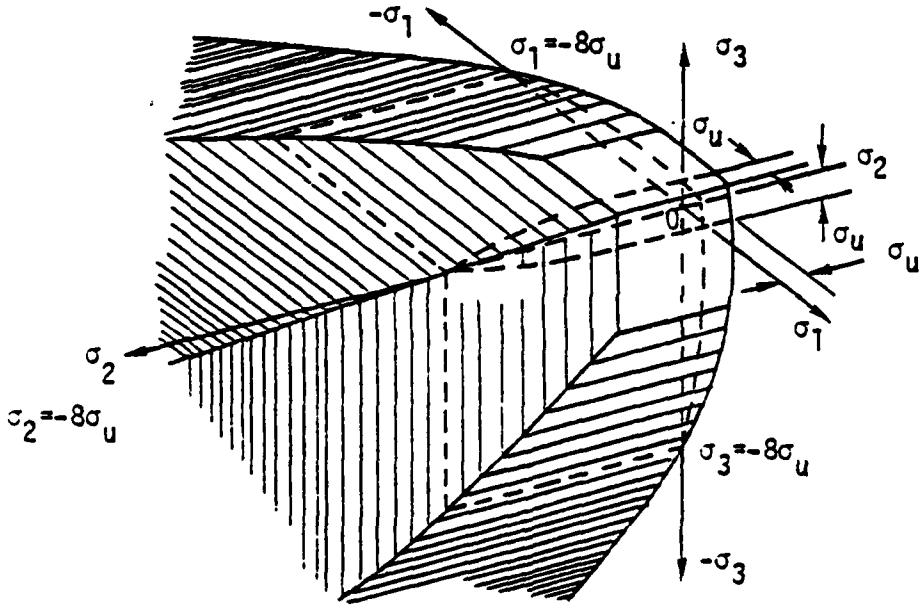

Figure 1.7. Brittle fracture solid representing the states of triaxial stress for brittle fracture.

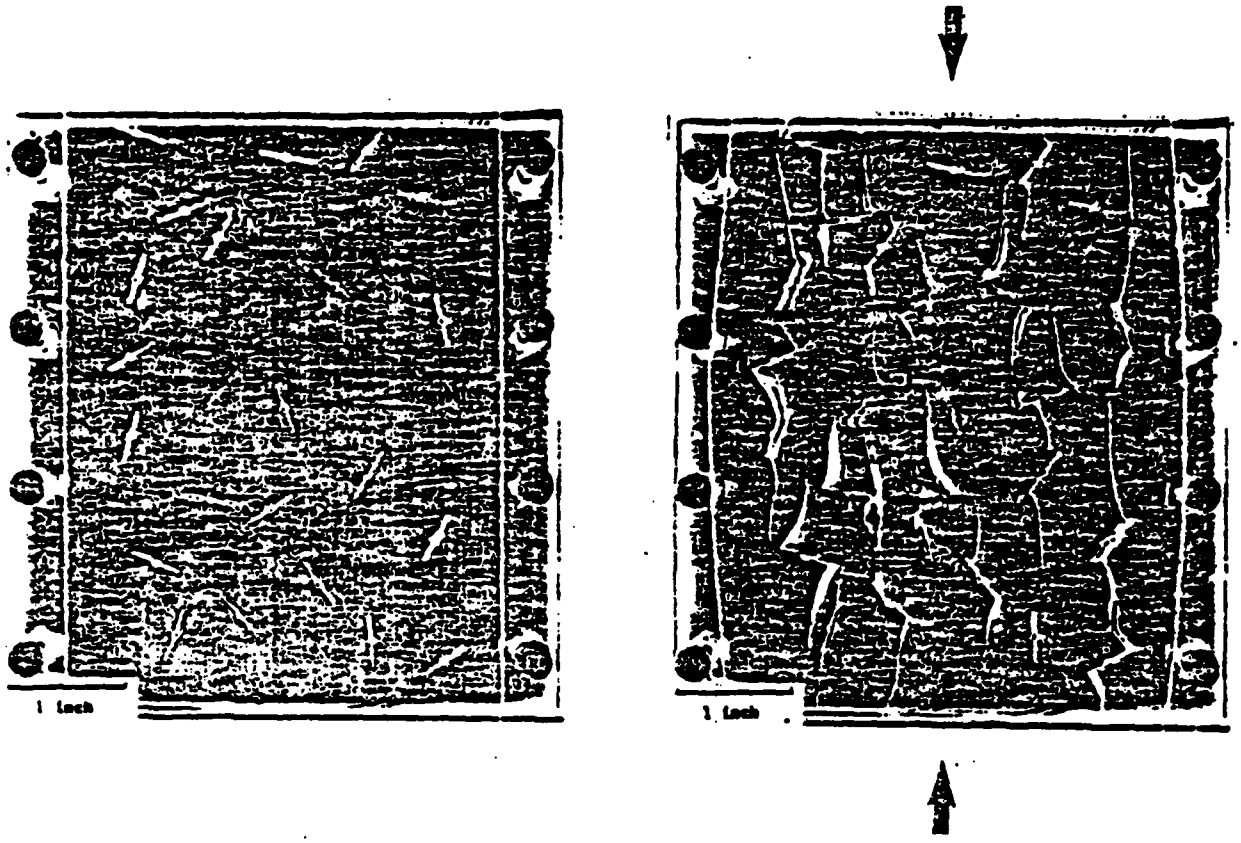

Figure 1.8. (a) Specimen with a number of randomly oriented cracks, and (b) the failure pattern under overall axial compression.

Of concern here is the Mode I crack since it is often observed on the failed seal [16]. Consider a through-the-thickness microcrack of length 2a in an infinite plate which is subjected to the uniaxial ultimate tensile stress as shown in Figure 1.10. The maximum stress occurs near the crack tip at $\theta = 0$ and has the value of $\sigma_{\theta\theta} = \sigma_U\sqrt{a/2r}$. Under this condition, the instability of the microcrack results in the fracture initiation predicted by Griffith's theory.

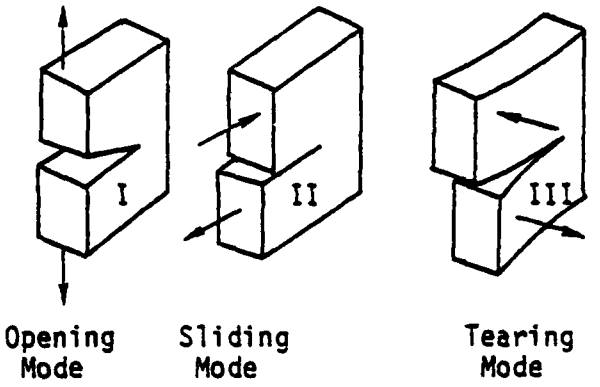

Figure 1.9. The three modes of cracking.

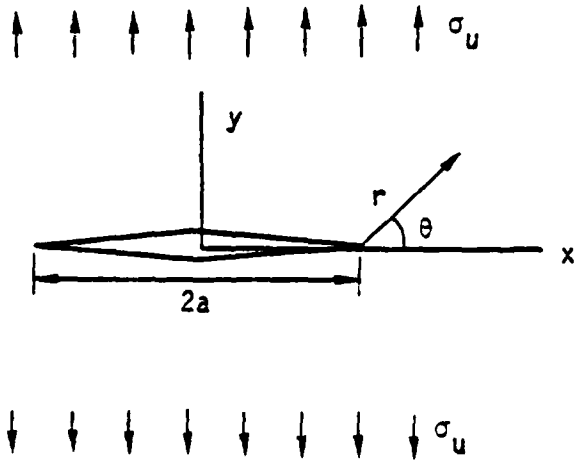

Figure 1.10. Crack in an infinite plate.

CHAPTER 2

A TWO-DIMENSIONAL MODEL OF A SINGLE MOVING ASPERITY

2.1 Mathematical Model[2]

In the present model, it is reiterated that the line asperity is on the insulated mating part of the cracked seal and the speed of the effective load is subsonic. The geometry of the contact area, as shown in Figure 2.1 is such a long narrow strip that the width of the area in the direction of motion is of small order to the radius of the seal surface. Accordingly, the latter may be represented by a planar half-space. The problem may then be described by a plane thermoelastic model as shown in Figure 2.2. The contact load is represented therein by a symmetrically distributed pressure over the contact zone. Coulomb friction is present, resisting the relative motion of the contacting surfaces, that is, the friction force is in the traverse direction of the load. Two sets of coordinates are employed: $(x_1' - x_3')$ are fixed to the seal; $(x_1 - x_3)$ are fixed to the moving load. The boundary values of this problem are therefore as follows: on the surface boundary $x_3 = 0$, there is a combined normal pressure $p(x_1)$ and tangential friction $\mu_f p(x_1)$ distributed over the contact zone $(-a \leq x_1 \leq a)$ and the half-plane is traction-free elsewhere. For the regions at infinity, regularity conditions hold.

The thermal load on the half-plane comes from the frictional heating in the contact zone. The mating surface is by postulation adiabatic. Therefore, all the dissipative energy is accounted for by the

---

[2]The present chapter is a revision of [71].

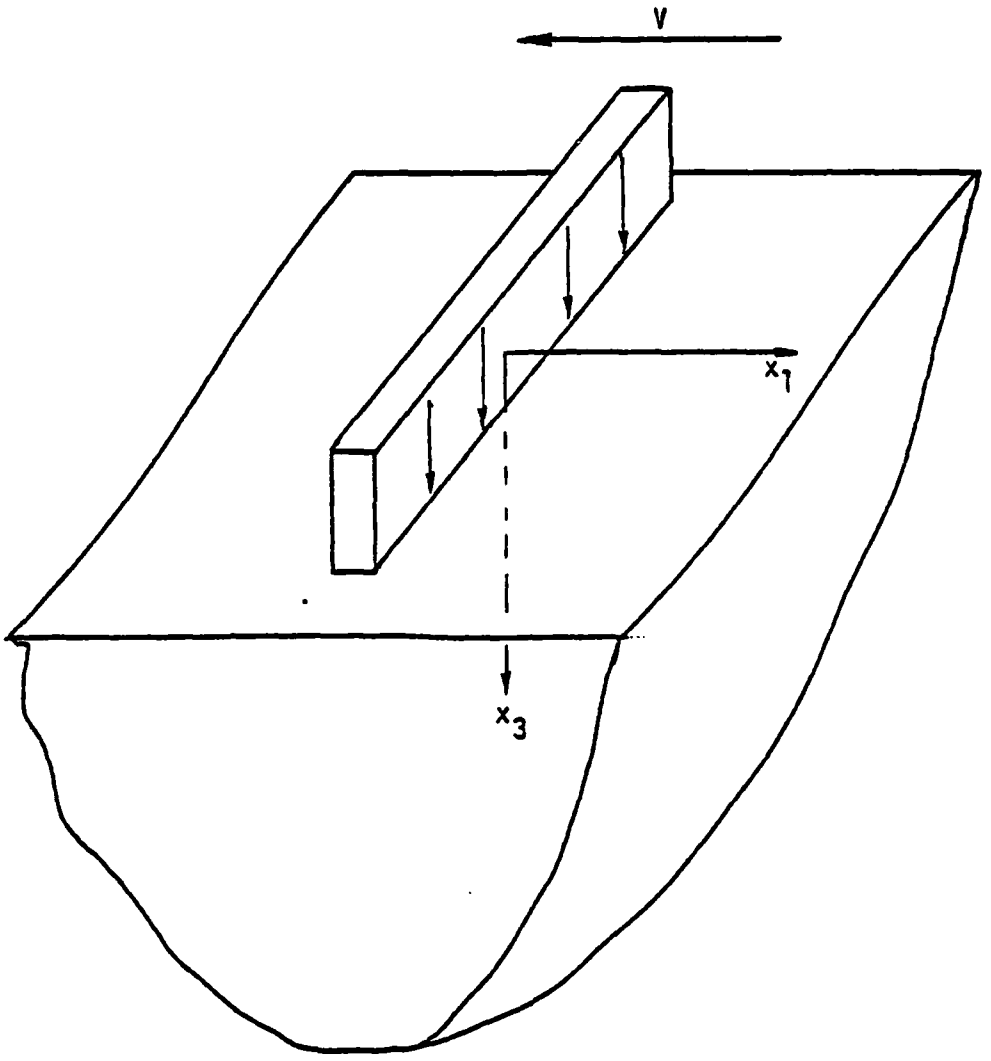

Figure 2.1. Two-dimensional asperity.

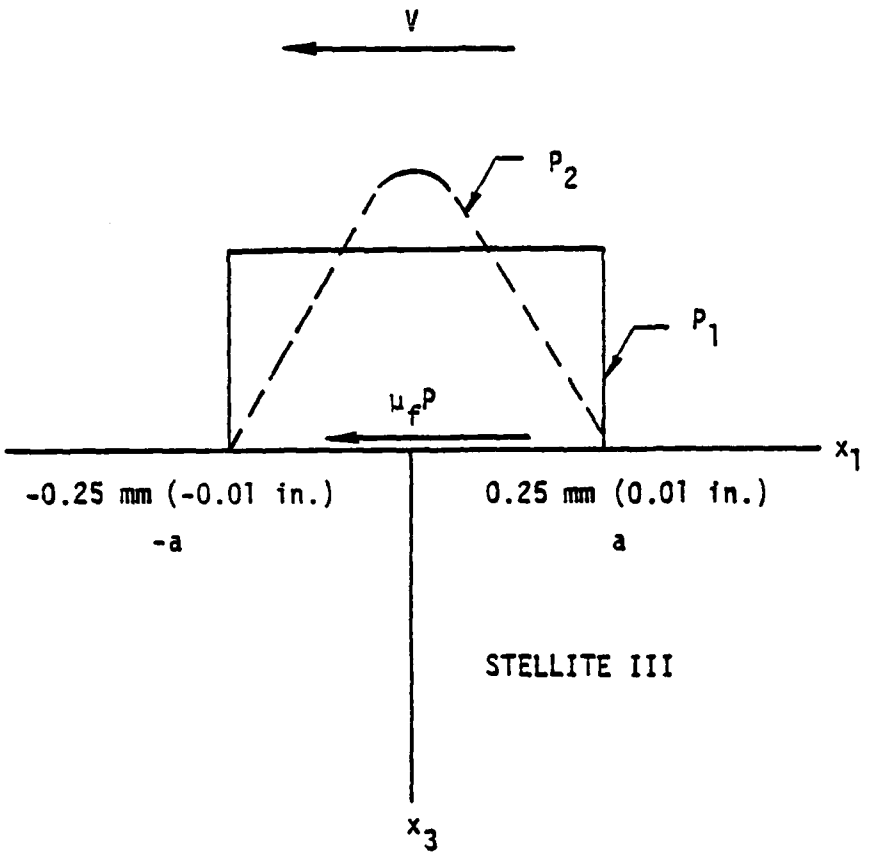

Figure 2.2. Plane model of the half-space problem for a plane moving load (P_1 and P_2 denote the uniform and parabolic pressure distributions, respectively).

heat input to the seal. The heat loss across the free boundary is also neglected.

The material properties affecting the thermomechanical stress field will be the elastic coefficients (E,ν), the density of the seal (ρ), the coefficient of friction (μ_f), the coefficient of thermal expansion (α), the thermal conductivity (k) and the thermal diffusivity (κ). The parameters characterizing the loading are the pressure distribution $p(x_1)$ over the contact zone and the velocity of the moving load (V) for the case when the traversing speed is the same as the rubbing speed.

The stress field from the mechanical loads of normal pressure and friction will at first be computed. The thermal load from the friction force will then be considered to compute the temperature rise and thus the resulting thermal stress field. The two sets of stresses should provide an insight to the separate effects on stresses from the mechanical and the thermal loads. The combined effect from superposing the two shall provide the information on impending failure by fracture.

2.2 Mechanical Stress Field

The solutions of the stress fields, corresponding to the mechanical loads as shown in Figure 2.2, may be obtained by the method of impulse response. For that method the stress field $\{\delta\sigma_{ij}^{n}\}$ from a moving normal force of one unit (Figure 2.3) is the impulse response for the normal pressure while $\{\delta\sigma_{ij}^{f}\}$ from a moving tangential force of one unit (Figure 2.4) is the impulse response for the friction. For

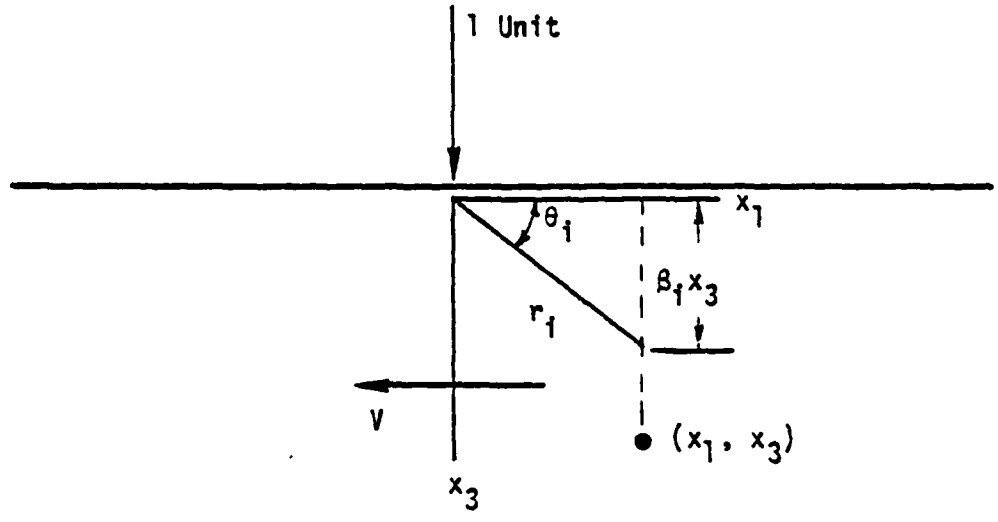

Figure 2.3. Unit normal load on a two-dimensional half-plane.

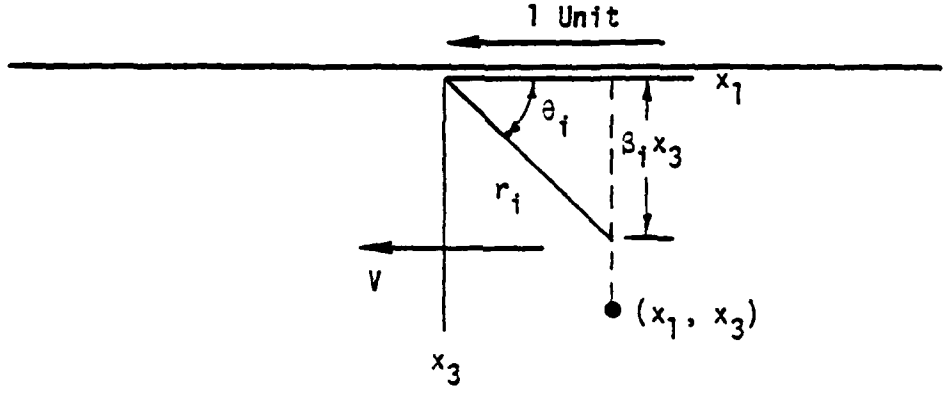

Figure 2.4. Unit tangent load on a two-dimensional half-plane.

loads with subsonic speed, the solutions follow Eringen and Suhubi [19]:

$$\delta\sigma_{11}^{n} = \frac{1}{\pi R}\left\{\frac{B}{r_d}\sin\theta_d - \frac{4\beta_d\beta_s}{r_s}\sin\theta_s\right\},$$

$$\delta\sigma_{33}^{n} = -\frac{1}{\pi R}\left\{\frac{(1+\beta_s^2)^2}{r_d}\sin\theta_d - \frac{4\beta_d\beta_s}{r_s}\sin\theta_s\right\},$$

$$\delta\sigma_{13}^{n} = \frac{1}{\pi R}\left\{-\frac{2\beta_d(2\beta_d^2-\beta_s^2+1)}{r_d}\cos\theta_d + \frac{2\beta_d(1+\beta_s^2)}{r_s}\cos\theta_s\right\}, \quad (2.1)$$

and

$$\delta\sigma_{11}^{f} = \frac{1}{\pi R}\left\{-\frac{2\beta_s(2\beta_d^2-\beta_s^2+1)}{r_d}\cos\theta_d + \frac{2\beta_s(1+\beta_s^2)}{r_s}\cos\theta_s\right\},$$

$$\delta\sigma_{33}^{f} = \frac{1}{\pi R}\left\{\frac{2\beta_s(1+\beta_s^2)}{r_d}\cos\theta_d - \frac{2\beta_s(1+\beta_s^2)}{r_s}\cos\theta_s\right\},$$

$$\delta\sigma_{13}^{f} = \frac{1}{\pi R}\left\{-\frac{4\beta_d\beta_s}{r_d}\sin\theta_d + \frac{(1+\beta_s^2)^2}{r_s}\sin\theta_s\right\} \quad (2.2)$$

where

$$\beta_i^2 = 1 - M_i^2 ,$$

$$\theta_i = \tan^{-1}\frac{\beta_i x_3}{x_1} ,$$

$$R = (1 + \beta_2^2)^2 - 4\beta_d\beta_s ,$$

$$B = (1 + \beta_s^2)(2\beta_d^2 - \beta_s^2 + 1) ,$$

$$M_i = \frac{V}{C_i} , \qquad 0 < M_i < 1 ,$$

$$r_i = [(x_1)^2 + (\beta_i x_3)^2]^{1/2} , \qquad i = d,s$$

and C_d and C_s are respectively the dilatational and the shear wave speeds.

The actual stress field due to the normal pressure is obtained by superposition as the Faltung product of the impulse response with the pressure distribution function $p(x_1)$, i.e.,

$$\sigma_{ij}^n = \delta\sigma_{ij}^n * p(x_1) . \tag{2.3}$$

Similarly, the stress field due to the friction force is the Faltung product of its impulse response with the friction distribution function:

$$\delta\sigma_{ij}^f = \delta\sigma_{ij}^f * \mu_f p(x_1) . \tag{2.4}$$

We shall use dimensionless variables such that

$$\sigma_{\xi\xi} = \frac{\sigma_{11}}{p_o} , \qquad \sigma_{\zeta\zeta} = \frac{\sigma_{33}}{p_o} , \qquad \sigma_{\xi\zeta} = \frac{\sigma_{13}}{p_o} ,$$

and

$$\tilde{p}(\lambda) = \frac{p}{p_o} , \qquad \xi = \frac{x_1}{a} , \qquad \zeta = \frac{x_3}{a}$$

where λ is a dummy variable of ξ, and p_o is the average pressure in the contact zone. The stress fields resulting from the normal pressure and the friction force in the contact zone are respectively obtained from Equations (2.3) and (2.4) as follows:

$$\sigma^n_{\xi\xi} = \frac{A_d}{\pi R}\int_{-1}^{1} \tilde{p}(\lambda)\left\{\frac{B}{(\xi-\lambda)^2 + A_d^2} - \frac{4\beta_s^2}{(\xi-\lambda)^2 + A_s^2}\right\} d\lambda ,$$

$$\sigma^n_{\zeta\zeta} = -\frac{A_d}{\pi R}\int_{-1}^{1} \tilde{p}(\lambda)\left\{\frac{(1+\beta_s^2)^2}{(\xi-\lambda)^2 + A_d^2} - \frac{4\beta_s^2}{(\xi-\lambda)^2 + A_s^2}\right\} d\lambda ,$$

$$\sigma^n_{\xi\zeta} = -\frac{2\beta_d(1+\beta_s^2)(\beta_s^2-\beta_d^2)\,\zeta^2}{\pi R}\int_{-1}^{1} \frac{\tilde{p}(\lambda)(\xi-\lambda)}{[(\xi-\lambda)^2 + A_d^2][(\xi-\lambda)^2 + A_s^2]}\, d\lambda \qquad (2.5)$$

and

$$\sigma^f_{\xi\xi} = -\frac{2\mu_f\beta_s}{\pi R}\int_{-1}^{1} \tilde{p}(\lambda)(\xi-\lambda)\left\{\frac{(2\beta_d^2 - \beta_s^2 + 1)}{(\xi-\lambda)^2 + A_d^2} - \frac{(1+\beta_s^2)}{(\xi-\lambda)^2 + A_s^2}\right\} d\lambda ,$$

$$\sigma^f_{\zeta\zeta} = \frac{2\mu_f\beta_s(1+\beta_s^2)(\beta_s^2-\beta_d^2)\,\zeta^2}{\pi R}\int_{-1}^{1} \frac{\tilde{p}(\lambda)(\xi-\lambda)}{[(\xi-\lambda)^2 + A_d^2][(\xi-\lambda)^2 + A_s^2]}\, d\lambda ,$$

$$\sigma^f_{\xi\zeta} = -\frac{\mu_f A_s}{\pi R}\int_{-1}^{1} \tilde{p}(\lambda)\left\{\frac{4\beta_d^2}{(\xi-\lambda)^2 + A_d^2} - \frac{(1+\beta_s^2)^2}{(\xi-\lambda)^2 + A_s^2}\right\} d\lambda \qquad (2.6)$$

where $A_i = \beta_i\zeta$, $i = d,s$.

When the pressure distribution function $\tilde{p}(\lambda)$ is given, the convolution integral can be evaluated. The simplest case is when the pressure distribution is uniform, $\tilde{p} = 1$, for which Equations (2.5) and (2.6) become

$$\sigma^n_{\xi\xi} = \frac{1}{\pi R}\,(B\psi_d - 4\beta_d\beta_s\psi_s) \ ,$$

$$\sigma^n_{\zeta\zeta} = -\frac{1}{\pi R}\,[(1+\beta_s^2)^2\,\psi_d - 4\beta_d\beta_s\psi_s]$$

$$\sigma^n_{\xi\zeta} = \frac{\beta_d(1+\beta_2^2)}{\pi R}\,\ln(\frac{F_d}{F_s}) \ ,$$

$$\sigma^f_{\xi\xi} = -\frac{\mu_f\beta_s}{\pi R}\,[(2\beta_d^2 - \beta_s^2 + 1)\,\ln F_d - (1+\beta_s^2)\,\ln F_s] \ ,$$

$$\sigma^f_{\zeta\zeta} = -\frac{\mu_f\beta_s(1+\beta_s^2)}{\pi R}\,\ln(\frac{F_d}{F_s}) \ ,$$

$$\sigma^f_{\xi\zeta} = -\frac{\mu_f}{\pi R}\,[4\beta_d\beta_s\psi_d - (1+\beta_s^2)^2\,\psi_s] \ , \qquad (2.7)$$

where

$$\psi_i = \tan^{-1}(\frac{1+\xi}{A_i}) + \tan^{-1}(\frac{1-\xi}{A_i}) \ ,$$

$$F_i = \frac{(\xi-1)^2 + A_i^2}{(\xi+1)^2 + A_i^2} \ , \qquad i = d,s \ .$$

The second case for which a parabolic pressure distribution, $\tilde{p} = 3/2(1 - \lambda^2)$, is considered yields

$$\sigma^n_{\xi\xi} = \frac{3}{2\pi R}\{B(A_d^2 - \xi^2 + 1)\,\psi_d - 4\beta_d\beta_s(A_s^2 - \xi^2 + 1)\,\psi_s$$

$$- A_d[B(2 + \xi \ln F_d) - 4\beta_s^2(2 + \xi \ln F_s)]\} ,$$

$$\sigma^n_{\zeta\zeta} = \frac{3}{2\pi R}\{-(1 + \beta_s^2)^2\,(A_d^2 - \xi^2 + 1)\,\psi_d + 4\beta_d\beta_s(A_s^2 - \xi^2 + 1)\,\psi_s$$

$$- A_d[-(1 + \beta_s^2)^2\,(2 + \xi \ln F_d) + 4\beta_s^2(2 + \xi \ln F_s)]\} ,$$

$$\sigma^n_{\xi\zeta} = \frac{3\beta_d(1 + \beta_s^2)}{2\pi R}[(A_d^2 - \xi^2 + 1) \ln F_d - (A_s^2 - \xi^2 + 1) \ln F_s$$

$$+ 4\xi(A_d\psi_d - A_s\psi_s)] ,$$

$$\sigma^f_{\xi\xi} = -\frac{3u_f\beta_s}{2\pi R}\{-(2\beta_d^2 - \beta_s^2 + 1)(A_d^2 - \xi^2 + 1) \ln F_d$$

$$+ (1 + \beta_s^2)(A_s^2 - \xi^2 + 1) \ln F_s - 4\xi[(2\beta_d^2 - \beta_s^2 + 1)\,A_d\psi_d$$

$$- (1 + \beta_s^2)\,A_s\psi_s - 2(\beta_d^2 - \beta_s^2)]\} ,$$

$$\sigma^f_{\zeta\zeta} = -\frac{3u_f\beta_s(1 + \beta_s^2)}{2\pi R}[(A_d^2 - \xi^2 + 1) \ln F_d - (A_s^2 - \xi^2 + 1) \ln F_s$$

$$+ 4\xi(A_d\psi_d - A_s\psi_s)] ,$$

$$\sigma^f_{\xi\zeta} = -\frac{3u_f}{2\pi R}\{4\beta_d\beta_s(A_d^2 - \xi^2 + 1)\,\psi_d - (1 + \beta_s^2)^2\,(A_s^2 - \xi^2 + 1)\,\psi_s$$

$$- A_s[4\beta_d^2(2 + \xi \ln F_d) - (1 + \beta_s^2)^2\,(2 + \xi \ln F_s)]\} . \qquad (2.8)$$

2.3 Temperature Field

The heating on the boundary is assumed to be caused principally by the friction. The analysis is therefore one with a half-space subjected to a fast-moving heat source. When the mating surface and its asperity are assumed to be adiabatic, the rate of energy dissipation from the friction force is converted entirely into the heat input q such that

$$q = V\mu_f p(x_1) \ .$$

Using the solution developed by Ling and Mow [20], we may obtain the temperature field as

$$\phi(\xi,\zeta) = 0 \ , \qquad -\infty < \xi \leq -1 \ ,$$

$$\phi(\xi,\zeta) = \frac{1}{(\pi P_e)^{1/2}} \int_{-1}^{\xi} \frac{Q(\lambda)}{(\xi - \lambda)^{1/2}} \exp\left\{-\frac{P_e \zeta^2}{4(\xi - \lambda)}\right\} d\lambda \ , \qquad -1 \leq \xi \leq 1 \ ,$$

$$\phi(\xi,\zeta) = \frac{1}{(\pi P_e)^{1/2}} \int_{-1}^{1} \frac{Q(\lambda)}{(\xi - \lambda)^{1/2}} \exp\left\{-\frac{P_e \zeta^2}{4(\xi - \lambda)}\right\} d\lambda \ , \qquad 1 \leq \xi < \infty \tag{2.9}$$

where

$\phi(\xi,\zeta) = \frac{Tk}{q_o a}$ is the dimensionless temperature,

$Q(\lambda) = \frac{q}{q_o}$ is the dimensionless heat input,

$P_e = \frac{Va}{\kappa}$ is the Peclet number,

T is the temperature above the stress-free ambient temperature and q_0 is the characteristic heat input ($\mu_f V p_0$). $Q(\lambda)$ is therefore identified with $\tilde{p}(\lambda)$.

Surface temperatures for the case of uniform and parabolic pressure distributions can be readily obtained by letting $\zeta = 0$. The results can be expressed as

$$\phi_s(\xi) = 0 , \qquad -\infty \leq \xi \leq -1 ,$$

$$\phi_s(\xi) = 2\left(\frac{\xi + 1}{\pi P_e}\right)^{1/2} , \qquad -1 \leq \xi \leq 1 ,$$

$$\phi_s(\xi) = \frac{2}{(\pi P_e)^{1/2}} \left[(\xi + 1)^{1/2} - (\xi - 1)^{1/2}\right] , \qquad 1 \leq \xi < \infty \tag{2.10}$$

and

$$\phi_s(\xi) = 0 , \qquad -\infty < \xi \leq -1 ,$$

$$\phi_s(\xi) = \frac{3}{(\pi P_e)^{1/2}} \left\{(1 - \xi^2)(\xi + 1)^{1/2} + \frac{2}{3} \xi(\xi + 1)^{3/2} - \frac{1}{5} (\xi + 1)^{5/2}\right\} , \qquad -1 \leq \xi \leq 1 ,$$

$$\phi_s(\xi) = \frac{3}{(\pi P_e)^{1/2}} \left\{(1 - \xi^2) \left[(\xi + 1)^{1/2} - (\xi - 1)^{1/2}\right] + \frac{2}{3} \xi\left[(\xi + 1)^{3/2} - (\xi - 1)^{3/2}\right] - \frac{1}{5} \left[(\xi + 1)^{5/2} - (\xi - 1)^{5/2}\right]\right\} , \qquad 1 \leq \xi < \infty \tag{2.11}$$

respectively.

2.4 Thermal Stress Field

The impulse response of a stress field corresponding to the heat input of a unit pressure is $\{\delta\sigma\}$, which is conveniently separated into the particular and the complementary solutions $\{\delta\sigma^P\}$ and $\{\delta\sigma^C\}$, respectively. Their expressions, following Mow and Cheng [22][3], are

$$\delta\sigma^P_{\xi\xi} = \frac{2g}{P_e(\pi P_e)^{1/2}}\left(-P_e\xi^{-1/2} - \frac{\xi}{2}^{-3/2} + \frac{P_e\zeta^2}{4}\xi^{-5/2}\right)\exp\left(-\frac{P_e\zeta^2}{4\xi}\right)H(\xi)\ ,$$

$$\delta\sigma^P_{\zeta\zeta} = -\frac{2g}{P_e(\pi P_e)^{1/2}}\left(-\frac{\xi^{-3/2}}{2} + \frac{P_e\zeta^2}{4}\xi^{-5/2}\right)\exp\left(-\frac{P_e\zeta^2}{4\xi}\right)H(\xi)\ ,$$

$$\delta\sigma^P_{\xi\zeta} = -\frac{g}{(\pi P_e)^{1/2}}\ \xi^{-3/2}\,\zeta\exp\left(-\frac{P_e\zeta^2}{4\xi}\right)H(\xi)\ , \qquad (2.12)$$

$$\delta\sigma^C_{\xi\xi} = \frac{1}{2}\{C_1(\xi^2+\zeta^2)^{-3/4}\left[\cos\tfrac{3}{2}\theta - \sin\tfrac{3}{2}\theta + \tfrac{3}{2}\cos\theta\,(\cos\tfrac{5}{2}\theta - \sin\tfrac{5}{2}\theta)\right] + C_3\xi^3(\xi^2+\zeta^2)^{-2}\}H(\xi)\ ,$$

$$\delta\sigma^C_{\zeta\zeta} = \frac{1}{2}\{C_1(\xi^2+\zeta^2)^{-3/4}\left[\cos\tfrac{3}{2}\theta - \sin\tfrac{3}{2}\theta + \tfrac{3}{2}\cos\theta\,(\cos\tfrac{5}{2}\theta - \sin\tfrac{5}{2}\theta) + C_3\xi\zeta^2(\xi^2+\zeta^2)^{-2}\right\}H(\xi)\ ,$$

$$\delta\sigma^C_{\xi\zeta} = \frac{1}{2}\{C_1(\xi^2+\zeta^2)^{-3/4}\left[\tfrac{3}{2}\cos\theta\,(\cos\tfrac{5}{2}\theta + \sin\tfrac{5}{2}\theta)\right] + \frac{4}{\pi^{1/2}}C_2\xi^2\zeta(\xi^2+\zeta^2)^{-2}\}H(\xi) \qquad (2.13)$$

---

[3]The equations listed are a corrected version of those given in the paper.

where

$$\theta = \tan^{-1} \frac{\xi}{\zeta} ,$$

$$C_1 = \left(\frac{2}{\pi}\right)^{1/2} \frac{g}{\rho_e^{3/2}} ,$$

$$C_2 = \frac{2}{\pi^{1/2}} \frac{g}{\rho_e} ,$$

$$C_3 = \frac{8}{\pi} \frac{g}{\rho_e} ,$$

$$g = \frac{E}{2(1 - \nu)} \frac{\alpha u_f}{k} Va ,$$

and

$$H(\xi) = \begin{cases} 0 & \xi < 0 \\ 1 & 0 \leq \xi \end{cases}$$

The thermal stresses are thus computed from the Faltung product:

$$\sigma_{ij} = \delta\sigma_{ij} * Q(\lambda)$$

where $\delta\sigma_{ij}$ is the combination of the particular and the complementary solutions. The results can be expressed in terms of convolution integrals, which are

$$\sigma_{ij} = 0 , \qquad -\infty < \xi \leq -1$$

$$\sigma_{ij} = \int_{-1}^{\xi} \tilde{p}(\lambda)\ \delta\tilde{\sigma}_{ij}(\xi - \lambda, \zeta)\ d\lambda , \qquad -1 \leq \xi \leq 1$$

$$\sigma_{ij} = \int_{-1}^{1} \tilde{p}(\lambda)\ \delta\tilde{\sigma}_{ij}(\xi - \lambda, \zeta)\ d\lambda\ , \qquad 1 \leq \xi < \infty \tag{2.14}$$

in which

$$\delta\tilde{\sigma}_{ij} = \delta\tilde{\sigma}^{p}_{ij} + \delta\tilde{\sigma}^{c}_{ij}\ . \tag{2.15}$$

Note that the expressions for $\delta\tilde{\sigma}^{p}_{ij}$ and $\delta\tilde{\sigma}^{c}_{ij}$ correspond to those in Equations (2.12) and (2.13), respectively, with the deletion of the Heaviside function.

With the notation

$$S_n = \int_{-1}^{\xi} (\xi - \lambda)^{-n/2}\ \exp\left\{-\frac{P_e\zeta^2}{4(\xi - \lambda)}\right\} d\lambda$$

and making the change of variable,

$$t = \frac{P_e\zeta^2}{4(\xi - \lambda)}\ ,$$

we have

$$S_1 = P_e^{1/2}\ \zeta\left\{\frac{2}{\zeta}\left(\frac{\xi + 1}{P_e}\right)^{1/2} \exp\left[-\frac{P_e\zeta^2}{4(\xi + 1)}\right] - \pi^{1/2}\left(1 - \operatorname{erf}\left[\frac{\zeta}{2}\left(\frac{P_e}{\xi + 1}\right)^{1/2}\right]\right)\right\}\ ,$$

$$S_3 = \frac{2}{\zeta}\left(\frac{\pi}{P_e}\right)^{1/2}\left\{1 - \operatorname{erf}\left[\frac{\zeta}{2}\left(\frac{P_e}{\xi + 1}\right)\right]\right\},$$

$$S_5 = \frac{8}{P_e^{3/2}\ \zeta^3}\left\{\frac{\pi^{1/2}}{2} - \int_0^{-\frac{P_e\zeta^2}{4(\xi+1)}} t^{1/2}\ e^{-t}\ dt\right\}. \tag{2.16}$$

Equation (2.14) for the uniform pressure loading case, on the substitution of Equations (2.15) and (2.16), gives

$$\sigma_{\xi\xi} = \sigma_{\zeta\zeta} = \sigma_{\xi\zeta} = 0 \ , \quad \text{for} \quad -\infty < \xi \leq -1 \ ,$$

$$\sigma_{\xi\xi} = -\frac{2g}{(\pi P_e)^{1/2}} S_1 - \frac{g}{P_e(\pi P_e)^{1/2}} S_3 + \frac{g\zeta^2}{2(\pi P_e)^{1/2}} S_5 + \int_{-1}^{\xi} \delta\tilde{\sigma}^c_{\xi\xi}(\xi - \lambda, \zeta)\, d\lambda \ ,$$

$$\sigma_{\zeta\zeta} = \frac{g}{P_e(\pi P_e)^{1/2}} S_3 - \frac{g\zeta^2}{2(\pi P_e)^{1/2}} S_5 + \int_{-1}^{\xi} \delta\tilde{\sigma}^c_{\zeta\zeta}(\xi - \lambda, \zeta)\, d\lambda \ ,$$

$$\sigma_{\xi\zeta} = -\frac{g\zeta}{(\pi P_e)^{1/2}} S_3 + \int_{-1}^{\xi} \delta\tilde{\sigma}^c_{\xi\zeta}(\xi - \lambda, \zeta)\, d\lambda \ ,$$

for $-1 \leq \xi \leq 1$ and

$$\sigma_{\xi\xi} = -\frac{2g}{(\pi P_e)^{1/2}} T_1 - \frac{g}{P_e(\pi P_e)^{1/2}} T_3 + \frac{g\zeta^2}{2(\pi P_e)^{1/2}} T_5 + \int_{-1}^{1} \delta\tilde{\sigma}^c_{\xi\xi}(\xi - \lambda, \zeta)\, d\lambda \ ,$$

$$\sigma_{\zeta\zeta} = \frac{g}{P_e(\pi P_e)^{1/2}} T_3 - \frac{g\zeta^2}{2(\pi P_e)^{1/2}} T_5 + \int_{-1}^{1} \delta\tilde{\sigma}^c_{\zeta\zeta}(\xi - \lambda, \zeta)\, d\lambda \ ,$$

$$\sigma_{\zeta\zeta} = -\frac{g\zeta}{(\pi P_e)^{1/2}} T_3 + \int_{-1}^{1} \delta\tilde{\sigma}_{\xi\zeta}(\xi - \lambda, \zeta)\, d\lambda \qquad (2.17)$$

for $1 \leq \xi < \infty$, where

$$T_n = \int_{-1}^{1} (\xi - \lambda)^{-n/2} \exp\left\{-\frac{P_e\zeta^2}{4(\xi - \lambda)}\right\} d\lambda \ , \qquad n = 1,3,5 \ .$$

Similarly, the stresses for the case of the parabolic pressure distribution can be obtained as follows:

For $\infty < \xi \leq -1$,

$$\sigma_{\xi\xi} = \sigma_{\zeta\zeta} = \sigma_{\xi\zeta} = 0 \ .$$

For $-1 \leq \xi \leq 1$,

$$\sigma_{\xi\xi} = -\frac{3g}{(\pi P_e)^{1/2}} F_1 - \frac{3g}{2P_e(\pi P_e)^{1/2}} F_3 + \frac{3g\zeta^2}{4(\pi P_e)^{1/2}} F_5$$

$$+ \frac{3}{2}\int_{-1}^{\xi} (1 - \lambda^2)\ \delta\tilde{\sigma}^c_{\xi\xi}(\xi - \lambda, \zeta)\ d\lambda$$

$$\sigma_{\zeta\zeta} = \frac{3g}{2P_e(\pi P_e)^{1/2}} F_3 - \frac{3g\zeta^2}{4(\pi P_e)^{1/2}} F_5 + \frac{3}{2}\int_{-1}^{\xi} (1 - \lambda^2)\ \delta\tilde{\sigma}^c_{\zeta\zeta}(\xi - \lambda, \zeta)\ d\lambda \ ,$$

$$\sigma_{\xi\zeta} = -\frac{3g\zeta}{2(\pi P_e)^{1/2}} F_3 + \frac{3}{2}\int_{-1}^{\xi} (1 - \lambda^2)\ \delta\tilde{\sigma}_{\xi\zeta}(\xi - \lambda, \zeta)\ d\lambda \ .$$

For $1 \leq \xi < \infty$,

$$\sigma_{\xi\xi} = -\frac{3g}{(\pi P_e)^{1/2}} G_1 - \frac{3g}{2P_e(\pi P_e)^{1/2}} G_3 + \frac{3g\zeta^2}{4(\pi P_e)^{1/2}} G_5$$

$$+ \frac{3}{2}\int_{-1}^{1} (1 - \lambda^2)\ \delta\tilde{\sigma}^c_{\xi\xi}(\xi - \lambda, \zeta)\ d\lambda \ ,$$

$$\sigma_{\zeta\zeta} = \frac{3g}{2P_e(\pi P_e)^{1/2}} G_3 - \frac{3g\zeta^2}{4(\pi P_e)^{1/2}} G_5 + \frac{3}{2}\int_{-1}^{1} (1 - \lambda^2)\ \delta\tilde{\sigma}^c_{\zeta\zeta}(\xi - \lambda, \zeta)\ d\lambda \ ,$$

$$\sigma_{\xi\zeta} = -\frac{3g\zeta}{2(\pi P_e)^{1/2}} G_3 + \frac{3}{2}\int_{-1}^{1} (1 - \lambda^2)\ \delta\tilde{\sigma}^c_{\xi\zeta}(\xi - \lambda, \zeta)\ d\lambda \qquad (2.18)$$

where

$$F_1 = \frac{1}{2} P_e^{1/2} \zeta \left\{ \frac{2}{\zeta} \left(\frac{\xi + 1}{P_e} \right)^{1/2} \left[2(1 - \xi^2) - \frac{2}{3} P_e \xi \zeta^2 - \frac{1}{30} P_e^2 \zeta^4 \right] \right.$$

$$\cdot \exp\left[- \frac{P_e \zeta^2}{4(\xi + 1)} \right] + \frac{8}{3\zeta} \left[\frac{(\xi + 1)^3}{P_e} \right]^{1/2} \left(\xi + \frac{1}{20} P_e \zeta^2 \right) \exp\left[- \frac{P_e \zeta^2}{4(\xi + 1)} \right]$$

$$- \frac{4}{5\zeta} \left[\frac{(\xi + 1)^5}{P_e} \right]^{1/2} \exp\left[- \frac{P_e \zeta^2}{4(\xi + 1)} \right] - \pi^{1/2} \left[1 - \operatorname{erf} \frac{\zeta}{2} \left(\frac{P_e}{\xi + 1} \right)^{1/2} \right]$$

$$\left. \cdot \left[2(1 - \xi^2) - \frac{2}{3} P_e \xi \zeta^2 - \frac{1}{30} P_e^2 \zeta^4 \right] \right\},$$

$$F_3 = \frac{2}{P_e^{1/2} \zeta} \left\{ 2\zeta P_e^{1/2} (\xi + 1)^{1/2} \left(\xi + \frac{1}{12} P_e \zeta^2 \right) \exp\left[- \frac{P_e \zeta^2}{4(\xi + 1)} \right] \right.$$

$$- \frac{\zeta}{3} P_e^{1/2} (\xi + 1)^{3/2} \exp\left[- \frac{P_e \zeta^2}{4(\xi + 1)} \right] + \pi^{1/2} \left[1 - \operatorname{erf} \frac{\zeta}{2} \left(\frac{P_e}{\xi + 1} \right)^{1/2} \right]$$

$$\left. \cdot \left(1 - \xi^2 - P_e \xi \zeta^2 - \frac{1}{12} P_e^2 \zeta^4 \right) \right\},$$

$$F_5 = \frac{8}{(P_e \zeta^3)^{1/2}} \left\{ (1 - \xi^2) \left[\frac{\pi^{1/2}}{2} - \int_0^{\frac{P_e \zeta^2}{4(\xi + 1)}} t^{1/2} e^{-t} \, dt \right] \right.$$

$$+ \frac{\pi^{1/2}}{2} P_e \zeta^2 \left(\xi + \frac{P_e \zeta^2}{4} \right) \left[1 - \operatorname{erf} \frac{\zeta}{2} \left(\frac{P_e}{\xi + 1} \right)^{1/2} \right]$$

$$\left. - \frac{1}{4} P_e^{3/2} \zeta^3 (\xi + 1)^{1/2} \exp\left[- \frac{P_e \zeta^2}{4(\xi + 1)} \right] \right\},$$

and

$$G_n = \int_{-1}^{1} (1 - \lambda^2)(\xi - \lambda)^{-n/2} \exp\left[-\frac{P_e \zeta^2}{4(\xi - \lambda)}\right] d\lambda , \qquad n = 1,3,5 .$$

2.5 Numerical Results

The numerical evaluation of the mechanical stress fields in Equations (2.7) and (2.8) can be readily obtained by direct substitution of the data for loading and material properties. Figure 2.5 shows $\sigma_{\xi\xi} = \sigma^n_{\xi\xi} + \sigma^f_{\xi\xi}$ for different depths ζ. The traversing speed V = 15 m/s (600 ips). The solid lines represent the uniform pressure distribution and the dotted lines represent the parabolic distribution. Because of the load discontinuity, the stress component $\sigma_{\xi\xi}$ has two singularities on the surface, for the case of uniform pressure, at $\xi = \pm 1$. In the real problem, the pressure distribution is closer to the case of a parabolic function, for which there is no singularity.

The temperature field for both cases is shown in Figure 2.6. Near the surface, there exists a high-temperature thermal layer. The temperature decays exponentially with respect to the depth as we can observe from Equations (2.9) and (2.10). As a result, the thermal stresses under the moving load may be compressive near the surface and become tensile at a certain depth where the maximum temperature gradient occurs. Indeed, this is the case and illustrated by the numerical evaluation of the thermal stress fields in Equations (2.17) and (2.18), and shown in Figure 2.7.

The maximum principal stress resulting from the combined stress field is shown in Figure 2.8 for depths ζ = 1.0 and 0.1. The

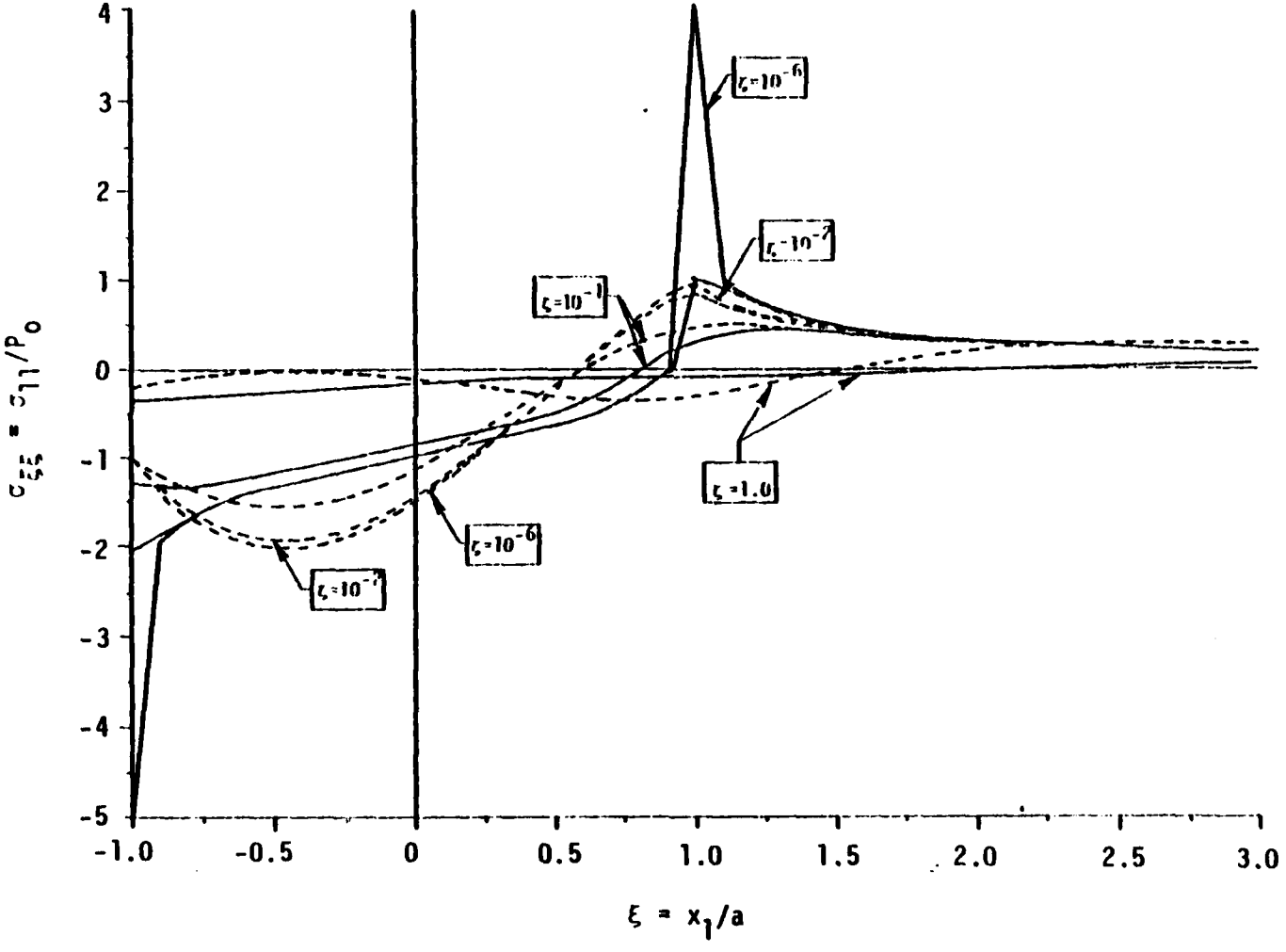

Figure 2.5. Mechanical stresses due to combined pressure and friction.

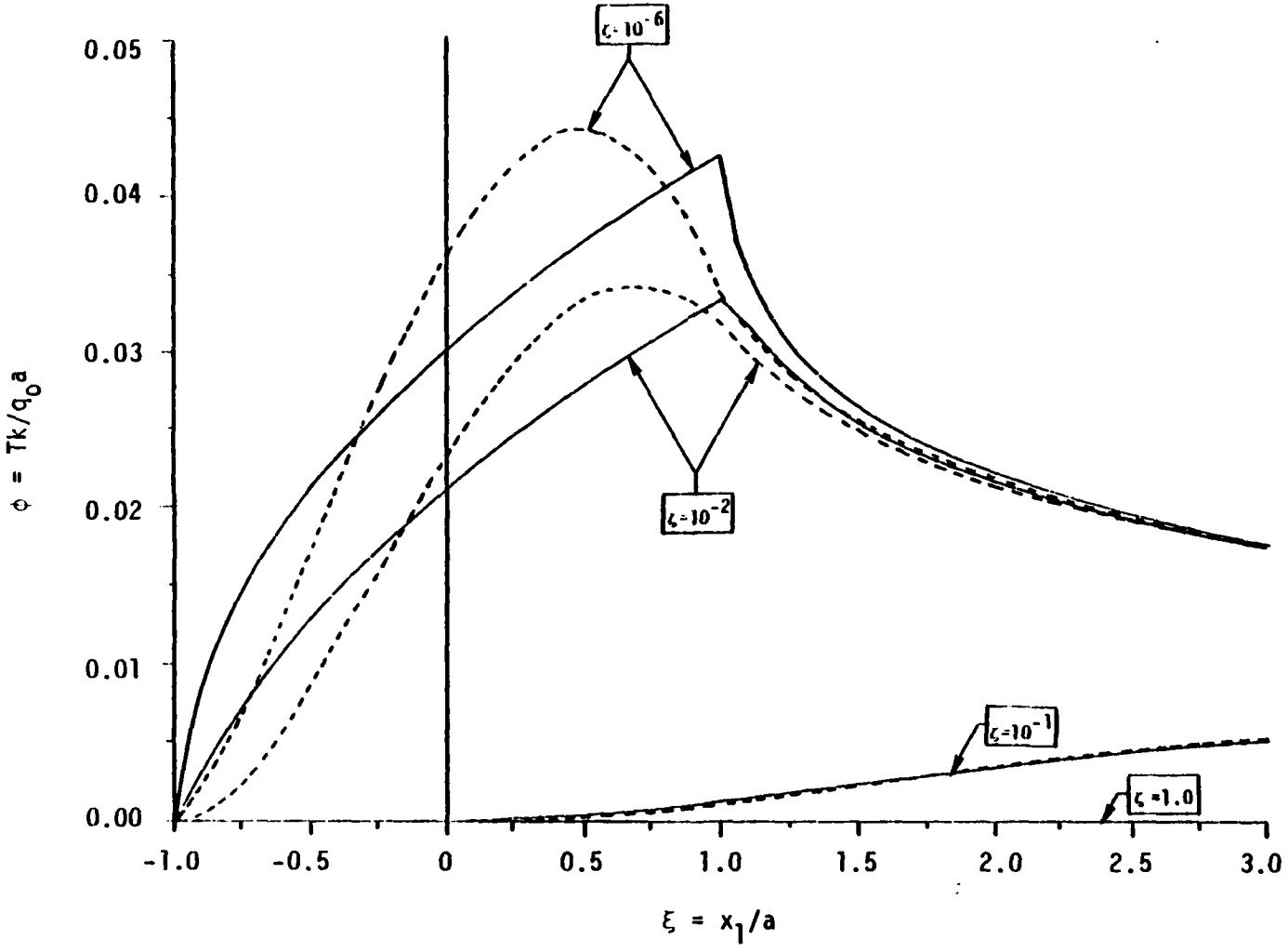

Figure 2.6. Temperatures due to friction.

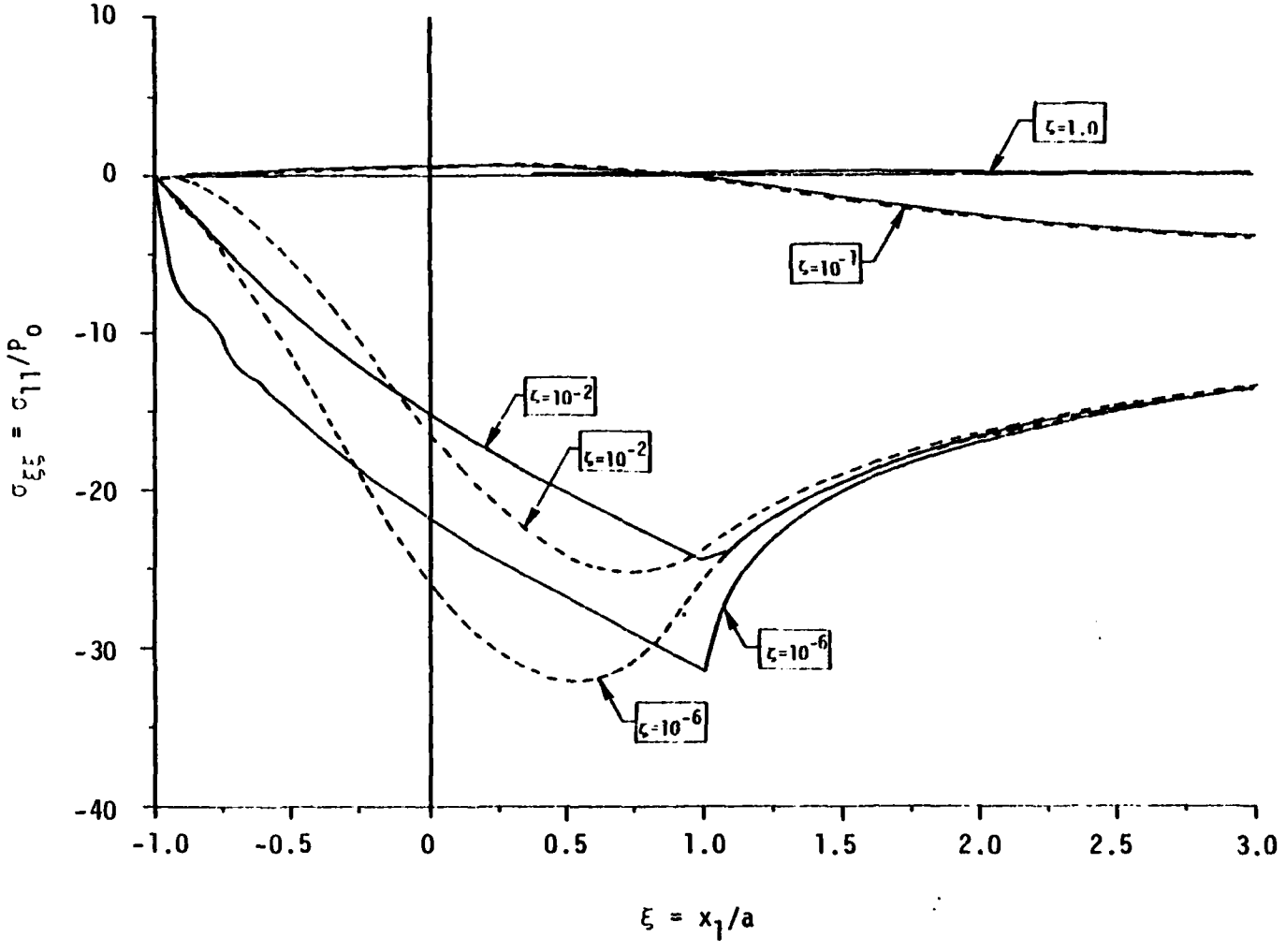

Figure 2.7. Thermostresses due to friction.

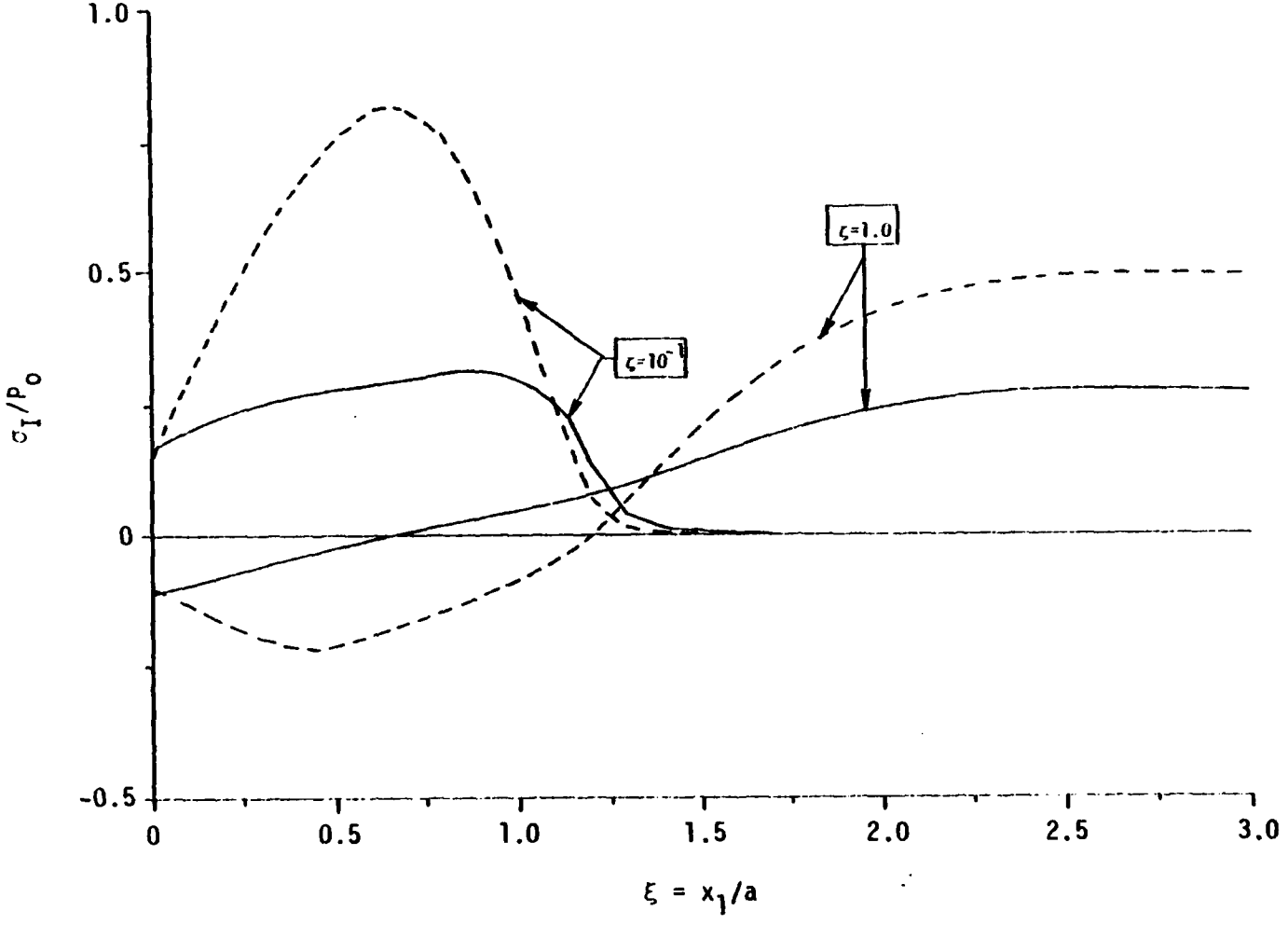

Figure 2.8. Principal stress fields.

compressive state of the thermal stress in the surface layer (Figure 2.7) is at a much higher level than that from the mechanical loading (Figure 2.5). However, the combined stress field does become tensile at a small depth and reaches the maximum principal stress at approximately a depth of one-twentieth of the asperity size. According to Figure 2.8, a tensile crack will not occur because $(\sigma_I)_{max}/P_o = 0.82$ is less than one. However, the temperature and the combined stress field strongly depend on the asperity size and the other parameters mentioned before. The details on the study of parameter effects will be given in Chapter 5. For the purpose of illustration, the maximum principal stress field for a typical asperity size of 1 mm (0.04 in.) is also obtained. These results are compared with the results obtained with an asperity size of 0.5 mm (0.02 in.) in Figure 2.9. At a pressure of 482 MPa (70,000 psi), the maximum principal stress reaches the ultimate tensile strength. The distributive friction force of 241 MPa (35,000 psi), using a coefficient of friction $\mu_f = 0.5$, is well below the ultimate shearing strength. Therefore, the crack could initiate at a depth of 0.05 mm (0.002 in.) from the surface for a typical asperity size of 1 mm (0.04 in.).

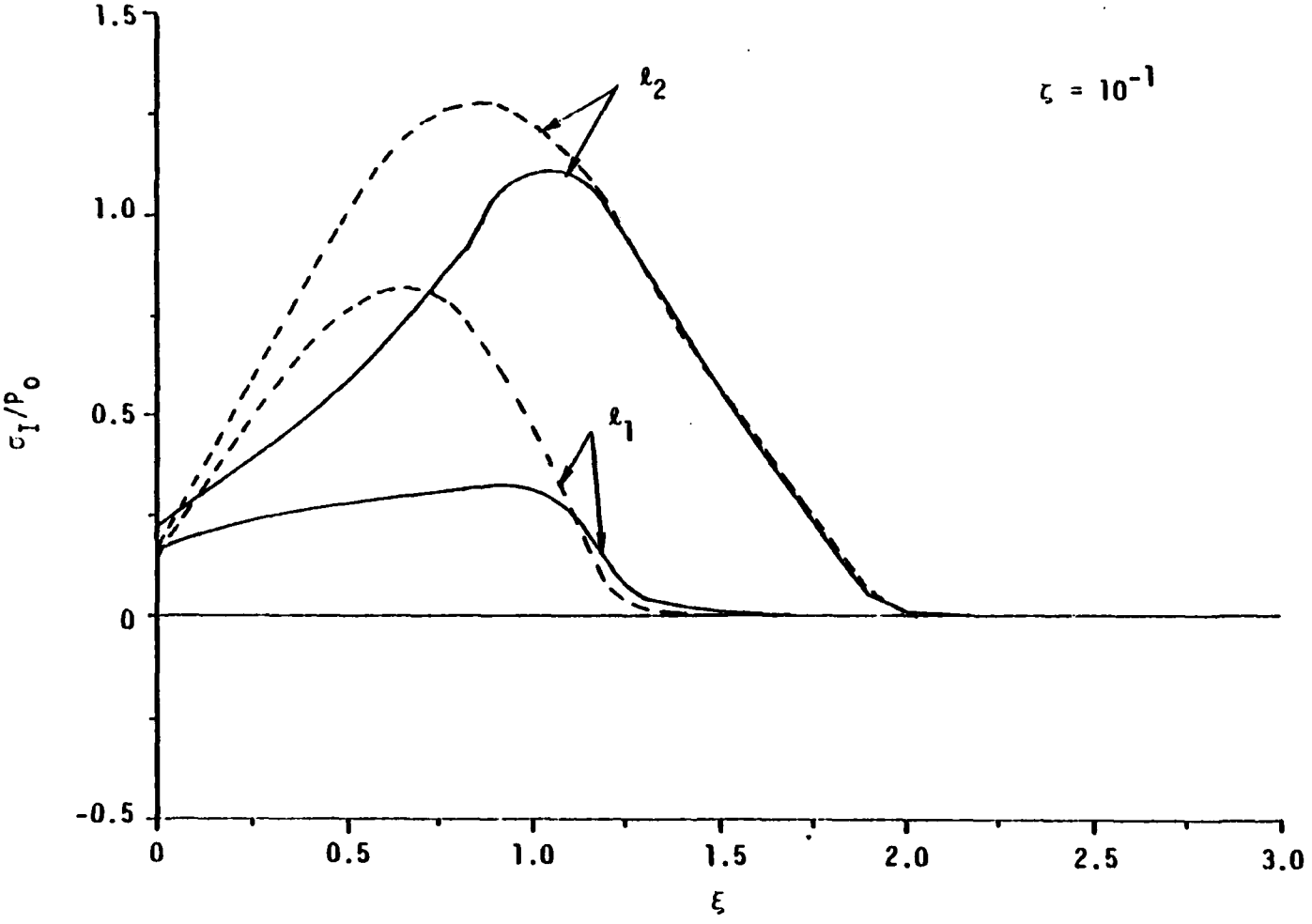

Figure 2.9. Principal stress fields for different half widths (ℓ_1 = 0.25 mm (0.01 in.), ℓ_2 = 0.5 mm (0.02 in.)).

CHAPTER 3

A THREE-DIMENSIONAL MODEL OF A SINGLE MOVING ASPERITY

3.1 Mathematical Model

In order to model a hot spot with a contact area that represents better the actual case and to investigate the three-dimensional effect, the three-dimensional problem of a single asperity moving with uniform velocity over the surface of a half space is presented in this chapter. The results can be used to compare with the two-dimensional results obtained previously. This half space representation of the seal is based on the same reasoning concerning the relative size between the seal material and the moving asperity as used in the two-dimensional analysis. The asperity contacts with the material on the otherwise traction-free surface in a small rectangular or circular region. The coordinates $\{x_i\}$ are fixed to the moving asperity such that x_1 points toward the trailing direction of the motion, x_2 is perpendicular to the traversing direction, and x_3 is a depth measure pointing from the surface into the material, Figure 3.1. For the rectangular contact area, the aspect ratio, $t = b/a$, is a significant parameter for the three-dimensional effect. For large aspect ratio, the asperity excitation is effectively a moving line load that was presented as a two-dimensional plane strain solution in Chapter 2.

In the three-dimensional formulation the potential theory approach in Chapter 2 is no longer applicable. Hence, the Fourier transform method (Appendix I) is used throughout in analyzing the mechanical and the thermal stress fields as well as the temperature field. The latter

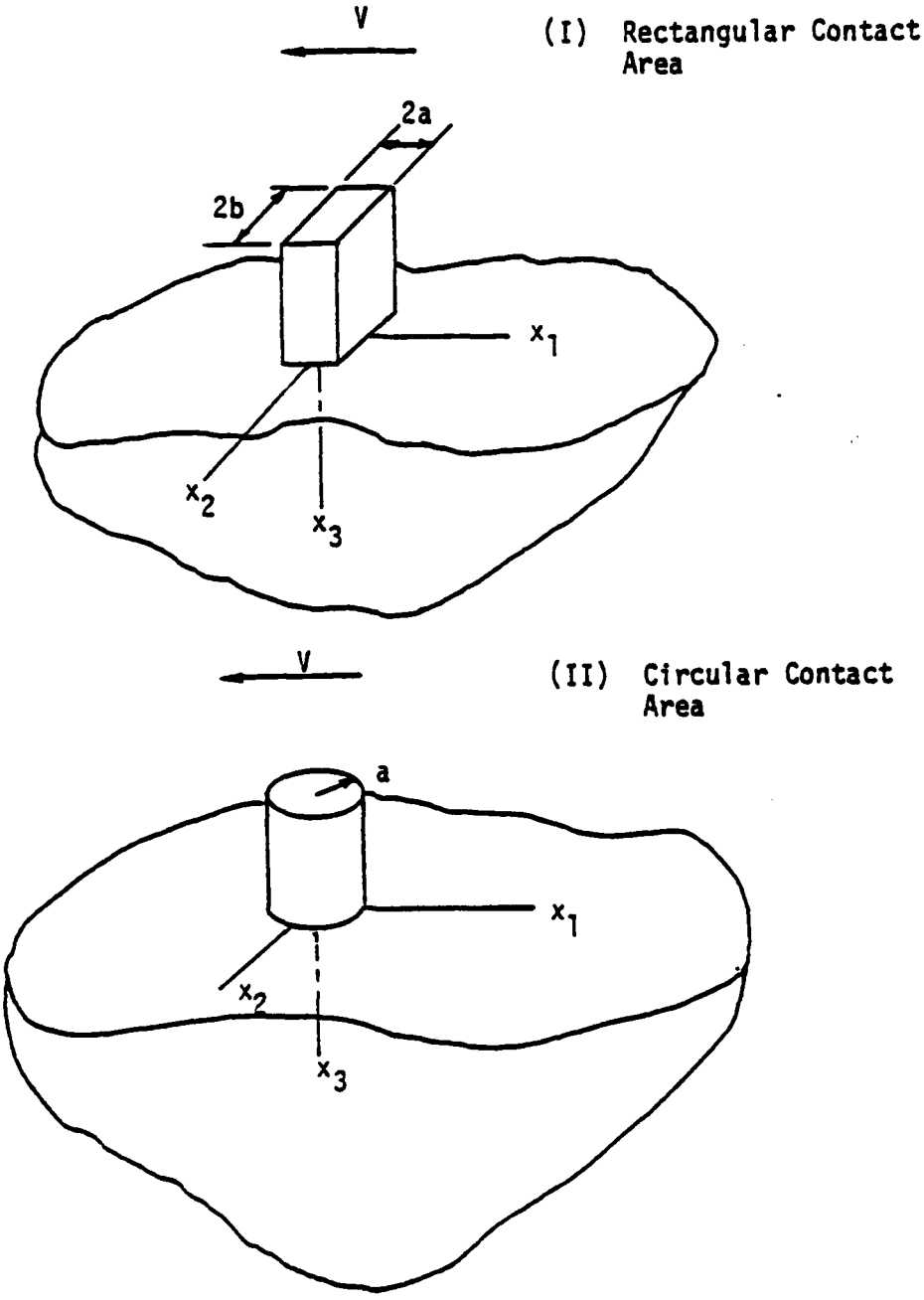

Figure 3.1. Moving asperities.

is also analytically checked with the Green's function approach. Because of the complexity, the general solutions given in Sections 2, 3, and 4 for the mechanical, the temperature, and the thermal stress fields respectively are left in the transformed space. The numerical solutions in Section 5 apply specifically to three cases: a moving rectangular contact area with uniform pressure (Case 1), a moving disk with uniform (Case 2), or nonuniform (Case 3) pressure. In the inverse Fourier transform the multiple integrals for the mechanical stress field are reduced to single finite integrals which are more suitable for numerical computation. However, the temperature and the thermal stress fields are quite complex and remain in the form of multiple integrals, for which numerical evaluations are obtained using a Simpson adaptive scheme in conjunction with a Gaussian-type quadrature (Appendix II). This numerical scheme is proven to be effective since it checks with the numerical result for the temperature field obtained from the Green's function method from which the resultant integrals are much easier to evaluate numerically.

3.2 Mechanical Stress Field

Basic Governing Equations. The governing equations come from Cauchy's law and Hooke's law. In terms of the moving convective coordinates $\{x_i\}$ and with the absence of body forces, the acceleration in Cauchy's law will have only convective terms. They are:

$$\partial_j \sigma^M_{ij} = \rho V^2 \partial_{11} u_i \ , \qquad (3.1)^4$$

[4]Summation convention is used for repeated indices of roman minuscules.

$$\sigma^M_{ij} = \lambda \partial_k u_k \delta_{ij} + \mu(\partial_i u_j + \partial_j u_i) \ , \qquad i,j,k = 1,2,3 \tag{3.2}$$

where u_i is the displacement field, σ^M_{ij} is the mechanical stress field, ∂_j denotes partial derivative with respect to x_j, δ_{ij} is the Kronecker delta, V is the asperity traverse speed and ρ, λ, and μ are material constants. The method used to solve the equations above is similar to the one used by Eason [21].

Equations (3.1) and (3.2) are conveniently solved by the method of double Fourier transform with respect to (x_1, x_2)

$$\bar{f}(\bar{x}_1,\bar{x}_2,x_3) = \frac{1}{2\pi} \int_{-\infty}^{\infty} \int_{-\infty}^{\infty} f(x_1,x_2,x_3)\, e^{i(\bar{x}_1 x_1 + \bar{x}_2 x_2)}\, dx_1\, dx_2 \ . \tag{3.3}$$

With the use of the relation

$$\overline{\partial_r^n f} = (-i\,\bar{x}_r)^n\, \bar{f} \ , \quad r = 1,2 \ ,$$

Equations (3.1) and (3.2) become

$$-i\bar{x}_r\, \bar{\sigma}^M_{jr} + D\, \bar{\sigma}^M_{j3} = -\rho V^2\, \bar{x}_1^2\, \bar{u}_j \ , \qquad j = 1,2,3 \ ; \ r = 1,2 \ , \tag{3.4}$$

and

$$\bar{\sigma}^M_{rs} = -i\lambda\, \bar{x}_k \bar{u}_k \delta_{rs} - i\mu(\bar{x}_r \bar{u}_s + \bar{x}_s \bar{u}_r) + \lambda D\bar{u}_3 \delta_{rs}$$

$$\bar{\sigma}^M_{3r} = -i\mu \bar{x}_r \bar{u}_3 + \mu D\bar{u}_r \qquad k,r,s = 1,2 \ ,$$

$$\bar{\sigma}^M_{33} = -i\lambda \bar{x}_k \bar{u}_k + (\lambda + 2\mu)\, D\bar{u}_3 \tag{3.5}$$

subject to the boundary conditions

$$\bar{\sigma}_{3i}^{M} = -\bar{R}_i \quad \text{at} \quad x_3 = 0 \tag{3.6}$$

and

$$\bar{u}_i \to 0 \quad \text{as} \quad x_3 \to \infty , \tag{3.7}$$

where the transformed quantities are denoted by a superposed ($\bar{}$). R_i is the traction on the surface $x_3 = 0$, D denotes derivative with respect to x_3 and the index i = 1,2,3.

Displacement and Stress Fields. The solution of the set of ordinary differential equations (3.4) and (3.5) is obtained by combining Equations (3.4) and (3.5) with the result

$$\begin{aligned}
&[D^2 + (M_2^2 - \beta^2)\,\bar{x}_1^2 - \bar{x}_2^2]\,\bar{u}_1 - \bar{x}_1\bar{x}_2(\beta^2 - 1)\,\bar{u}_2 - i\bar{x}_1(\beta^2 - 1)\,D\bar{u}_3 = 0 \\
&-\bar{x}_1\bar{x}_2(\beta^2 - 1)\,\bar{u}_1 + [D^2 + (M_2^2 - 1)\,\bar{x}_1^2 - \beta^2\bar{x}_2^2]\,\bar{u}_2 - i\bar{x}_2(\beta^2 - 1)\,D\bar{u}_3 = 0 \\
&-i\bar{x}_1(\beta^2 - 1)\,D\bar{u}_1 - i\bar{x}_2(\beta^2 - 1)\,D\bar{u}_2 + [\beta^2 D^2 + (M_2^2 - 1)\,\bar{x}_1^2 - \bar{x}_2^2]\,\bar{u}_3 = 0
\end{aligned} \tag{3.8}$$

in which

$$M_1 = V\left(\frac{\rho}{\lambda + 2\mu}\right)^{1/2} ; \qquad M_2 = V\left(\frac{\rho}{\mu}\right)^{1/2} ; \qquad \beta^2 = (\lambda + 2\mu)/\mu .$$

Equation (3.8) is a system of three simultaneous homogeneous linear

equations for three unknowns $\{\bar{u}_i\}$. For nontrivial solutions the determinant of coefficients should be zero identically, that is

$$\Delta = \begin{vmatrix} D^2 + (M_2^2-\beta^2)\,\bar{x}_1^2 - \bar{x}_2^2 & -\bar{x}_1\bar{x}_2(\beta^2-1) & -i\bar{x}_1(\beta^2-1)\,D \\ -\bar{x}_1\bar{x}_2(\beta^2-1) & D^2 + (M_2^2-1)\,\bar{x}_1^2 - \beta^2\,\bar{x}_2^2 & -i\bar{x}_2(\beta^2-1)\,D \\ -i\bar{x}_1(\beta^2-1)\,D & -i\bar{x}_2(\beta^2-1)\,D & \beta^2 D^2 + (M_2^2-1)\,\bar{x}_1^2 - \bar{x}_2^2 \end{vmatrix}$$

$$= \beta^2(D^2 - n_1^2)\,(D^2 - n_2^2)^2 = 0 \ ,$$

where the distorted distances are

$$n_r = (\bar{x}_1^2 + \bar{x}_2^2 - M_r^2\bar{x}_1^2)^{1/2} \ , \quad r = 1,2 \ .$$

Hence, Equation (3.8) results in

$$(D^2 - n_1^2)\,(D^2 - n_2^2)^2\,(\bar{u}_1, \bar{u}_2, \bar{u}_3) = 0 \qquad (3.9)$$

whose solutions, with the consideration of the regularity condition (3.7), are

$$\bar{u}_1 = A_1 e^{-n_1 x_3} + (B_1 + C_1 x_3)\, e^{-n_2 x_3} \ ,$$

$$\bar{u}_2 = A_2 e^{-n_1 x_3} + (B_2 + C_2 x_3)\, e^{-n_2 x_3} \ ,$$

$$\bar{u}_3 = A_3 e^{-n_1 x_3} + (B_3 + C_3 x_3)\, e^{-n_2 x_3} \ , \qquad (3.10)$$

where the coefficients $\{A_i, B_i, C_i,\}$ are independent of x_3.

Substituting Equations (3.10) into (3.8) gives certain relations between these quantities as follows:

$$A_r = \frac{i\bar{x}_r}{n_1} A_3 , \quad r = 1,2 ,$$

$$B_3 = -i\left(\frac{\bar{x}_1 B_1 + \bar{x}_2 B_2}{n_2}\right) ,$$

and

$$C_j = 0 , \quad j = 1,2,3 .$$

A_3, B_1, and B_2 are to be determined by the surface traction conditions. Thus, Equation (3.10) can be rewritten as

$$\bar{u}_1 = \frac{i\bar{x}_1 A_3}{n_1} e^{-n_1 x_3} + B_1 e^{-n_2 x_3} ,$$

$$\bar{u}_2 = \frac{i\bar{x}_2 A_3}{n_1} e^{-n_1 x_3} + B_2 e^{-n_2 x_3} ,$$

$$\bar{u}_3 = A_3 e^{-n_1 x_3} - \frac{i}{n_2} (\bar{x}_1 B_1 + \bar{x}_2 B_2) e^{-n_2 x_3} . \qquad (3.11)$$

Expressions for the transformed stress components may be obtained by the substitution of Equations (3.11) into (3.5). In particular

$$\bar{\sigma}_{33} = \frac{\lambda M_1^2 \bar{x}_1^2 - 2\mu n_1^2}{n_1} A_3 e^{-n_1 x_3} + i2\mu(\bar{x}_1 B_1 + \bar{x}_2 B_2) e^{-n_2 x_3} ,$$

$$\bar{\sigma}_{32} = -i2\mu\bar{x}_2 A_3 e^{-n_1 x_3} - \frac{\mu}{n_2} [\bar{x}_1 \bar{x}_2 B_1 + (n_2^2 + \bar{x}_2^2) B_2] e^{-n_2 x_3} ,$$

$$\bar{\sigma}_{31} = -i2\mu\bar{x}_1 A_3 e^{-n_1 x_3} - \frac{\mu}{n_2} [(n_2^2 + \bar{x}_1^2) B_1 + \bar{x}_1 \bar{x}_2 B_2] e^{-n_2 x_3} . \qquad (3.12)$$

In view of the boundary condition (3.6), A_3 and B_1, B_2 can be readily solved and expressed in terms of $\bar{R}_i$.

$$2\mu F A_3 = n_1[(\bar{x}_1^2 + \bar{x}_2^2 - \tfrac{1}{2} M_2^2 \bar{x}_1^2)\,\bar{R}_3 + i n_2(\bar{x}_1 \bar{R}_1 + \bar{x}_2 \bar{R}_2)] ,$$

$$2\mu F B_1 = -i\bar{x}_1 n_1 n_2 \bar{R}_3 + \frac{1}{n_2}\{[\bar{x}_2^2(\bar{x}_1^2 + \bar{x}_2^2 - \tfrac{1}{2} M_2^2 \bar{x}_1^2 - 2n_1 n_2) + n_2^2(\bar{x}_1^2 + \bar{x}_2^2 - \tfrac{1}{2} M_2^2 \bar{x}_1^2)]\,\bar{R}_1 - \bar{x}_1 \bar{x}_2(\bar{x}_1^2 + \bar{x}_2^2 - \tfrac{1}{2} M_2^2 \bar{x}_1^2 - 2n_1 n_2)\,\bar{R}_2\} ,$$

$$2\mu F B_2 = -i\bar{x}_2 n_1 n_2 \bar{R}_3 + \frac{1}{n_2}\{-\bar{x}_1 \bar{x}_2(\bar{x}_1^2 + \bar{x}_2^2 - \tfrac{1}{2} M_2^2 \bar{x}_1^2 - 2n_1 n_2)\,\bar{R}_1 + [\bar{x}_1^2(\bar{x}_1^2 + \bar{x}_2^2 - \tfrac{1}{2} M_2^2 \bar{x}_1^2 - 2n_1 n_2) + n_2^2(\bar{x}_1^2 + \bar{x}_2^2 - \tfrac{1}{2} M_2^2 \bar{x}_1^2)]\,\bar{R}_2\} . \tag{3.13}$$

Following the substitution of Equations (3.13) into (3.11)

$$2\mu F\,\bar{u}_1 = (i\bar{x}_1 n_3 \bar{R}_3 - \bar{x}_1^2 n_2 \bar{R}_1 - \bar{x}_1 \bar{x}_2 n_2 \bar{R}_2)\, e^{-n_1 x_3} - \left\{ i\bar{x}_1 n_1 n_2 \bar{R}_3 - \left[\frac{\bar{x}_2^2}{n_2}(n_3 - 2n_1 n_2) + n_2 n_3\right]\bar{R}_1 + \frac{\bar{x}_1 \bar{x}_2}{n_2}(n_3 - 2n_1 n_2)\,\bar{R}_2 \right\} e^{-n_2 x_3} ,$$

$$2\mu F\,\bar{u}_2 = (i\bar{x}_2 n_3 \bar{R}_3 - \bar{x}_1 \bar{x}_2 n_2 \bar{R}_1 - \bar{x}_2^2 n_2 \bar{R}_2)\, e^{-n_1 x_3} - \left\{ i\bar{x}_2 n_1 n_2 \bar{R}_3 + \frac{\bar{x}_1 \bar{x}_2}{n_2}(n_3 - 2n_1 n_2)\,\bar{R}_1 - \left[\frac{\bar{x}_1^2}{n_2}(n_3 - 2n_1 n_2) + n_2 n_3\right]\bar{R}_2 \right\} e^{-n_2 x_3} ,$$

$$2\mu F\,\bar{u}_3 = (n_1 n_3 \bar{R}_3 + i\bar{x}_1 n_1 n_2 \bar{R}_1 + i\bar{x}_2 n_1 n_2 \bar{R}_2)\, e^{-n_1 x_3}$$

$$- [n_1(\bar{x}_1^2 + \bar{x}_2^2)\,\bar{R}_3 + i\bar{x}_1 n_3 \bar{R}_1 + i\bar{x}_2 n_3 \bar{R}_2]\, e^{-n_2 x_3}\,, \qquad (3.14)$$

where

$$n_3 = \bar{x}_1^2 + \bar{x}_2^2 - \tfrac{1}{2} M_2^2\, \bar{x}_1^2\,, \qquad F = n_3^2 - n_1 n_2(\bar{x}_1^2 + \bar{x}_2^2)\,.$$

Stress components can then be determined by the substitution of (3.14) into (3.5) in accordance with the new variables as follows:

$$N_1 = n_3 - 2n_1 n_2\,; \qquad N_2 = N_1/n_2\,; \qquad \bar{B} = n_3 \bar{R}_3 + i n_2(\bar{x}_1 \bar{R}_1 + \bar{x}_2 \bar{R}_2)\,.$$

Thus we have

$$2\mu F\,\bar{\sigma}_{11}^{M} = \bar{B}\,[(\bar{x}_1^2 + \bar{x}_2^2 - n_1^2)\,\lambda + 2\,\bar{x}_1^2]\, e^{-n_1 x_3} - 2\,\{\bar{x}_1^2 n_1 n_2 \bar{R}_3$$

$$+ i\bar{x}_1[\bar{x}_2^2 N_2 + n_2 n_3]\,\bar{R}_1 - i\bar{x}_1^2 \bar{x}_2 N_2 \bar{R}_2\}\, e^{-n_2 x_3}\,,$$

$$2\mu F\,\bar{\sigma}_{22}^{M} = \bar{B}\,[(\bar{x}_1^2 + \bar{x}_2^2 - n_1^2)\,\lambda + 2\mu\bar{x}_2^2]\, e^{-n_1 x_3} - 2\mu\{\bar{x}_2^2 n_1 n_2 \bar{R}_3$$

$$- i\bar{x}_1 \bar{x}_2^2 N_2 \bar{R}_1 + i\bar{x}_2[\bar{x}_1^2 N_2 + n_2 n_3]\,\bar{R}_2\}\, e^{-n_2 x_3}\,,$$

$$2\mu F\,\bar{\sigma}_{33}^{M} = \bar{B}[(\bar{x}_1^2 + \bar{x}_2^2 - n_1^2)\,\lambda - 2\mu n_1^2]\, e^{-n_1 x_3}$$

$$+ 2\mu n_2[(\bar{x}_1^2 + \bar{x}_2^2)\, n_1 \bar{R}_3 + i n_3(\bar{x}_1 \bar{R}_1 + \bar{x}_2 \bar{R}_2)]\, e^{-n_2 x_3}\,,$$

$$2\mu F\,\bar{\sigma}^{M}_{12} = 2\mu\bar{x}_1\bar{x}_2\bar{B}\,e^{-n_1x_3} - 2\mu\{\bar{x}_1\bar{x}_2n_1n_2\bar{R}_3 + \frac{i}{2}\,\bar{x}_2[n_2n_3 - (\bar{x}_1^2 - \bar{x}_2^2)\,N_2]\,\bar{R}_1 + \frac{i}{2}\,\bar{x}_1[n_2n_3 + (\bar{x}_1^2 - \bar{x}_2^2)\,N_2]\,\bar{R}_2\}\,e^{-n_2x_3}\,,$$

$$2\mu F\,\bar{\sigma}^{M}_{23} = -2\mu i\bar{x}_2n_1\bar{B}\,e^{-n_1x_3} + \mu\{i\bar{x}_2n_1(\bar{x}_1^2 + \bar{x}_2^2 + n_2^2)\,\bar{R}_3 - 2\bar{x}_1\bar{x}_2n_1n_2\bar{R}_1 - [\bar{x}_1^2N_1 + n_3(n_2^2 + \bar{x}_2^2)]\,\bar{R}_2\}\,e^{-n_2x_3}\,,$$

$$2\mu F\,\bar{\sigma}^{M}_{31} = -2\mu i\bar{x}_1n_1\bar{B}\,e^{-n_1x_3} + \mu\{i\bar{x}_1n_1(\bar{x}_1^2 + \bar{x}_2^2 + n_2^2)\,\bar{R}_3 - [\bar{x}_2^2N_1 + n_3(n_2^2 + \bar{x}_1^2)]\,\bar{R}_1 - 2\bar{x}_1\bar{x}_2n_1n_2R_2\}\,e^{-n_2x_3}\,. \qquad (3.15)$$

The general solutions of displacement and stress fields are left in the Fourier transformed expressions (3.14) and (3.15). The actual fields are to be obtained through an inverse transform after the substitution of the specific boundary values $\{\bar{R}_i\}$.

3.3 Temperature Field

The heat equation with constant thermal properties, assuming quasi-steady state and no heat generation in the medium, as expressed in terms of the convective coordinates $\{x_i\}$, is

$$\partial_{jj}T = \frac{V}{\kappa}\,\partial_1T \qquad (3.16)$$

where κ is the thermal diffusivity.

The boundary conditions at $x_3 = 0$, are

$$k\partial_3 T = \begin{cases} -q(x_1, x_2) , & \text{in the contact region} \\ 0 , & \text{elsewhere} \end{cases} \tag{3.17}$$

$$T, \partial_i T \to 0 \quad \text{as} \quad (x_i x_i)^{1/2} \to \infty . \tag{3.18}$$

Note that T is the temperature above the stress-free ambient, k is the thermal conductivity, q is the heat flux ($-R_1 V = \mu_f p V$), where μ_f is Coulomb coefficient and p is normal pressure distribution on the surface $x_3 = 0$. It is assumed that the mating seal which contains the asperity is an insulator.

The double Fourier transform of Equations (3.16) through (3.18) become, respectively,

$$[D^2 - (s^2 + in)] \bar{T} = 0 , \tag{3.19}$$

$$kD\bar{T} = \bar{Q} = \begin{cases} -\bar{q}(\bar{x}_1, \bar{x}_2) , & \text{in the contact region} \\ 0 , & \text{elsewhere} \end{cases} \tag{3.20}$$

$$\bar{T} \to 0 \quad \text{as} \quad x_3 \to \infty , \tag{3.21}$$

where $s^2 = \bar{x}_1^2 + \bar{x}_2^2$ and $n = -(V/\kappa)\, \bar{x}_1$. Now let $\bar{T} = \bar{T}_1 + i\bar{T}_2$ and $\bar{Q}/k = \bar{P}_1 + i\bar{P}_2$, then Equations (3.19) and (3.20) result in

$$(D^2 - s^2)\, \bar{T}_1 = -n\bar{T}_2 ,$$

$$(D^2 - s^2)\,\bar{T}_2 = n\bar{T}_1 \tag{3.22}$$

and

$$D\bar{T}_1 = \bar{P}_1 ,$$

$$D\bar{T}_2 = \bar{P}_2 \quad \text{at} \quad x_3 = 0 . \tag{3.23}$$

Also, (3.21) becomes

$$\bar{T}_1,\ \bar{T}_2 \to 0 \quad \text{as} \quad x_3 \to \infty . \tag{3.24}$$

Equation (3.22) can be expressed as a fourth-order homogeneous ordinary differential equation which is

$$[D^4 - 2s^2D^2 + (n^2 + s^4)]\,\bar{T}_r = 0 , \quad r = 1,2 . \tag{3.25}$$

In view of the regularity condition (3.24), the solution of Equation (3.25) has the form

$$\bar{T}_r = e^{-\omega x_3}[A_r \cos(\theta x_3) + B_r \sin(\theta x_3)] \tag{3.26}$$

where

$$\theta = \left[\frac{(s^4 + n^2)^{1/2} - s^2}{2}\right]^{1/2} ,$$

$$\omega = \left[\frac{(s^4 + n^2)^{1/2} + s^2}{2}\right]^{1/2} .$$

Substituting (3.26) into (3.22) and (3.23) gives

$$\bar{P}_r = -\omega A_r + \theta B_r , \quad r = 1,2 \tag{3.27}$$

and

$$A_1 = -\frac{n}{2\omega\theta} B_2 , \tag{3.28}$$

$$B_1 = \frac{n}{2\omega\theta} A_2 . \tag{3.29}$$

Hence, we have four equations for four unknowns A_1, A_2, B_1 and B_2, which can be readily solved.

$$A_1 = -\frac{2\omega^2\bar{P}_1 + n\bar{P}_2}{2\omega(\omega^2 + \theta^2)} ,$$

$$A_2 = \frac{n\bar{P}_1 - 2\omega^2\bar{P}_2}{2\omega(\omega^2 + \theta^2)} ,$$

$$B_1 = \frac{2\theta^2\bar{P}_1 - n\bar{P}_2}{2\theta(\omega^2 + \theta^2)} ,$$

$$B_2 = \frac{n\bar{P}_1 + 2\theta^2\bar{P}_2}{2\theta(\omega^2 + \theta^2)} . \tag{3.30}$$

Following the substitution of the expression (3.30) into (3.26) and according to $\bar{T} = \bar{T}_1 + i\bar{T}_2$, we obtain $\bar{T}$ as

$$\bar{T} = e^{-\omega x_3} \{[C_1 \cos(\theta x_3) + C_2 \sin(\theta x_3)] \bar{P}_1 + [C_3 \cos(\theta x_3) + C_4 \sin(\theta x_3)] \bar{P}_2\} , \tag{3.31}$$

where

$$C_1 = \frac{-2\omega^2 + in}{2\omega(\omega^2 + \theta^2)} ,$$

$$C_2 = \frac{2\theta^2 + in}{2\theta(\omega^2 + \theta^2)} ,$$

$$C_3 = \frac{-n - i2\omega^2}{2\omega(\omega^2 + \theta^2)} ,$$

$$C_4 = \frac{-n + i2\theta^2}{2\theta(\omega^2 + \theta^2)} .$$

Again, the temperature field is left in the Fourier transformed expression, which will be used in solving the thermal stress field. To be complete and also for comparison, the Green's function solution approach for the temperature field is given in the following.

The Green's function solution, following Carslaw and Jaeger [47], can be expressed as

$$g(x_1 - x_1', x_2 - x_2', x_3, t - t') = \frac{1}{4\rho c[\pi\kappa(t - t')]^{3/2}}$$

$$\cdot \exp\left\{ - \frac{[(x_1 - x_1') - V(t - t')]^2 + (x_2 - x_2')^2 + x_3^2}{4\kappa(t - t')} \right\} \quad (3.32)$$

which is the temperature at time t at the location (x_1, x_2, x_3) due to the unit heat flux input emitted at time t' at the location $(x_1', x_2', 0)$. It can be easily shown that Equation (3.32) satisfies the governing heat equation (3.16).

The temperature field can be obtained by the convolution integral as

$$T(x_1,x_2,x_3,t) = \int_{B_H} q(x_1',x_2')\, K_o(x_1 - x_1',\ x_2 - x_2',\ x_3,\ t - t')\, dx_1'\, dx_2' \tag{3.33}$$

where B_H indicates the heat-flux input region and

$$K_o = \int_o^t g(x_1 - x_1',\ x_2 - x_2',\ x_3,\ t - t')\, dt' \ . \tag{3.34}$$

After substituting (3.32) into (3.34) and changing the variable by letting $\tau = R/2\sqrt{\kappa(t - t')}$, K_o becomes

$$K_o = \frac{e^{V(x_1 - x_1')/2\kappa}}{\pi^{3/2}\, kR} \int_{R/2\sqrt{\kappa t}}^{\infty} e^{-\tau^2 - (V^2R^2/16\kappa^2\tau^2)}\, d\tau \tag{3.35}$$

where ρ = density

c = specific heat

$k = \rho c \kappa$

$R = [(x_1 - x_1')^2 + (x_2 - x_2')^2 + x_3^2]^{1/2}$.

For the steady-state solution, i.e., $t \to \infty$, Equation (3.35) results in

$$G(x_1 - x_1',\ x_2 - x_2',\ x_3) = \lim_{t \to \infty} K_o$$

$$= \frac{1}{2\pi kR}\, e^{-V[R - (x_1 - x_1')]/2\kappa} \ . \tag{3.36}$$

Accordingly, the steady-state temperature field can be obtained as

$$T(x_1,x_2,x_3) = \frac{1}{2\pi k} \int_{B_H} q(x_1',x_2') \frac{e^{-V[R-(x_1-x_1')]/2\kappa}}{R} \, dx_1' \, dx_2' \qquad (3.37)$$

which will be employed to give numerical results for different cases of application.

3.4 Thermal Stress Field

The governing equations for the thermal stress solutions are based on the theory of quasi-static uncoupled thermoelasticity. The governing equations are then

$$\mu\nabla^2 u_j + (\lambda + \mu)\, \partial_j(\partial_k u_k) = (3\lambda + 2\mu)\, \alpha \partial_j T \qquad (3.38)$$

and

$$\sigma_{ij}^T = \lambda \partial_k u_k \delta_{ij} + \mu(\partial_j u_i + \partial_i u_j) - (3\lambda + 2\mu)\, \alpha T \delta_{ij} \qquad (3.39)$$

subject to the boundary conditions

$$\sigma_{3i}^T = 0 , \qquad i = 1,2,3 \quad \text{at} \quad x_3 = 0 , \qquad (3.40)$$

$$\sigma_{ij}^T , \; u_i \to 0 \quad \text{as} \quad (x_i x_i)^{1/2} \to \infty . \qquad (3.41)$$

The double Fourier transform of Equations (3.38) through (3.41) are

$$[D^2 - (a_1\bar{x}_1^2 + \bar{x}_2^2)]\, \bar{u}_1 - a_2\bar{x}_1\bar{x}_2\bar{u}_2 - ia_2\bar{x}_1 D\bar{u}_3 = -ia_3\bar{x}_1\bar{T} , \qquad (3.42)$$

$$- a_2\bar{x}_1\bar{x}_2\bar{u}_1 + [D^2 - (a_1\bar{x}_2^2 + \bar{x}_1^2)]\, \bar{u}_2 - ia_2\bar{x}_2 D\bar{u}_3 = -ia_3\bar{x}_2\bar{T} , \qquad (3.43)$$

$$- ia_2\bar{x}_1 D\bar{u}_1 - ia_2\bar{x}_2 D\bar{u}_2 + (a_1 D^2 - s^2)\,\bar{u}_3 = a_3 D\bar{T}\,, \tag{3.44}$$

$$\frac{\bar{\sigma}_{11}^{T}}{\mu} = -i(a_1\bar{x}_1\bar{u}_1 + a_4\bar{x}_2\bar{u}_2) + a_4 D\bar{u}_3 - a_3\bar{T}\,, \tag{3.45}$$

$$\frac{\bar{\sigma}_{22}^{T}}{\mu} = -i(a_4\bar{x}_1\bar{u}_1 + a_1\bar{x}_2\bar{u}_2) + a_4 D\bar{u}_3 - a_3\bar{T}\,, \tag{3.46}$$

$$\frac{\bar{\sigma}_{33}^{T}}{\mu} = -ia_4(\bar{x}_1\bar{u}_1 + \bar{x}_2\bar{u}_2) + a_1 D\bar{u}_3 - a_3\bar{T}\,, \tag{3.47}$$

$$\frac{\bar{\sigma}_{12}^{T}}{\mu} = -i(\bar{x}_2\bar{u}_1 + \bar{x}_1\bar{u}_2)\,, \tag{3.48}$$

$$\frac{\bar{\sigma}_{23}^{T}}{\mu} = D\bar{u}_2 - i\bar{x}_2\bar{u}_3\,, \tag{3.49}$$

$$\frac{\bar{\sigma}_{31}^{T}}{\mu} = D\bar{u}_1 - i\bar{x}_1\bar{u}_3\,, \tag{3.50}$$

$$\bar{\sigma}_{3i}^{T} = 0\,, \qquad i = 1,2,3 \quad \text{at} \quad x_3 = 0\,, \tag{3.51}$$

$$\bar{\sigma}_{ij}^{T}\,, \qquad \bar{u}_i \to 0 \quad \text{as} \quad (\bar{x}_i\bar{x}_i)^{1/2} \to \infty\,, \tag{3.52}$$

where $a_4 = \lambda/\mu$, $a_1 = a_4 + 2$, $a_2 = a_4 + 1$ and $a_3 = (3a_4 + 2)\,\alpha$.

Having a known temperature expression as in Equation (3.31), we may choose the solution for the displacement components $\bar{u}_1$ and $\bar{u}_2$ in the form

$$\bar{u}_1 = f(x_3)\, e^{-\omega x_3} ,$$

$$\bar{u}_2 = g(x_3)\, e^{-\omega x_3} \tag{3.53}$$

where functions f and g are to be determined later by combining Equation (3.43) and Equation (3.42) which results in

$$(D^2 - s^2)(\bar{x}_2\bar{u}_1 - \bar{x}_1\bar{u}_2) = 0 .$$

Considering Equation (3.53), it follows that

$$f = \frac{\bar{x}_1}{\bar{x}_2}\, g . \tag{3.54}$$

Equation (3.42) can be rewritten as

$$D\bar{u}_3 = \frac{i}{a_2\bar{x}_1}\left[-ia_3\bar{x}_1\bar{T} + (a_1\bar{x}_1^2 + \bar{x}_2^2)\,\bar{u}_1 - D^2\bar{u}_1 + a_2\bar{x}_1\bar{x}_2\bar{u}_2\right] . \tag{3.55}$$

In view of $D^2\bar{u}_3$ obtained by taking the differentiation of Equation (3.55) with respect to x_3, it follows from Equation (3.44) that

$$\bar{u}_3 = \frac{i}{a_2\bar{x}_1 s^2}\left[-a_1D^3\bar{u}_1 + (a_1s^2 + a_2\bar{x}_1^2)\,D\bar{u}_1 + a_2\bar{x}_1\bar{x}_2D\bar{u}_2 - ia_3\bar{x}_1D\bar{T}\right] . \tag{3.56}$$

Differentiating $\bar{u}_3$ with respect to x_3 and then equating the result with Equation (3.55), the ODE governing the displacement field becomes

$$-a_1D^4\bar{u}_1 + (a_1^2\bar{x}_1^2 + s^2 + a_1\bar{x}_2^2 - a_2\bar{x}_1^2)\,D^2\bar{u}_1 - s^2(a_1\bar{x}_1^2 + \bar{x}_2^2)\,\bar{u}_1$$

$$+ a_2\bar{x}_1\bar{x}_2D^2\bar{u}_2 - a_2s^2\bar{x}_1\bar{x}_2\bar{u}_2 = ia_3\bar{x}_1(D^2 - s^2)\,\bar{T} . \tag{3.57}$$

From Equations (3.31), (3.53), and (3.54), Equation (3.57) leads to

$$-D^4g + 4\omega D^3g + 2(s^2 - 3\omega^2)\, D^2g + 4\omega\theta^2 Dg - \theta^4 g$$

$$= \frac{2a_3}{a_1}\bar{x}_2\omega\theta[(B_2 - iB_1)\cos(\theta x_3) + (-A_2 + iA_1)\sin(\theta x_3)] \quad (3.58)$$

where A_1, A_2, B_1, and B_2 are the same as in Equation (3.30).

The complementary solution of Equation (3.58) (g^H) is obtained by solving the corresponding characteristic equation which is

$$-m^4 + 4\omega m^3 + 2(s^2 - 3\omega^2)\, m^2 + 4\omega\theta^2 m + \theta^4 = 0$$

or

$$(m - \omega - s)^2\,(m - \omega + s)^2 = 0\ . \quad (3.59)$$

Taking account of the regularity condition the complementary solution is

$$g^H = (h_1 + h_2 x_3)\, e^{(\omega - s)\, x_3} \quad (3.60)$$

where h_1 and h_2 are contants of integration.

The particular solution of Equation (3.58) (g^P) is determined by the method of undetermined coefficients as follows.

$$g^P = \frac{a_3\bar{x}_2}{2a_1\omega\theta}[G_1\cos(\theta x_3) + H_1\sin(\theta x_3)] \quad (3.61)$$

where $G_1 = B_2 - iB_1$ and $H_1 = -A_2 + iA_1$.

With g^H and g^P known, the particular and homogeneous solutions of $\bar{u}_1$ can be readily obtained

$$\bar{u}_1^c = \frac{\bar{x}_1}{\bar{x}_2}(h_1 + h_2 x_3)\, e^{-sx_3} ,$$

$$\bar{u}_2^c = (h_1 + h_2 x_3)\, e^{-sx_3} ,$$

$$\bar{u}_3^c = -\frac{i}{a_2 \bar{x}_2}[a_2 s(h_1 + h_2 x_3) + (a_2 + 2)\, h_2]\, e^{-sx_3} ,$$

$$\bar{u}_r^p = \frac{a_3 \bar{x}_r}{2a_1 \omega\theta}[G_r \cos(\theta\, x_3) + H_r \sin(\theta\, x_3)]\, e^{-\omega x_3} , \qquad r = 1,2 ,$$

$$\bar{u}_3^p = \frac{a_3}{2a_1 \omega\theta}[G_3 \cos(\theta\, x_3) + H_3 \sin(\theta\, x_3)]\, e^{-\omega x_3} \tag{3.62}$$

where

$$G_1 = G_2 , \qquad H_1 = H_2$$

$$G_3 = -i(\omega G_1 - \theta H_1) , \qquad H_3 = -i(\omega H_1 + \theta G_1) .$$

As a result, the general solutions are

$$\bar{u}_i = \bar{u}_i^p + \bar{u}_i^c . \tag{3.63}$$

The two unknown constants h_1 and h_2 will be determined by substituting Equation (3.63) into Equations (3.47) and (3.49) and employing the boundary condition (3.51). Thus we have

$$h_1 = \frac{a_3\bar{x}_2}{2a_1a_2s^2\omega\theta}\left[a_1s\theta\, H_1 + (s^2 - a_1s\omega + a_1\theta^2)\, G_1\right],$$

$$h_2 = \frac{a_3\bar{x}_2}{2a_1s\omega\theta}\left[-s\theta\, H_1 - (s^2 - s\omega + a_1\theta^2)\, G_1\right]. \qquad (3.64)$$

Following the substitution of the displacement solution, (3.62) through (3.64), into Equations (3.45) through (3.50), the thermal stress field can be readily obtained.

$$\frac{\bar{\sigma}^T_{11}}{\mu} = i\left[(-b_1H_1 + b_2G_1)\, e^{-\omega x_3} + (-b_3H_1 + b_4G_1)\, e^{-sx_3}\right],$$

$$\frac{\bar{\sigma}^T_{22}}{\mu} = i\left[(-b_5H_1 + b_6G_1)\, e^{-\omega x_3} + (-b_7H_1 + b_8G_1)\, e^{-sx_3}\right],$$

$$\frac{\bar{\sigma}^T_{33}}{\mu} = i\left[(-b_9H_1 + b_{10}G_1)\, e^{-\omega x_3} + (b_{11}H_1 - b_{12}G_1)\, e^{-sx_3}\right],$$

$$\frac{\bar{\sigma}^T_{12}}{\mu} = i\bar{x}_1\bar{x}_2\left[(-b_{13}H_1 + b_{14}G_1)\, e^{-\omega x_3} + (-b_{15}H_1 + b_{16}G_1)\, e^{-sx_3}\right],$$

$$\frac{\bar{\sigma}^T_{23}}{\mu} = -\bar{x}_2\left[(b_{17}H_1 - b_{18}G_1)\, e^{-\omega x_3} - (b_{19}H_1 - b_{20}G_1)\, e^{-sx_3}\right],$$

$$\frac{\bar{\sigma}^T_{31}}{\mu} = -\bar{x}_1\left[(b_{17}H_1 - b_{18}G_1)\, e^{-\omega x_3} - (b_{19}H_1 - b_{20}G_1)\, e^{-sx_3}\right], \qquad (3.65)$$

where

$$H_1 = \frac{-(n + i2\omega^2)\,\overline{P}_1 + (2\omega^2 - in)\,\overline{P}_2}{2\omega(\omega^2 + \theta^2)} = i(C_1\overline{P}_1 + C_3\overline{P}_2) ,$$

$$G_1 = \frac{(n - i2\theta^2)\,\overline{P}_1 + (2\theta^2 + in)\,\overline{P}_2}{2\theta(\omega^2 + \theta^2)} = -i(C_2\overline{P}_1 + C_4\overline{P}_2) ,$$

$$b_1 = \frac{-a_3}{a_1\omega\theta}\,[2\omega\theta\,\cos(\theta x_3) - \overline{x}_1^2\,\sin(\theta x_3)] ,$$

$$b_2 = \frac{-a_3}{a_1\omega\theta}\,[\overline{x}_1^2\,\cos(\theta x_3) + 2\omega\theta\,\sin(\theta x_3)] ,$$

$$b_3 = \frac{a_3}{\omega}\left(\frac{\overline{x}_1^2}{a_2 s} + \frac{rs}{a_1 a_2} - \frac{\overline{x}_1^2\,x_3}{a_1}\right),$$

$$b_4 = \frac{a_3}{a_1\omega\theta}\left[\frac{a_1\omega - s}{a_2 s}\,\overline{x}_1^2 + \frac{r(s\omega - s^2)}{a_2} + (s - \omega)\,\overline{x}_1^2\,x_3\right] ,$$

$$b_5 = \frac{-a_3}{a_1\omega\theta}\,[2\omega\theta\,\cos(\theta x_3) - \overline{x}_2^2\,\sin(\theta x_3)] ,$$

$$b_6 = \frac{-a_3}{a_1\omega\theta}\,[\overline{x}_2^2\,\cos(\theta x_3) + 2\omega\theta\,\sin(\theta x_3)] ,$$

$$b_7 = \frac{a_3}{\omega}\left(\frac{\overline{x}_2^2}{a_2 s} + \frac{rs}{a_1 a_2} - \frac{\overline{x}_2^2\,x_3}{a_1}\right),$$

$$b_8 = \frac{a_3}{a_1\omega\theta}\left[\frac{a_1\omega - s}{a_2 s}\,\overline{x}_2^2 + \frac{r(s\omega - s^2)}{a_2} + (s - \omega)\,\overline{x}_2^2\,x_3\right] ,$$

$$b_9 = \frac{-a_3 s^2}{a_1\omega\theta}\,\sin(\theta x_3) ,$$

$$b_{10} = \frac{a_3 s^2}{a_1 \omega\theta} \cos(\theta x_3) ,$$

$$b_{11} = - \frac{a_3 s^2}{a_1 \omega} x_3 ,$$

$$b_{12} = \frac{a_3 s^2}{a_1 \omega\theta} [1 + (s - \omega) x_3] ,$$

$$b_{13} = \frac{a_3}{a_1 \omega\theta} \sin(\theta x_3) ,$$

$$b_{14} = - \frac{a_3}{a_1 \omega\theta} \cos(\theta x_3) ,$$

$$b_{15} = \frac{a_3}{\omega} \left(\frac{1}{a_2 s} - \frac{x_3}{a_1} \right) ,$$

$$b_{16} = \frac{a_3}{a_1 \omega\theta} \left[\frac{a_1 \omega - s}{a_2 s} + (s - \omega) x_3 \right] ,$$

$$b_{17} = \frac{a_3}{a_1 \omega\theta} [-\theta \cos(\theta x_3) + \omega \sin(\theta x_3)] ,$$

$$b_{18} = \frac{-a_3}{a_1 \omega\theta} [\omega \cos(\theta x_3) + \theta \sin(\theta x_3)] ,$$

$$b_{19} = \frac{a_3}{a_1 \omega} (-1 + s x_3) ,$$

$$b_{20} = \frac{a_3}{a_1 \omega\theta} [-\omega + s(\omega - s) x_3] ,$$

Note that $\bar{P}_1$ and $\bar{P}_2$ are the real and imaginary part of $\bar{Q}/k$. Therefore

$$\bar{P}_1 = \frac{1}{2\pi k} \int_{B_H} Q(x_1, x_2) \cos (\bar{x}_1 x_1 + \bar{x}_2 x_2) \, dx_1 \, dx_2 ,$$

$$\bar{P}_2 = \frac{1}{2\pi k} \int_{B_H} Q(x_1, x_2) \sin (\bar{x}_1 x_1 + \bar{x}_2 x_2) \, dx_1 \, dx_2 . \qquad (3.66)$$

For the case $\bar{P}_2 = 0$, Equations (3.65) become

$$\frac{\bar{\sigma}^T_{11}}{\mu} = \bar{P}_1 \left[(b_1 C_1 + b_2 C_2) \, e^{-\omega x_3} + (b_3 C_1 + b_4 C_2) \, e^{-s x_3} \right] ,$$

$$\frac{\bar{\sigma}^T_{22}}{\mu} = \bar{P}_1 \left[(b_5 C_1 + b_6 C_2) \, e^{-\omega x_3} + (b_7 C_1 + b_8 C_2) \, e^{-s x_3} \right] ,$$

$$\frac{\bar{\sigma}^T_{33}}{\mu} = \bar{P}_1 \left[(b_9 C_1 + b_{10} C_2) \, e^{-\omega x_3} - (b_{11} C_1 + b_{12} C_2) \, e^{-s x_3} \right] ,$$

$$\frac{\bar{\sigma}^T_{12}}{\mu} = \bar{P}_1 \bar{x}_1 \bar{x}_2 \left[(b_{13} C_1 + b_{14} C_2) \, e^{-\omega x_3} + (b_{15} C_1 + b_{16} C_2) \, e^{-s x_3} \right] ,$$

$$\frac{\bar{\sigma}^T_{23}}{\mu} = -i \bar{x}_2 \bar{P}_1 \left[(b_{17} C_1 + b_{18} C_2) \, e^{-\omega x_3} - (b_{19} C_1 + b_{20} C_2) \, e^{-s x_3} \right] ,$$

$$\frac{\bar{\sigma}^T_{31}}{\mu} = -i \bar{x}_1 \bar{P}_1 \left[(b_{17} C_1 + b_{18} C_2) \, e^{-\omega x_3} - (b_{19} C_1 + b_{20} C_2) \, e^{-s x_3} \right] . \qquad (3.67)$$

3.5 Numerical Results

Previous sections have shown the general expressions for the transformed mechanical and thermal stress fields. After applying the

inverse Fourier transform and following through the simplification of the multiple integrals, results for several cases can be obtained numerically.

3.5.1 Rectangular Contact Area with Uniform Pressure (Case 1) Mechanical Stress Field

The tractions of the mechanical loading are

$$\sigma_{33} = -R_3(x_1, x_2, 0) , \quad \sigma_{32} = -R_2 = 0 , \quad \sigma_{31} = -R_1(x_1, x_2, 0)$$

where

$$R_3 = \begin{cases} p_o = \text{constant} , & x_1 \leq a, \ x_2 \leq b \\ 0 , & \text{elsewhere} \end{cases}$$

$$R_1 = -\mu_f R_3 .$$

The corresponding transformed boundary conditions can be readily obtained

$$\bar{R}_3(\bar{x}_1, \bar{x}_2, 0) = \frac{1}{2\pi} \int_{-\infty}^{\infty} \int_{-\infty}^{\infty} R_3 \, e^{i(\bar{x}_1 x_1 + \bar{x}_2 x_2)} \, dx_1 \, dx_2$$

$$= \frac{1}{2\pi} \int_{-b}^{b} \int_{-a}^{a} p_o \, e^{i(\bar{x}_1 x_1 + \bar{x}_2 x_2)} \, dx_1 \, dx_2$$

$$= \frac{p_o}{2\pi} \left[\int_{-b}^{b} e^{i\bar{x}_2 x_2} \, dx_2 \right] \left[\int_{-a}^{a} e^{i\bar{x}_1 x_1} \, dx_1 \right]$$

$$= \frac{2p_o}{\pi \bar{x}_1 \bar{x}_2} \sin(\bar{x}_1 a) \sin(\bar{x}_2 b) ,$$

$$\bar{R}_1 = -\mu_f \bar{R}_3 , \quad \bar{R}_2 = 0 . \tag{3.68}$$

By following the substitution of (3.68) into (3.15) and applying the inverse transform, the mechanical stress components can be expressed as

$$\{\sigma_{ij}\} = \{\sigma_{ij}^{n}\} + \{\sigma_{ij}^{f}\}$$

where the first term on the right-hand side of this equation denotes the stress components resulting from the normal loading $\bar{R}_3$, and the second the frictional loading $\bar{R}_1$. The expressions are

$$\sigma_{11}^{n} = \frac{P_o}{\pi^2}\int_0^{2\pi}\frac{\cot\phi}{H}\int_0^{\infty}\left[\gamma_3(1+\tfrac{1}{2}M_2^2-M_1^2)\,e^{-s\gamma_1 x_3}-\gamma_1\gamma_2\,e^{-s\gamma_2 x_3}\right]$$

$$\cdot\, W(s,\phi)\,ds\,d\phi\,,$$

$$\sigma_{22}^{n} = \frac{P_o}{\pi^2}\int_0^{2\pi}\frac{1}{H\sin\phi\cos\phi}\int_0^{\infty}\left\{\left[\gamma_3(\tfrac{1}{2}\beta^2-1)\,M_1^2\cos^2\phi+\sin^2\phi\right]\right.$$

$$\left.\cdot\, e^{-s\gamma_1 x_3}-\gamma_1\gamma_2\sin^2\phi\,e^{-s\gamma_2 x_3}\right\}W(s,\phi)\,ds\,d\phi\,,$$

$$\sigma_{33}^{n} = \frac{-P_o}{\pi^2}\int_0^{2\pi}\frac{1}{H\sin\phi\cos\phi}\int_0^{\infty}\left[\gamma_3^2\,e^{-s\gamma_1 x_3}-\gamma_1\gamma_2\,e^{-s\gamma_2 x_3}\right]$$

$$\cdot\, W(s,\phi)\,ds\,d\phi\,,$$

$$\sigma_{12}^{n} = \frac{P_o}{\pi^2}\int_0^{2\pi}\frac{1}{H}\int_0^{\infty}\left[\gamma_3\,e^{-s\gamma_1 x_3}-\gamma_1\gamma_2\,e^{-s\gamma_2 x_3}\right]W(s,\phi)\,ds\,d\phi\,,$$

$$\sigma_{23}^{n} = \frac{-iP_o}{\pi^2}\int_0^{2\pi}\frac{\gamma_1\gamma_3}{H\cos\phi}\int_0^{\infty}\left[e^{-s\gamma_1 x_3}-e^{-s\gamma_2 x_3}\right]W(s,\phi)\,ds\,d\phi\,,$$

$$\sigma_{31}^{n} = \frac{-iP_o}{\pi^2}\int_0^{2\pi}\frac{\gamma_1\gamma_3}{H\sin\phi}\int_0^{\infty}\left[e^{-s\gamma_1 x_3}-e^{-s\gamma_2 x_3}\right]W(s,\phi)\,ds\,d\phi\,,$$

$$\sigma_{11}^f = \frac{-i\mu_f p_o}{\pi^2} \int_0^{2\pi} \frac{1}{H \sin\phi} \int_0^{\infty} \left\{ \gamma_2 \cos^2\phi \left(1 + \frac{1}{2} M_2^2 - M_1^2\right) e^{-s\gamma_1 x_3} \right.$$

$$\left. - \left[\frac{(\gamma_3 - 2\gamma_1\gamma_2)}{\gamma_2} \sin^2\phi + \gamma_2\gamma_3 \right] e^{-s\gamma_2 x_3} \right\} W(s,\phi)\, ds\, d\phi \,,$$

$$\sigma_{22}^f = \frac{-i\mu_f p_o}{\pi^2} \int_0^{2\pi} \frac{1}{H \sin\phi} \int_0^{\infty} \left\{ \gamma_2 \left[\left(\frac{1}{2}\beta^2 - 1\right) M_1^2 \cos^2\phi + \sin^2\phi \right] e^{-s\gamma_1 x_3} \right.$$

$$\left. + \left[\frac{(\gamma_3 - 2\gamma_1\gamma_2)}{\gamma_2} \sin^2\phi \right] e^{-s\gamma_2 x_3} \right\} W(s,\phi)\, ds\, d\phi \,,$$

$$\sigma_{33}^f = \frac{-i\mu_f p_o}{\pi^2} \int_0^{2\pi} \frac{\gamma_2}{H \sin\phi} \int_0^{\infty} \left\{ \left[\left(\frac{1}{2}\beta^2 - 1\right) M_1^2 \cos^2\phi - \gamma_1^2 \right] \right.$$

$$\left. \cdot\, e^{-s\gamma_1 x_3} + \gamma_3\, e^{-s\gamma_2 x_3} \right\} W(s,\phi)\, ds\, d\phi \,,$$

$$\sigma_{12}^f = \frac{-i\mu_f p_o}{\pi^2} \int_0^{2\pi} \frac{\gamma_2}{H \cos\phi} \int_0^{\infty} \left\{ \cos^2\phi\, e^{-s\gamma_1 x_3} - \frac{1}{2} \left[\frac{(\gamma_3 - 2\gamma_1\gamma_2)}{\gamma_2^2} \right. \right.$$

$$\left. \left. \cdot\, (\sin^2\phi - \cos^2\phi) + \gamma_3 \right] e^{-s\gamma_2 x_3} \right\} W(s,\phi)\, ds\, d\phi \,,$$

$$\sigma_{23}^f = \frac{-\mu_f p_o}{\pi^2} \int_0^{2\pi} \frac{\gamma_1\gamma_2}{H} \int_0^{\infty} \left(e^{-s\gamma_1 x_3} - e^{-s\gamma_2 x_3} \right) W(s,\phi)\, ds\, d\phi \,,$$

$$\sigma_{31}^f = \frac{-\mu_f p_o}{\pi^2} \int_0^{2\pi} \frac{1}{H \sin\phi \cos\phi} \int_0^{\infty} \left[\gamma_1\gamma_2 \cos^2\phi\, e^{-s\gamma_1 x_3} \right.$$

$$\left. - (\gamma_3^2 - \gamma_1\gamma_2 \sin^2\phi)\, e^{-s\gamma_2 x_3} \right] W(s,\phi)\, ds\, d\phi \,, \qquad (3.69)$$

where

$$W(s,\phi) = \frac{\sin(sa\cos\phi)\,\sin(sb\sin\phi)}{s}\, e^{-is\gamma\cos(\theta-\phi)},$$

$$\gamma = (x_1^2 + x_2^2)^{1/2}, \qquad \gamma_3 = (1 - \tfrac{1}{2}M_2^2\cos^2\phi),$$

$$\gamma_t = (1 - M_t^2\cos^2\phi)^{1/2}, \qquad t = 1,2,$$

$$H = \gamma_3^2 - \gamma_1\gamma_2, \qquad \theta = \tan^{-1}\frac{x_2}{x_1}.$$

Equations (3.69) can be reduced to single integrals by using the techniques of change of variables and the following equalities:

$$\frac{\sin(sa\cos\phi)\,\sin(sb\sin\phi)}{s}\, e^{-s\gamma_t x_3}\cos(s\gamma\cos(\theta-\phi))$$

$$= \frac{1}{4}\frac{1}{s}\, e^{-s\gamma_t x_3}\{[\cos s(a\cos\phi - b\sin\phi - \gamma\cos(\theta-\phi)) + \cos s(a\cos\phi - b\sin\phi + \gamma\cos(\theta-\phi))] - [\cos s(a\cos\phi + b\sin\phi - \gamma\cos(\theta-\phi)) + \cos s(a\cos\phi + b\sin\phi + \gamma\cos(\theta-\phi))]\},$$

$$\frac{\sin(sa\cos\phi)\,\sin(sb\sin\phi)}{s}\, e^{-s\gamma_t x_3}\sin(s\gamma\cos(\theta-\phi))$$

$$= \frac{1}{4}\frac{1}{s}\, e^{-s\gamma_t x_3}\{[\sin s(a\cos\phi - b\sin\phi + \gamma\cos(\theta-\phi)) - \sin s(a\cos\phi - b\sin\phi - \gamma\cos(\theta-\phi))] - [\sin s(a\cos\phi + b\sin\phi + \gamma\cos(\theta-\phi)) - \sin s(a\cos\phi + b\sin\phi - \gamma\cos(\theta-\phi))]\},$$

$$\int_0^\infty \frac{1}{s}\, e^{-sd}\sin(sh)\,ds = \tan^{-1}\left(\frac{h}{d}\right),$$

$$\int_0^\infty \frac{1}{s}\, e^{-sd}\cos(sh)\,ds = \int_0^\infty \frac{1}{s}\, e^{-sd}\,ds - \frac{1}{2}\ln\left(\frac{h^2+d^2}{d^2}\right).$$

The term $\int_0^\infty \frac{1}{s} e^{-sd}\, ds$ cancels out during simplification. Thus, the stress fields are expressed as

$$\sigma_{11}^n = \frac{P_o}{4\pi^2}\int_0^\pi \frac{\cot\phi}{H}\left[\gamma_3\left(1 + \frac{1}{2}M_2^2 - M_1^2\right) S_1 - \gamma_1\gamma_2 S_2\right] d\phi ,$$

$$\sigma_{22}^n = \frac{P_o}{2\pi^2}\int_0^\pi \frac{1}{H \sin 2\phi}\left\{\left[\gamma_3\left(\frac{1}{2}\beta^2 - 1\right) M_1^2 \cos^2\phi + \sin^2\phi\right] \cdot S_1 - \gamma_1\gamma_2 \sin^2\phi\, S_2\right\} d\phi ,$$

$$\sigma_{33}^n = \frac{-P_o}{2\pi^2}\int_0^\pi \frac{1}{H \sin 2\phi}\left[\gamma_3^2 S_1 - \gamma_1\gamma_2 S_2\right] d\phi ,$$

$$\sigma_{12}^n = \frac{P_o}{4\pi^2}\int_0^\pi \frac{1}{H}\left[\gamma_3 S_1 - \gamma_1\gamma_2 S_2\right] d\phi ,$$

$$\sigma_{23}^n = \frac{-P_o}{2\pi^2}\int_0^\pi \frac{\gamma_1\gamma_3}{H\cos\phi}\left[W_1 - W_2\right] d\phi ,$$

$$\sigma_{31}^n = \frac{-P_o}{2\pi^2}\int_0^\pi \frac{\gamma_1\gamma_3}{H\sin\phi}\left[W_1 - W_2\right] d\phi ,$$

$$\sigma_{11}^f = \frac{-\mu_f P_o}{2\pi^2}\int_0^\pi \frac{1}{H\sin\phi}\left\{\gamma_2\cos^2\phi\left(1 + \frac{1}{2}M_2^2 - M_1^2\right) W_1 - \left[\frac{(\gamma_3 - 2\gamma_1\gamma_2)}{\gamma^2}\sin^2\phi + \gamma_2\gamma_3\right] W_2\right\} d\phi ,$$

$$\sigma_{22}^f = \frac{-\mu_f P_o}{2\pi^2} \int_0^\pi \frac{1}{H \sin\phi} \left\{ \gamma_2 [(\tfrac{1}{2}\beta^2 - 1) M_1^2 \cos^2\phi + \sin^2\phi] W_1 \right.$$

$$\left. + \left[\frac{(\gamma_3 - 2\gamma_1\gamma_2)}{\gamma_2} \sin^2\phi \right] W_2 \right\} d\phi ,$$

$$\sigma_{33}^f = \frac{-\mu_f P_o}{2\pi^2} \int_0^\pi \frac{\gamma_2}{H \sin\phi} \{[(\tfrac{1}{2}\beta^2 - 1 M_1^2 \cos^2\phi - \gamma_1^2] W_1 + \gamma_3 W_2\} d\phi ,$$

$$\sigma_{12}^f = \frac{-\mu_f H_o}{2\pi^2} \int_0^\pi \frac{\gamma_2}{H \cos\phi} \left\{ \cos^2\phi W_1 - \frac{1}{2} \left[\frac{(\gamma_3 - 2\gamma_1\gamma_2)}{\gamma_2^2} \right.\right.$$

$$\left.\left. \cdot (\sin^2\phi - \cos^2\phi) + \gamma_3 \right] W_2 \right\} d\phi ,$$

$$\sigma_{23}^f = \frac{-\mu_f P_o}{4\pi^2} \int_0^\pi \frac{\gamma_1\gamma_2}{H} [S_1 - S_2] d\phi ,$$

$$\sigma_{31}^f = \frac{-\mu_f P_o}{2\pi^2} \int_0^\pi \frac{1}{H \sin^2\phi} [\gamma_1\gamma_2 \cos^2\phi S_1 - (\gamma_3^2 - \gamma_1\gamma_2 \sin^2\phi) S_2] d\phi \qquad (3.70)$$

in which

$$S_t = \ln \frac{\{[a \cos\phi + b \sin\phi + \gamma \cos(\theta - \phi)]^2 + \gamma_t^2 x_3^2\}}{\{[a \cos\phi - b \sin\phi - \gamma \cos(\theta - \phi)]^2 + \gamma_t^2 x_3^2\}}$$

$$+ \ln \frac{\{[a \cos\phi + b \sin\phi - \gamma \cos(\theta - \phi)]^2 + \gamma_t^2 x_3^2\}}{\{[a \cos\phi - b \sin\phi + \gamma \cos(\theta - \phi)]^2 + \gamma_t^2 x_3^2\}}$$

$$W_t = \tan^{-1} \frac{a \cos\phi - b \sin\phi + \gamma \cos(\theta - \phi)}{\gamma_t x_3}$$

$$+ \tan^{-1} \frac{a \cos\phi + b \sin\phi - \gamma \cos(\theta - \phi)}{\gamma_t x_3}$$

$$- \tan^{-1} \frac{a \cos\phi - b \sin\phi - \gamma \cos(\theta - \phi)}{\gamma_t x_3}$$

$$- \tan^{-1} \frac{a \cos\phi + b \sin\phi + \gamma \cos(\theta - \phi)}{\gamma_t x_3}$$

$t = 1,2$.

The integrals appearing in Equations (3.70) are suitable for numerical evaluation at any point inside the solid. However, most integrals are not defined at $\phi = 0$, $\pi/2$ or π. Limiting processes are imperative so that singularities can be removed.

Temperature Field

Replacing $Q(x_1,x_2)$ in (3.66) by expressions (3.20) and (3.17), the heat flux input in the transformed space is

$$\bar{P}_1 = \frac{-1}{2\pi k} \int_{B_H} q(x_1, x_2) \cos(\bar{x}_1 x_1 + \bar{x}_2 x_2)\, dx_1\, dx_2$$

$$= \frac{-\mu_f P_o V}{2\pi k} \int_{-a}^{a} \int_{-b}^{b} \cos(\bar{x}_1 x + \bar{x}_2 x)\, dx_2\, dx_1$$

$$= \frac{-\mu_f P_o V}{\pi k} \cdot \frac{\sin(\bar{x}_2 b)}{\bar{x}_2} \int_{-a}^{a} \cos(\bar{x}_1 x)\, dx_1$$

$$= \frac{-2\mu_f P_o V}{\pi k} \cdot \frac{1}{\bar{x}_1 \bar{x}_2} \sin(\bar{x}_1 a) \sin(\bar{x}_2 b) ,$$

$$\bar{P}_2 = \frac{-1}{2\pi k} \int_{B_H} q(x_1, x_2) \sin(\bar{x}_1 x_1 + \bar{x}_2 x_2)\, dx_1\, dx_2$$

$$= \frac{-\mu_f P_o V}{2\pi k} \int_{-a}^{a} \int_{-b}^{b} \sin(\bar{x}_1 x + \bar{x}_2 x)\, dx_2\, dx_1$$

$$= 0 .$$

Expressions above are substituted into Equation (3.31) for the transformed temperature field. The inverse Fourier transform, after certain simplications, results in:

$$T = \frac{-4\mu_f P_o V}{\pi^2 k} \int_0^{\infty} \int_0^{\infty} f_1 \cos(\bar{x}_2 x_2)\ e^{-\omega x_3} [D_1 \cos(\theta x_3) + D_2 \sin(\theta x_3)]\, d\bar{x}_1\, d\bar{x}_2 \qquad (3.71)$$

where

$$f_1 = \frac{1}{\bar{x}_1 \bar{x}_2} \sin(\bar{x}_1 a) \sin(\bar{x}_2 b) ,$$

$$D_1 = -\frac{1}{\omega^2 + \theta^2} [\omega \cos(\bar{x}_1 x_1) - \frac{n}{2\omega} \sin(\bar{x}_1 x_1)] ,$$

$$D_2 = \frac{1}{\omega^2 + \theta^2} [\theta \cos(\bar{x}_1 x_1) + \frac{n}{2\theta} \sin(\bar{x}_1 x_1)] .$$

Alternately, the temperature distribution can also be obtained by Green's function method which will serve as a double check for numerical results. The temperature field results by substituting Equation (3.35) into (3.33) and letting $t \to \infty$,

$$T = \frac{\mu_f V P_o}{\pi^{3/2} k} \int_0^\infty \int_{-a}^{a} \int_{-b}^{b} \frac{\exp\{\frac{V}{2\kappa}(x_1 - x_1') - \tau^2 - (V^2R^2/16\kappa^2\tau^2)\}}{R}$$

$$dx_2' \, dx_1' \, d\tau \, .$$

With the introduction of the variable $\tau = \sqrt{2u}R$

$$T = \frac{\mu_f V P_o}{4\sqrt{2\pi}\, k} \int_0^\infty \frac{e^{-2ux_3^2}}{\sqrt{u}} \left[\int_{-a}^{a} \exp\{-2u[(x_1 - x_1') - \frac{V}{8\kappa u}]^2\} \, dx_1' \int_{-b}^{b} \right.$$

$$\left. \cdot \exp\{-2u(x_2 - x_2')\} \, dx_2' \right] du$$

which can be further simplified as

$$T = \frac{\mu_f V P_o}{4\sqrt{2\pi}\, k} \int_0^\infty \frac{\exp\left(-\frac{x_3^2}{2y}\right)}{\sqrt{y}} \left[\operatorname{erf}\left(\frac{x_2 + b}{\sqrt{2y}}\right) - \operatorname{erf}\left(\frac{x_2 - b}{\sqrt{2y}}\right) \right]$$

$$\cdot \left[\operatorname{erf}\left(\frac{x_1 + a - \frac{V}{2\kappa} y}{\sqrt{2y}}\right) - \operatorname{erf}\left(\frac{x_1 - a - \frac{V}{2\kappa} y}{\sqrt{2y}}\right) \right] dy \, . \qquad (3.72)$$

This integral expression is more conducive to numerical computation.

Thermal Stress Field

Following the substitution of the expression $\bar{P}_1$ into Equations (3.67) and applying the inverse Fourier transform, the thermal stress field is thus

$$\frac{\sigma_{11}^T}{\mu} = \frac{-4\mu_f P_o V}{\pi^2 k}\int_0^\infty\int_0^\infty f_1 \cos(\bar{x}_2 x_2)\left[e^{-\omega x_3}(b_1 D_1 + b_2 D_2)\right.$$

$$\left. + e^{-sx_3}(b_3 D_1 + b_4 D_2)\right] d\bar{x}_1\, d\bar{x}_2 ,$$

$$\frac{\sigma_{22}^T}{\mu} = \frac{-4\mu_f P_o V}{\pi^2 k}\int_0^\infty\int_0^\infty f_1 \cos(\bar{x}_2 x_2)\left[e^{-\omega x_3}(b_5 D_1 + b_6 D_2)\right.$$

$$\left. + e^{-sx_3}(b_7 D_1 + b_8 D_2)\right] d\bar{x}_1\, d\bar{x}_2 ,$$

$$\frac{\sigma_{33}^T}{\mu} = \frac{-4\mu_f P_o V}{\pi^2 k}\int_0^\infty\int_0^\infty f_1 \cos(\bar{x}_2 x_2)\left[e^{-\omega x_3}(b_9 D_1 + b_{10} D_2)\right.$$

$$\left. - e^{-sx_3}(b_{11} D_1 + b_{12} D_2)\right] d\bar{x}_1\, d\bar{x}_2 ,$$

$$\frac{\sigma_{12}^T}{\mu} = \frac{-4\mu_f P_o V}{\pi^2 k}\int_0^\infty\int_0^\infty \bar{x}_1\bar{x}_2 f_1 \sin(\bar{x}_2 x_2)\left[e^{-\omega x_3}(-b_{13} D_3 - b_{14} D_4)\right.$$

$$\left. - e^{-sx_3}(b_{15} D_3 + b_{16} D_4)\right] d\bar{x}_1\, d\bar{x}_2 ,$$

$$\frac{\sigma_{23}^T}{\mu} = \frac{-4\mu_f P_o V}{\pi^2 k}\int_0^\infty\int_0^\infty \bar{x}_2 f_1 \sin(\bar{x}_2 x_2)\left[e^{-\omega x_3}(b_{17} D_5 + b_{18} D_6)\right.$$

$$\left. - e^{-sx_3}(b_{19} D_5 + b_{20} D_6)\right] d\bar{x}_1\, d\bar{x}_2 ,$$

$$\frac{\sigma_{31}^{T}}{\mu} = \frac{-4\mu_f P_o V}{\pi^2 k}\int_0^\infty\int_0^\infty \bar{x}_1 f_1 \cos(\bar{x}_2 x_2)\left[e^{-\omega x_3}(b_{17}D_7 + b_{18}D_8)\right.$$

$$\left. - e^{-sx_3}(b_{19}D_7 + b_{20}D_8)\right] d\bar{x}_1\, d\bar{x}_2 \,, \qquad (3.73)$$

$$D_3 = -\frac{1}{\omega^2 + \theta^2}\left[\omega \sin(\bar{x}_1 x_1) + \frac{n}{2\omega}\cos(\bar{x}_1 x_1)\right] ,$$

$$D_4 = \frac{1}{\omega^2 + \theta^2}\left[\theta \sin(\bar{x}_1 x_1) - \frac{n}{2\theta}\cos(\bar{x}_1 x_1)\right] ,$$

$$D_5 = \frac{1}{\omega^2 + \theta^2}\left[-\frac{n}{2\omega}\sin(\bar{x}_1 x_1) + \omega\cos(\bar{x}_1 x_1)\right] ,$$

$$D_6 = -\frac{1}{\omega^2 + \theta^2}\left[\frac{n}{2\theta}\sin(\bar{x}_1 x_1) + \theta\cos(\bar{x}_1 x_1)\right] ,$$

$$D_7 = \frac{1}{\omega^2 + \theta^2}\left[\frac{n}{2\omega}\cos(\bar{x}_1 x_1) + \omega\sin(\bar{x}_1 x_1)\right] ,$$

$$D_8 = \frac{1}{\omega^2 + \theta^2}\left[\frac{n}{2\theta}\cos(\bar{x}_1 x_1) - \theta\sin(\bar{x}_1 x_1)\right] .$$

Due to the complexity of the expressions, no existing automatic integration scheme for the integrals above is efficient. Hence the Gaussian-Laguerre quadrature formulas and Simpson's integration scheme are used for the numerical approximation (Appendix II).

3.5.2 Disk Contact Area with Uniform Pressure (Case 2)

Mechanical Stress Field

The pressure distributions are assumed to be of the form

$$\sigma_{33} = -R_3(x_1, x_2, 0) , \quad \sigma_{32} = -R_2 = 0 , \quad \sigma_{31} = -R_1(x_1, x_2, 0)$$

where

$$R_3 = \begin{cases} P_o , & \gamma^2 = x_1^2 + x_2^2 \leq a^2 \\ 0 , & \text{elsewhere} \end{cases} ,$$

$$R_1 = -\mu_f R_3 .$$

The transformed boundary conditions can be obtained by using Equation (3.3).

$$\bar{R}_3(\bar{x}_1, \bar{x}_2, 0) = \frac{P_o}{2\pi} \int_{-a}^{a} \int_{-[a^2-x_1^2]^{1/2}}^{[a^2-x_1^2]^{1/2}} e^{i(\bar{x}_1 x_1 + \bar{x}_2 x_2)} \, dx_2 \, dx_1$$

$$= \frac{P_o}{2\pi} \int_0^a \gamma d\gamma \int_0^{2\pi} e^{is\gamma \cos(\theta-\phi)} \, d\theta$$

$$= P_o \int_0^a \gamma J_o(s\gamma) \, d\gamma$$

$$= \frac{aP_o}{s} J_1(sa) ,$$

$$\bar{R}_1 = -\mu_f \bar{R}_3 , \quad \bar{R}_2 = 0 .$$

Following the same procedure as in Case 1, expressions are obtained for the stress components of the forms

$$\sigma_{11}^{n} = \frac{aP_o}{\pi} \int_0^{\pi} \frac{\cos^2 \phi}{H} [\gamma_3(1 + \tfrac{1}{2} M_2^2 - M_1^2)\, S_1' - \gamma_1\gamma_2 S_2'] \, d\phi \,,$$

$$\sigma_{22}^{n} = \frac{aP_o}{\pi} \int_0^{\pi} \frac{1}{H} \{[\gamma_3(\tfrac{1}{2}\beta^2 - 1) M_1^2 \cos^2 \phi + \sin^2 \phi]$$

$$\cdot S_1' - \gamma_1\gamma_2 \sin^2 \phi\, S_2'\} \, d\phi \,,$$

$$\sigma_{33}^{n} = \frac{-aP_o}{\pi} \int_0^{\pi} \frac{1}{H} [\gamma_3^2 S_1' - \gamma_1\gamma_2 S_2'] \, d\phi \,,$$

$$\sigma_{12}^{n} = \frac{aP_o}{2\pi} \int_0^{\pi} \frac{\sin 2\phi}{H} [\gamma_3 S_1' - \gamma_1\gamma_2 S_2'] \, d\phi \,,$$

$$\sigma_{23}^{n} = \frac{-aP_o}{\pi} \int_0^{\pi} \frac{\gamma_1\gamma_3 \sin \phi}{H} [W_1' - W_2'] \, d\phi \,,$$

$$\sigma_{31}^{n} = \frac{-aP_o}{\pi} \int_0^{\pi} \frac{\gamma_1\gamma_3 \cos \phi}{H} [W_1' - W_2'] \, d\phi \,,$$

$$\sigma_{11}^{f} = \frac{-au_f P_o}{\pi} \int_0^{\pi} \frac{\cos \phi}{H} \left\{\gamma_2 \cos^2 \phi(1 + \tfrac{1}{2} M_2^2 - M_1^2)\, W_1' \right.$$

$$\left. - \left[\frac{(\gamma_3 - 2\gamma_1\gamma_2)}{\gamma_2} \sin^2 \phi + \gamma_2\gamma_3\right] W_2' \right\} d\phi \,,$$

$$\sigma_{22}^{f} = \frac{-au_f P_o}{\pi} \int_0^{\pi} \frac{\cos \phi}{H} \left\{\gamma_2[(\tfrac{1}{2}\beta^2 - 1) M_1^2 \cos^2 \phi + \sin^2 \phi]\, W_1' \right.$$

$$\left. + \left[\frac{(\gamma_3 - 2\gamma_1\gamma_2)}{\gamma_2} \sin^2 \phi\right] W_2' \right\} d\phi \,,$$

$$\sigma_{33}^f = \frac{-a\mu_f p_o}{\pi} \int_0^\pi \frac{\gamma_2 \cos\phi}{H} \{[(\tfrac{1}{2}\beta^2 - 1) M_1^2 \cos^2\phi - \gamma_1^2] W_1' + \gamma_3 W_2'\} d\phi ,$$

$$\sigma_{12}^f = \frac{-a\mu_f p_o}{\pi} \int_0^\pi \frac{\gamma_2 \sin\phi}{H} \left\{ \cos^2\phi \, W_1' - \frac{1}{2}\left[\frac{(\gamma_3 - 2\gamma_1\gamma_2)}{\gamma_2^2}(\sin^2\phi - \cos^2\phi) + \gamma_3\right] W_2' \right\} d\phi ,$$

$$\sigma_{23}^f = \frac{-a\mu_f p_o}{2\pi} \int_0^\pi \frac{\sin 2\phi}{H} \gamma_1\gamma_2 [S_1' - S_2'] \, d\phi ,$$

$$\sigma_{31}^f = \frac{-a\mu_f p_o}{\pi} \int_0^\pi \frac{1}{H} [\gamma_1\gamma_2 \cos^2\phi \, S_1' - (\gamma_3^2 - \gamma_1\gamma_2 \sin^2\phi) S_2'] \, d\phi , \quad (3.74)$$

where

$$S_t' = \int_0^\infty J_1(sa) \cos(s\gamma \cos(\theta - \phi)) \, e^{-s\gamma_t x_3} \, ds ,$$

$$W_t' = \int_0^\infty J_1(sa) \sin(s\gamma \cos(\theta - \phi)) \, e^{-s\gamma_t x_3} \, ds ,$$

$$t = 1,2 .$$

The integrals for S_t' and W_t' can be solved analytically so that the stress expressions have the form of single integrals which can be evaluated numerically.

Temperature Field

$\bar{P}_1$ and $\bar{P}_2$ are given by

$$\bar{P}_1 = \frac{-\mu_f P_o V}{2\pi k} \int_{-a}^{a} \int_{-[a^2-x_1^2]^{1/2}}^{[a^2-x_1^2]^{1/2}} \cos(\bar{x}_1 x_1 + \bar{x}_2 x_2)\, dx_2\, dx_1$$

$$= \frac{-\mu_f P_o V}{2\pi k} \mathrm{Re} \int_{-a}^{a} \int_{-[a^2 - x_1^2]^{1/2}}^{[a^2-x_1^2]^{1/2}} e^{i(\bar{x}_1 x_1 + \bar{x}_2 x_2)}\, dx_2\, dx_1$$

$$= \frac{-\mu_f P_o V}{k} \cdot \frac{a J_1(sa)}{s} ,$$

$$\bar{P}_2 = \frac{-\mu_f P_o V}{2\pi k} \int_{-a}^{a} \int_{-[a^2-x_1^2]^{1/2}}^{[a^2-x_1^2]^{1/2}} \sin(\bar{x}_1 x_1 + \bar{x}_2 x_2)\, dx_2\, dx_1$$

$$= \frac{-\mu_f P_o V}{\pi k} \int_{-a}^{a} \sin(\bar{x}_1 x_1) \sin\left(\bar{x}_2 \sqrt{a^2 - x_1^2}\right) dx_1$$

$$= 0 .$$

Substitution of $\bar{P}_1$ and $\bar{P}_2$ into Equation (3.31) and again application of the inverse transform results in

$$T = \frac{-2\mu_f P_o V}{\pi k} \int_0^{\infty} \int_0^{\infty} f_2 \cos(\bar{x}_2 x_2)\, e^{-\omega x_3}$$

$$\cdot [D_1 \cos(\vartheta x_3) + D_2 \sin(\vartheta x_3)]\, d\bar{x}_1\, d\bar{x}_2 \qquad (3.75)$$

AD-A146 271 THERMOMECHANICAL CRACKING DUE TO MOVING FRICTION LOADS (U) NEW MEXICO UNIV ALBUQUERQUE BUREAU OF ENGINEERING RESEARCH F D JU ET AL. MAY 84 ME-125(84)ONR-233-2 2/2

UNCLASSIFIED N00014-83-K-0304 F/G 12/1 NL

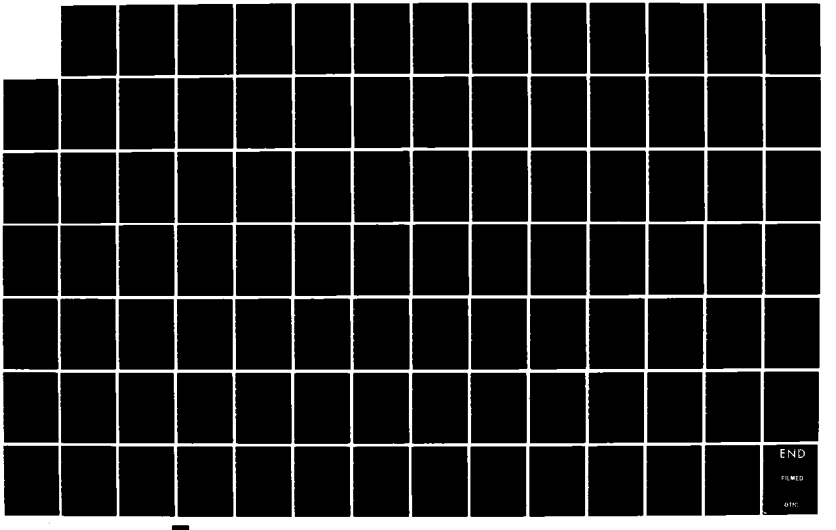

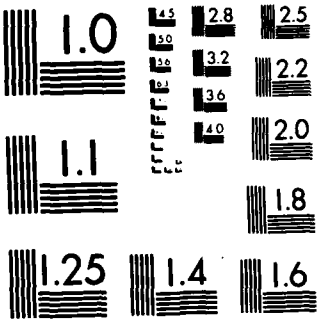

where

$$f_2 = \frac{aJ_1(sa)}{s} .$$

According to Equation (3.37), the corresponding Green's function solution for this case is

$$T(x_1,x_2,x_3) = \frac{\mu_f P_o V}{2\pi k} \int_{-a}^{a} \int_{-[a^2-x_1'^2]^{1/2}}^{[a^2-x_1'^2]^{1/2}} \frac{e^{-V[R - (x_1 - x_1')]/2\kappa}}{R} dx_2' dx_1' , \tag{3.76}$$

for which the numerical evaluation can be done by double Simpson's schemes. Since Equation (3.76) is integrated within finite intervals, it is advantageous to compute the numerical results through Equation (3.76) instead of (3.75) where the integral is improper.

Thermal Stress Field

In the same fashion as in Case 1, it can be shown that

$$\frac{\sigma_{11}^T}{\mu} = \frac{-2\mu_f P_o V}{\pi k} \int_0^{\infty} \int_0^{\infty} f_2 \cos(\bar{x}_2 x_2) \left[e^{-\omega x_3}(b_1 D_1 + b_2 D_2) + e^{-sx_3}(b_3 D_1 + b_4 D_2) \right] d\bar{x}_1 \, d\bar{x}_2 ,$$

$$\frac{\sigma_{22}^T}{\mu} = \frac{-2\mu_f P_o V}{\pi k} \int_0^{\infty} \int_0^{\infty} f_2 \cos(\bar{x}_2 x_2) \left[e^{-\omega x_3}(b_5 D_1 + b_6 D_2) + e^{-sx_3}(b_7 D_1 + b_8 D_2) \right] d\bar{x}_1 \, d\bar{x}_2 ,$$

$$\frac{\sigma_{33}^T}{\mu} = \frac{-2\mu_f P_o V}{\pi k}\int_0^\infty\int_0^\infty f_2 \cos(\bar{x}_2 x_2)\left[e^{-\omega x_3}(b_9 D_1 + b_{10} D_2)\right.$$

$$\left. - e^{-sx_3}(b_{11} D_1 + b_{12} D_2)\right] d\bar{x}_1\, d\bar{x}_2 ,$$

$$\frac{\sigma_{12}^T}{\mu} = \frac{-2\mu_f P_o V}{\pi k}\int_0^\infty\int_0^\infty \bar{x}_1\bar{x}_2 f_2 \sin(\bar{x}_2 x_2)\left[e^{-\omega x_3}(-b_{13} D_3 - b_{14} D_4)\right.$$

$$\left. - e^{-sx_3}(b_{15} D_3 + b_{16} D_4)\right] d\bar{x}_1\, d\bar{x}_2 ,$$

$$\frac{\sigma_{23}^T}{\mu} = \frac{-2\mu_f P_o V}{\pi k}\int_0^\infty\int_0^\infty \bar{x}_2 f_2 \sin(\bar{x}_2 x_2)\left[e^{-\omega x_3}(b_{17} D_5 + b_{18} D_6)\right.$$

$$\left. - e^{-sx_3}(b_{19} D_5 + b_{20} D_6)\right] d\bar{x}_1\, d\bar{x}_2 ,$$

$$\frac{\sigma_{31}^T}{\mu} = \frac{-2\mu_f P_o V}{\pi k}\int_0^\infty\int_0^\infty \bar{x}_1 f_2 \cos(\bar{x}_2 x_2)\left[e^{-\omega x_3}(b_{17} D_7 + b_{18} D_8)\right.$$

$$\left. - e^{-sx_3}(b_{19} D_7 + b_{20} D_8)\right] d\bar{x}_1\, d\bar{x}_2 , \qquad (3.77)$$

3.5.3 Disk Contact Area with Paraboloidal Distribution of Pressure (Case 3)

Mechanical Stress Field. The traction boundary conditions are

$$\sigma_{33} = -R_3(x_1, x_2, 0) , \quad \sigma_{32} = -R_2 = 0 , \quad \sigma_{31} = -R_1(x_1, x_2, 0)$$

where

$$R_3 = \begin{cases} 2P_o(1 - r^2/a^2) , & x_1^2 + x_2^2 \le a^2 \\ 0 , & \text{elsewhere} \end{cases}$$

$$\bar{R}_3(\bar{x}_1, \bar{x}_2, 0) = \frac{P_o}{\pi} \int_{-a}^{a} \int_{-[a^2-x_1^2]^{1/2}}^{[a^2-x_1^2]^{1/2}} (1 - \gamma^2/a^2)\, e^{i(\bar{x}_1 x_1 + \bar{x}_2 x_2)}\, dx_2\, dx_1$$

$$= \frac{P_o}{\pi} \int_0^a \int_0^{2\pi} (1 - \gamma^2/a^2)\, e^{is\gamma \cos(\theta-\phi)}\, \gamma\, d\gamma\, d\theta$$

$$= \frac{4P_o J_2(sa)}{s^2} ,$$

$$\bar{R}_1 = -\mu_f \bar{R}_3 , \qquad \bar{R}_2 = 0 .$$

The expressions of the stress components are similar to those (3.74) in Case 2 except S_t' and W_t' being replaced by S_t'' and W_t'' which are of the forms

$$S_t'' = \frac{4}{a} \int_0^\infty \frac{J_2(sa)}{s} \cos(s\gamma \cos(\theta - \phi))\, e^{-s\gamma_t x_3}\, ds ,$$

$$W_t'' = \frac{4}{a} \int_0^\infty \frac{J_2(sa)}{s} \sin(s\gamma \cos(\theta - \phi))\, e^{-s\gamma_t x_3}\, ds ,$$

$$t = 1,2 .$$

Again S_t'' and W_t'' can be solved analytically and accordingly numerical results of the stress components can be readily obtained by automatic integration schemes for single integrals.

Temperature Field

It is found that

$$\bar{P}_1 = \frac{-u_f P_o V}{\pi k} \int_{-a}^{a} \int_{-[a^2-x_1^2]^{1/2}}^{[a^2-x_1^2]^{1/2}} \left(1 - \frac{\gamma^2}{a^2}\right) \cos(\bar{x}_1 x_1 + \bar{x}_2 x_2)\, dx_2\, dx_1$$

$$= \frac{-4u_f P_o V}{k} \frac{J_2(sa)}{s^2} ,$$

$$\bar{P}_2 = 0 .$$

The temperature field can be obtained by replacing f_2 in Equations (3.75) by f_3 which has the following form

$$f_3 = \frac{4J_2(sa)}{s^2} .$$

The expression of Green's function solution is

$$T(x_1,x_2,x_3) = \frac{u_f P_o V}{2\pi k} \int_{-a}^{a} \int_{-[a^2-x_1'^2]^{1/2}}^{[a^2-x_1'^2]^{1/2}} \left(1 - \frac{r'^2}{a^2}\right) \cdot \frac{e^{-V[R-(x_1-x_1')]/2\kappa}}{R} dx_2'\, dx_1' \qquad (3.78)$$

where

$$r'^2 = x_1'^2 + x_2'^2 .$$

Thermal Stress Field

The expressions have the same form as Equation (3.77) in Case 2 except f_2 being replaced by f_3.

As an illustration of the numerical evaluation of the integrals, graphical results are presented in dimensionless form. The coordinates are normalized by the half width of the asperity and the stress components by the average pressure P_o, i.e.,

$$(\xi,\eta,\zeta) = (x_1,x_2,x_3)/a$$

and

$$(\sigma_{\xi\xi},\sigma_{\eta\eta},\sigma_{\zeta\zeta},\sigma_{\xi\eta},\sigma_{\eta\zeta},\sigma_{\zeta\xi}) = (\sigma_{11},\sigma_{22},\sigma_{33},\sigma_{12},\sigma_{23},\sigma_{31})/P_o \ .$$

The temperature rise from the cold state is $\phi = Tk/q_o a$, where q_o is the heat flux due to the average frictional load, that is, $q_o = \mu_f P_o V$. Figures 3.2 to 3.4 show the mechanical principal stresses (σ_I^M) on the trailing side with different depth, ζ, for Cases 1, 2, and 3, respectively. It is noticed that stresses rise sharply in the neighborhood of $\xi = 1$, as ζ approaches zero for Cases 1 and 2. Such stress singularities at $\xi = \pm 1$ are expected because of the discontinuities in the loading functions. Temperature fields for different cases are shown in Figures 3.5 to 3.7, in which the temperature decays rapidly with respect to the depth. Consequently, thermal stresses are compressive only in a very thin surface layer due to the thermal effect. The magnitude of compressive stresses also decreases rapidly with the increase of the depth until it becomes tensile. Figures 3.8 to 3.10 show the corresponding thermal principal stress (σ_I^T) at depths $\zeta = 10^{-1}$ and 1.0, where tensile stresses dominate, for each case. The combined effects from mechanical and thermal fields for three cases are given in Figures 3.11 to 3.13. Accordingly, the critical asperity pressure to

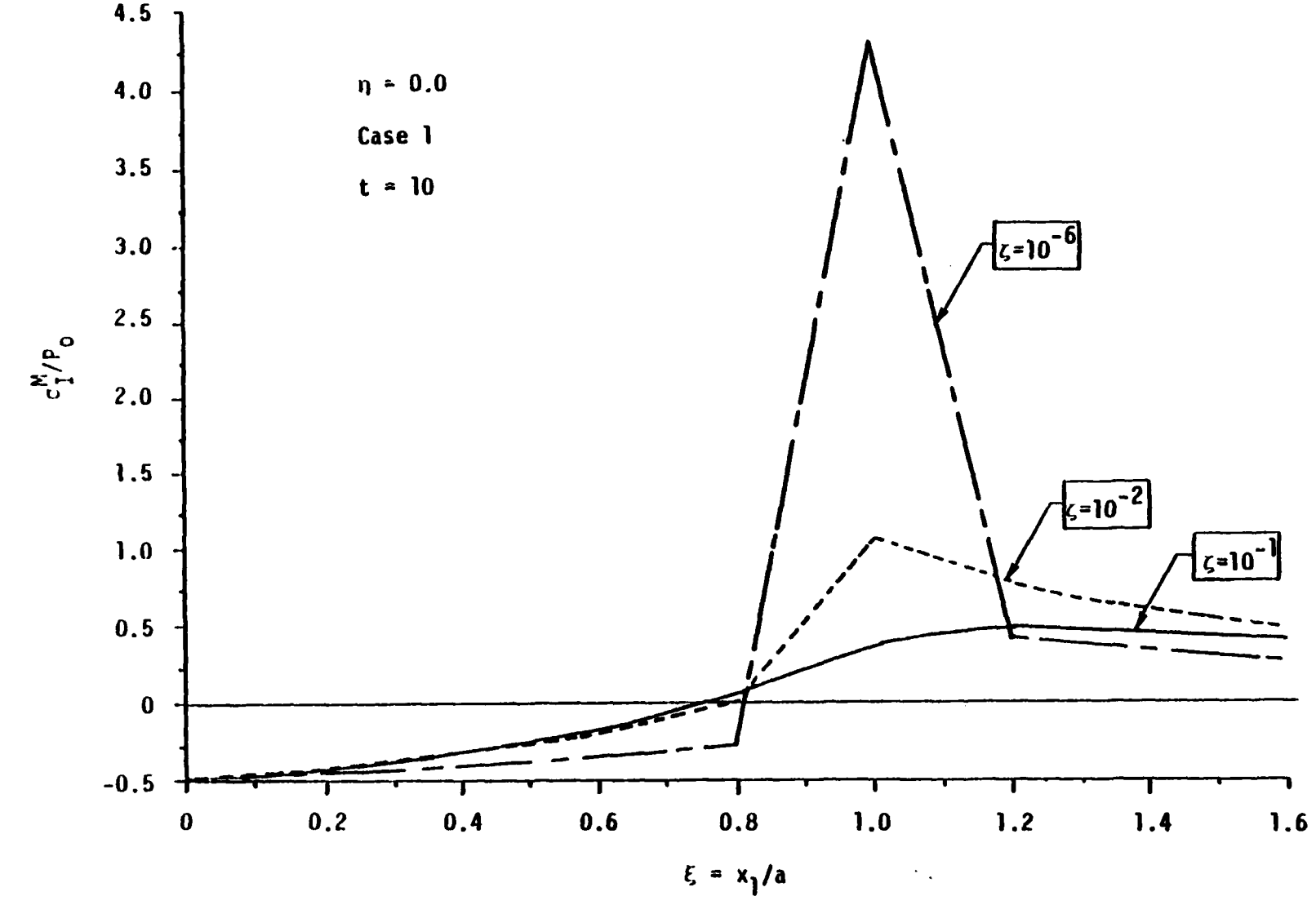

Figure 3.2. Maximum mechanical principal stresses in the surface layer (Case 1).

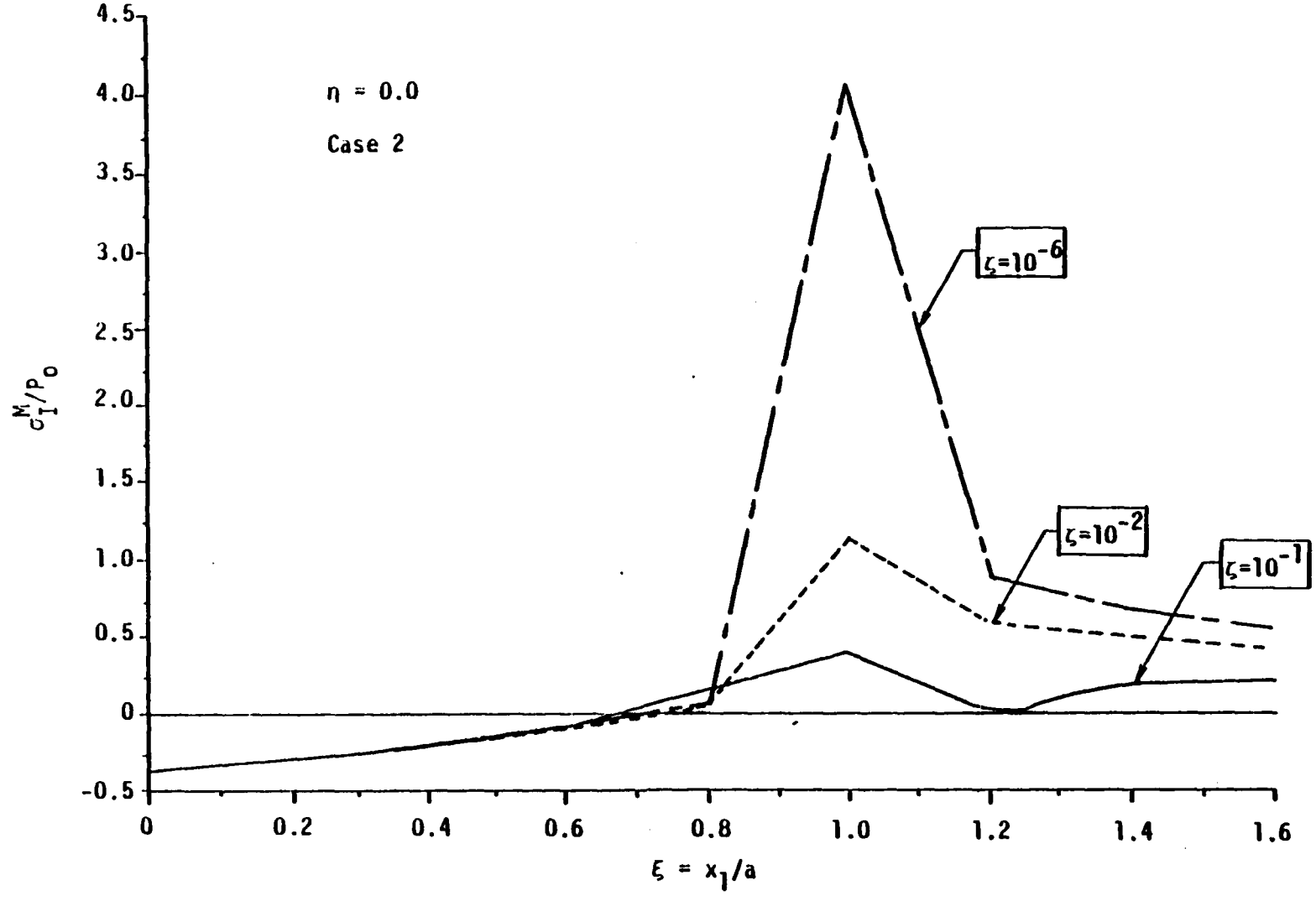

Figure 3.3. Maximum mechanical principal stresses in the surface layer (Case 2).

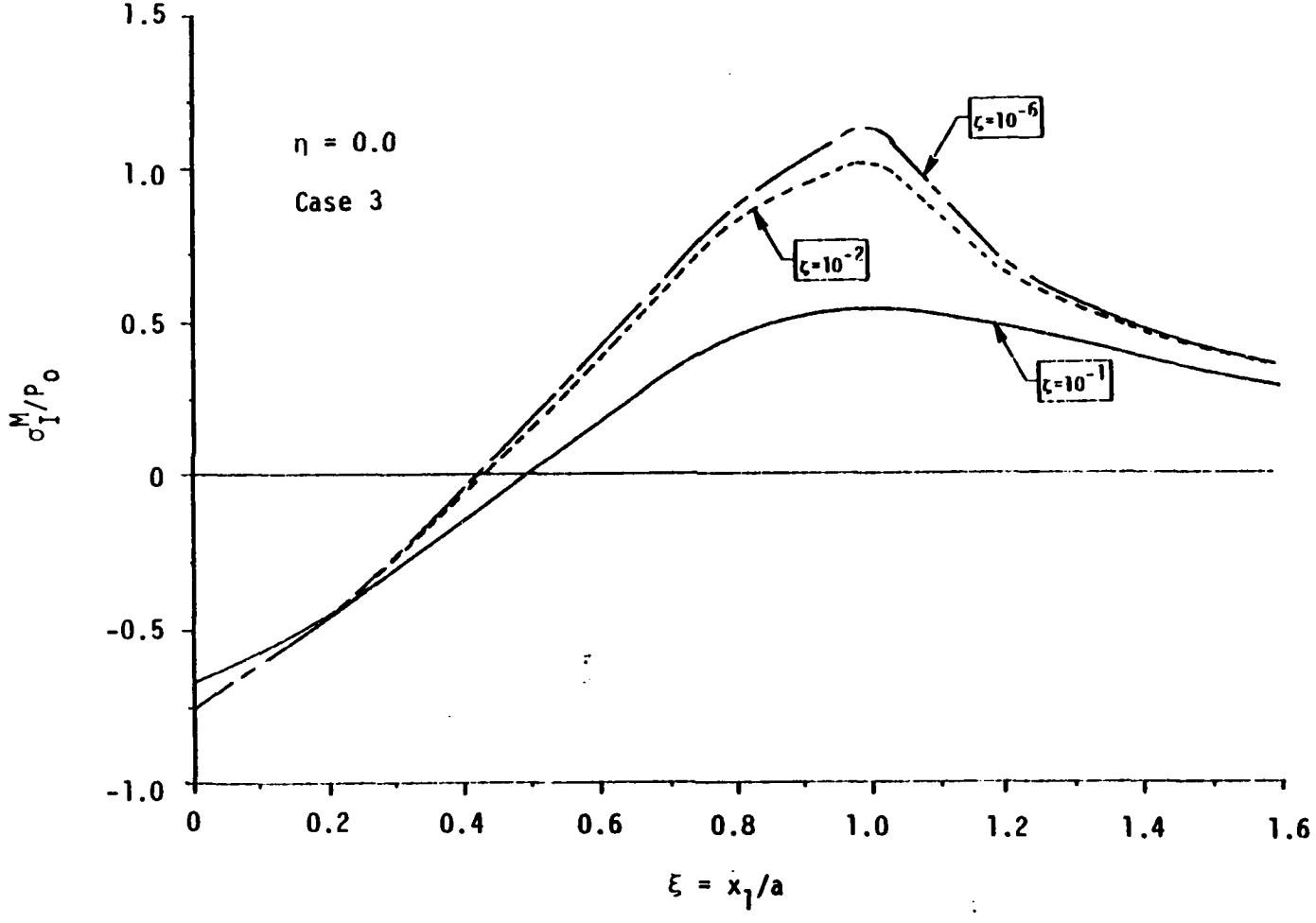

Figure 3.4. Maximum mechanical principal stresses in the surface layer (Case 3).

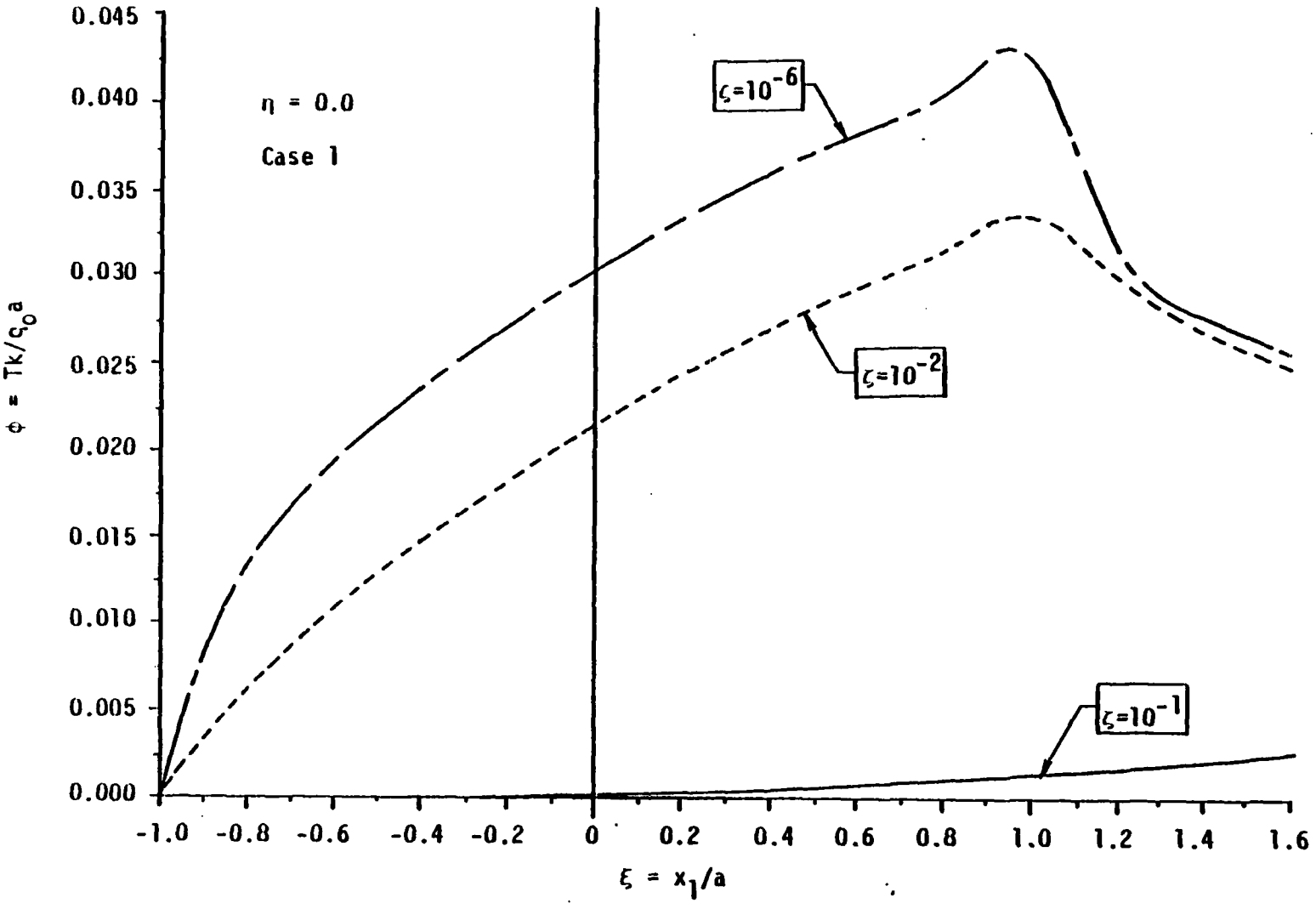

Figure 3.5. Temperature field in the surface layer (Case 1).

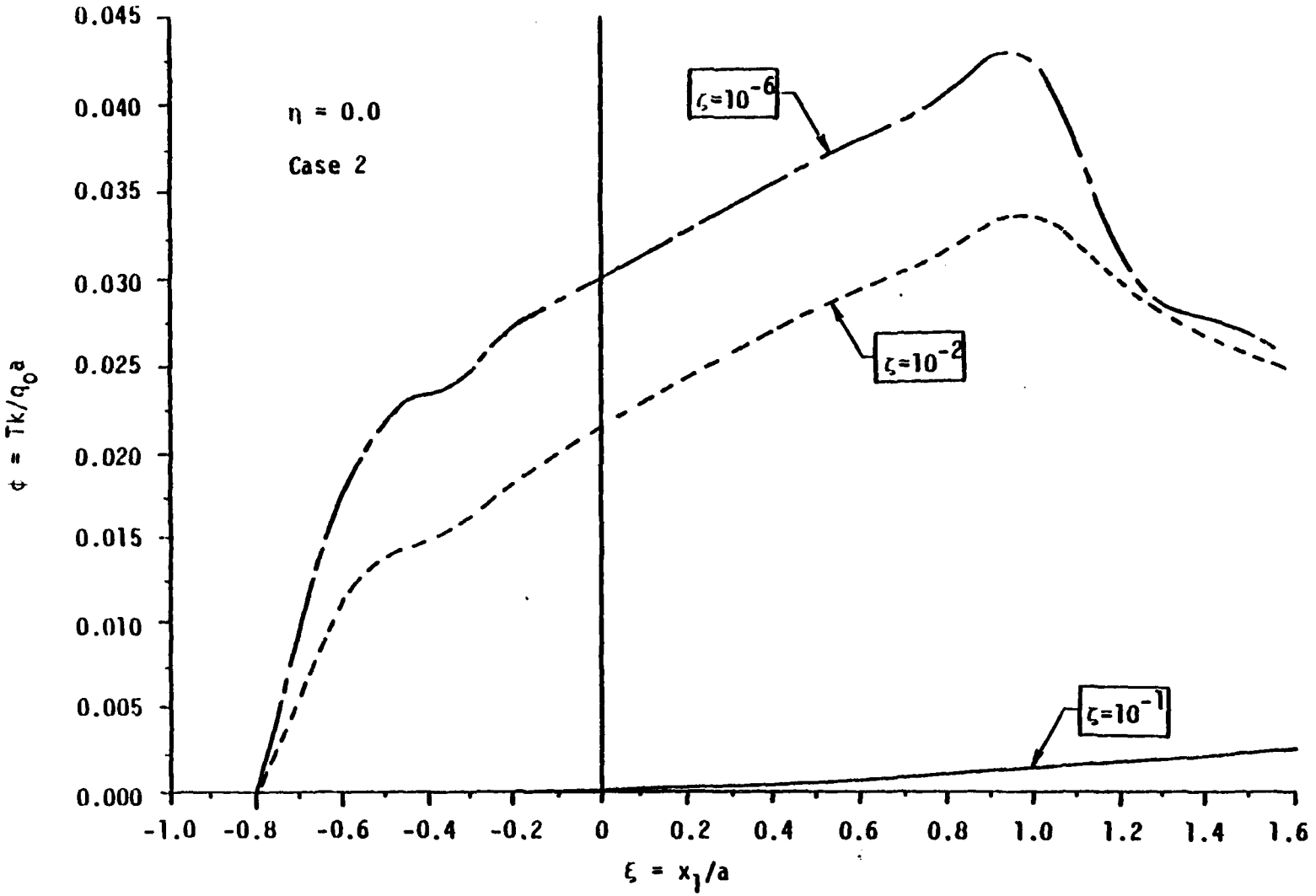

Figure 3.6. Temperature field in the surface layer (Case 2).

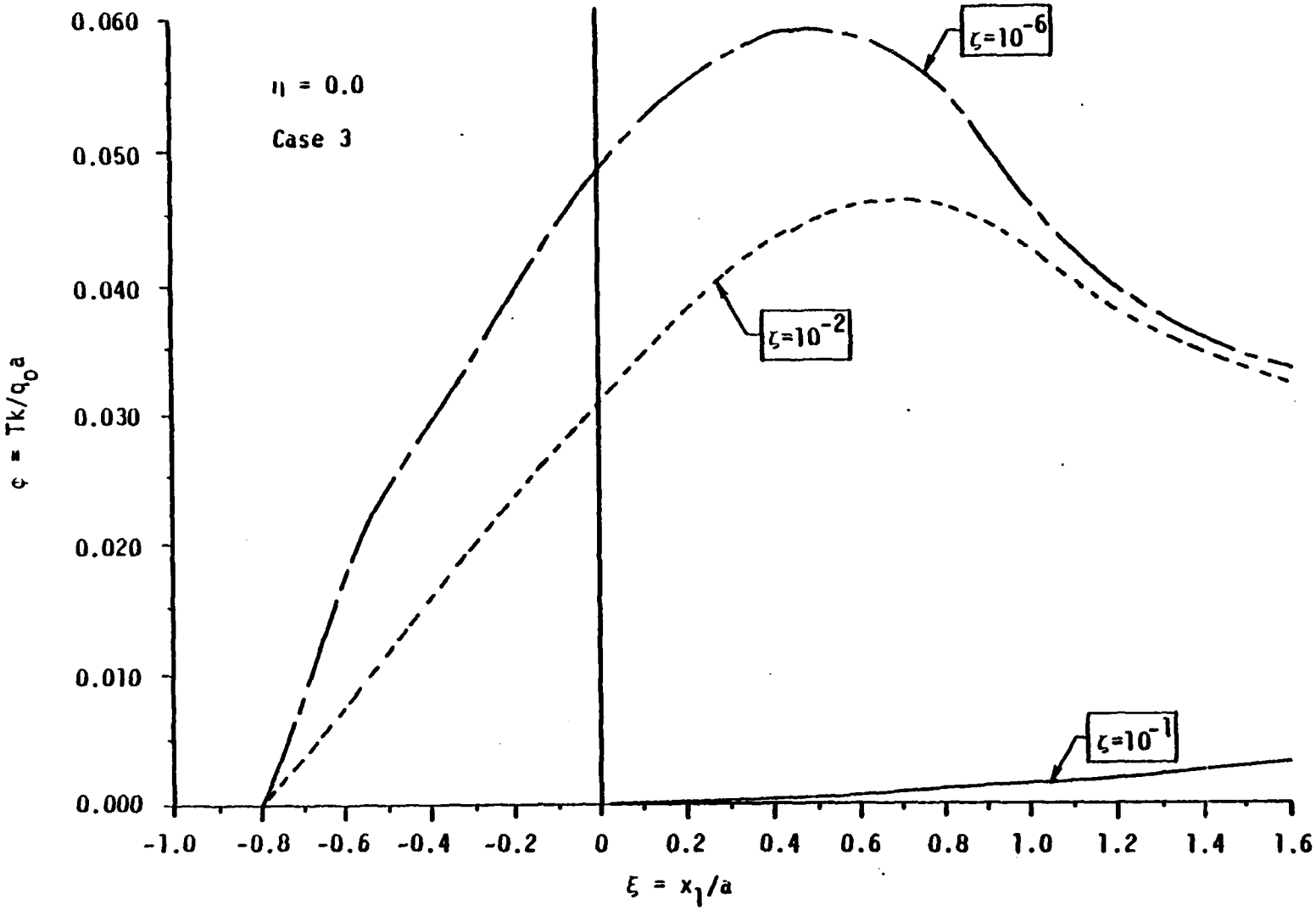

Figure 3.7. Temperature field [illegible] face layer (Case 3).

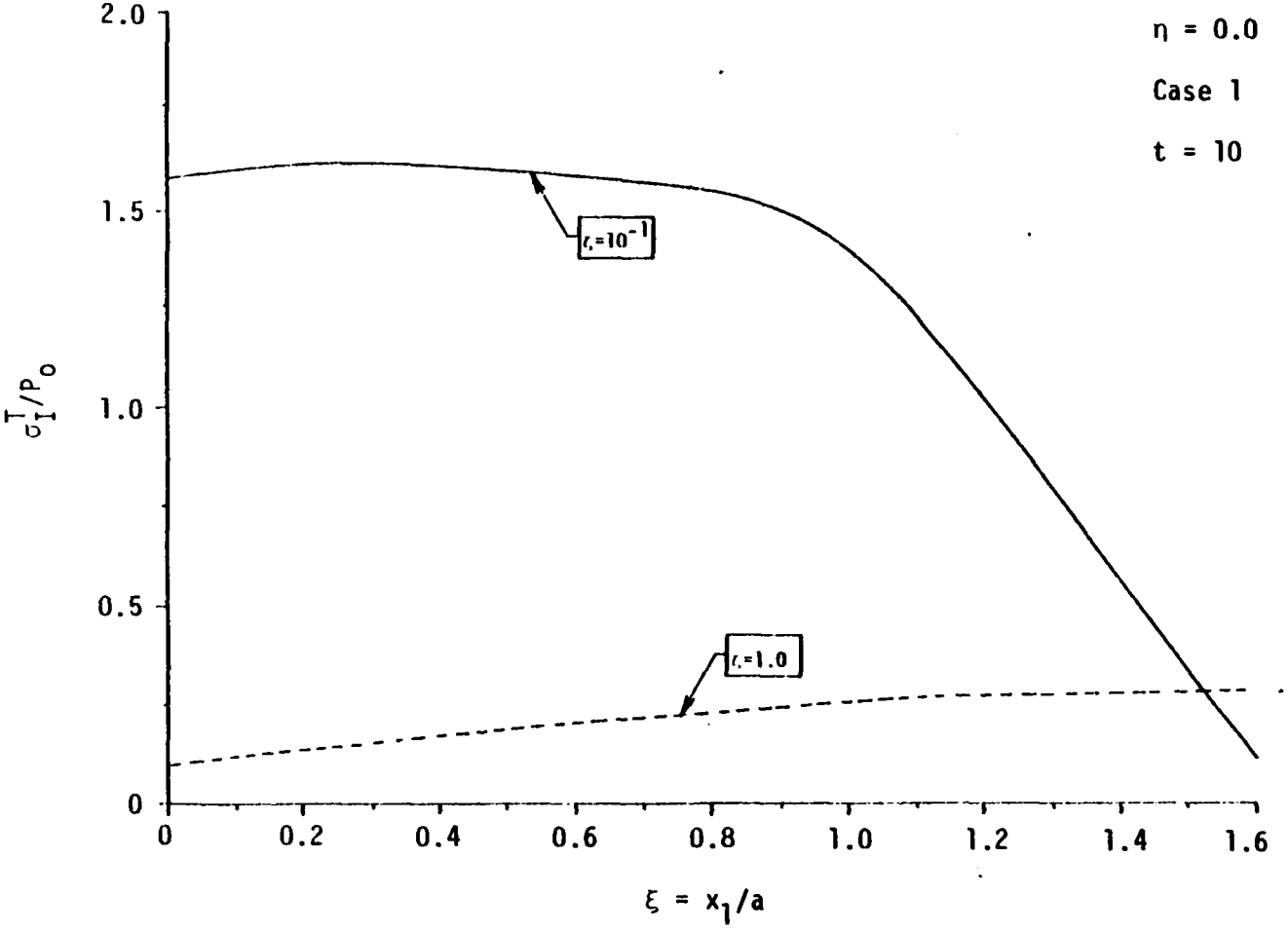

Figure 3.8. Maximum thermal principal stresses (Case 1).

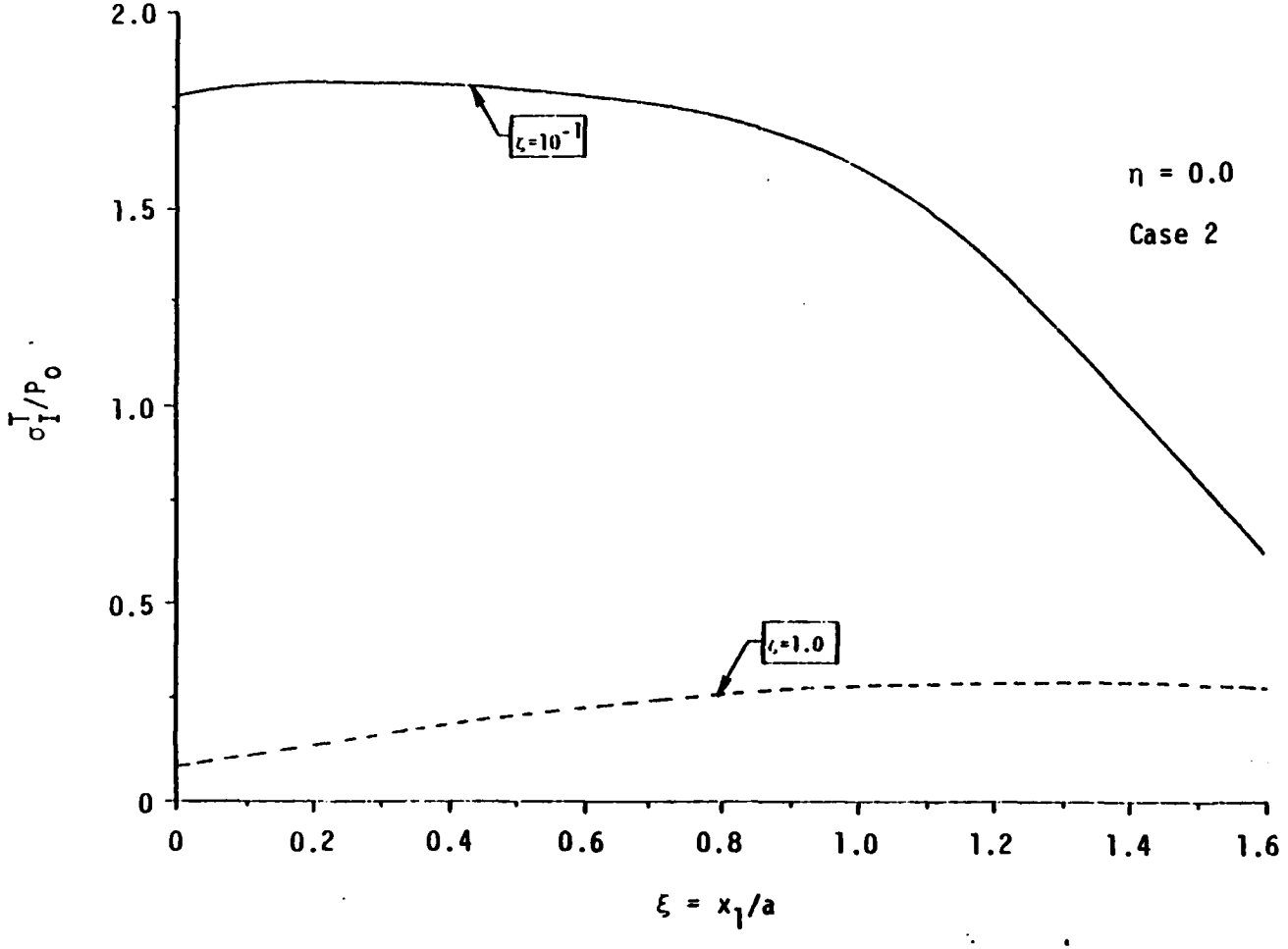

Figure 3.9. Maximum thermal principal stresses (Case 2).

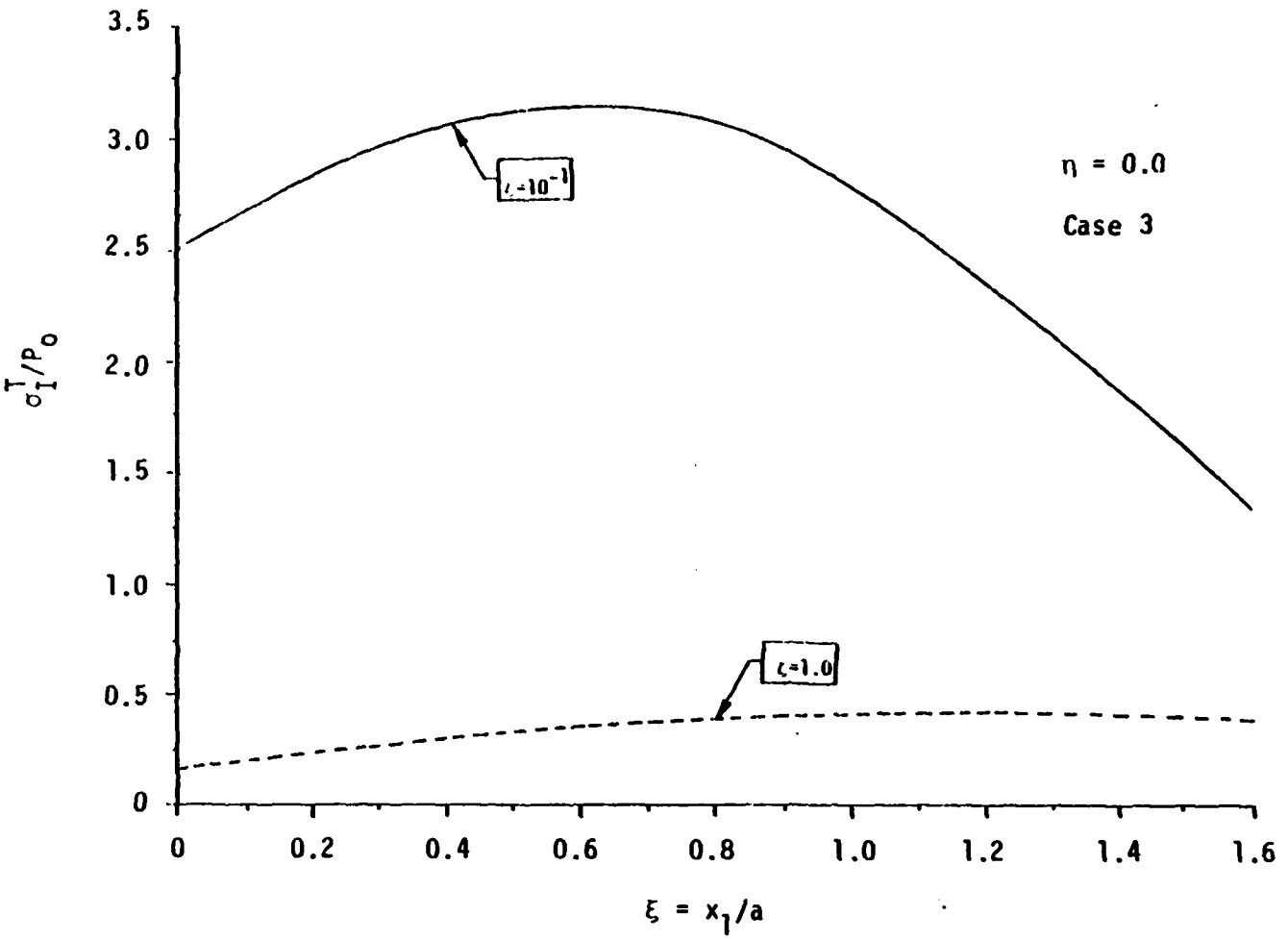

Figure 3.10. Maximum thermal principal stresses (Case 3).

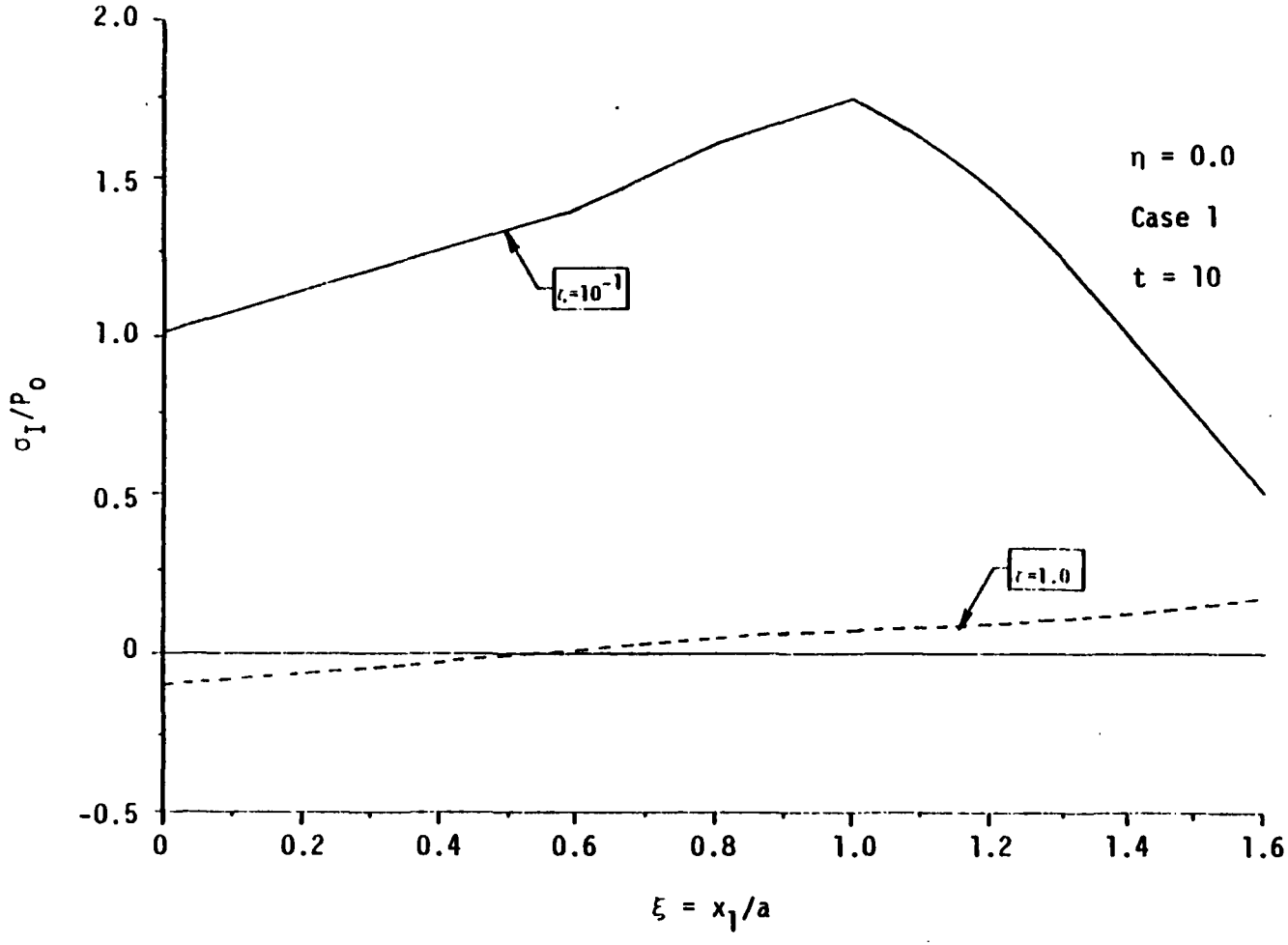

Figure 3.11. Maximum combined thermomechanical principal stress field (Case 1).

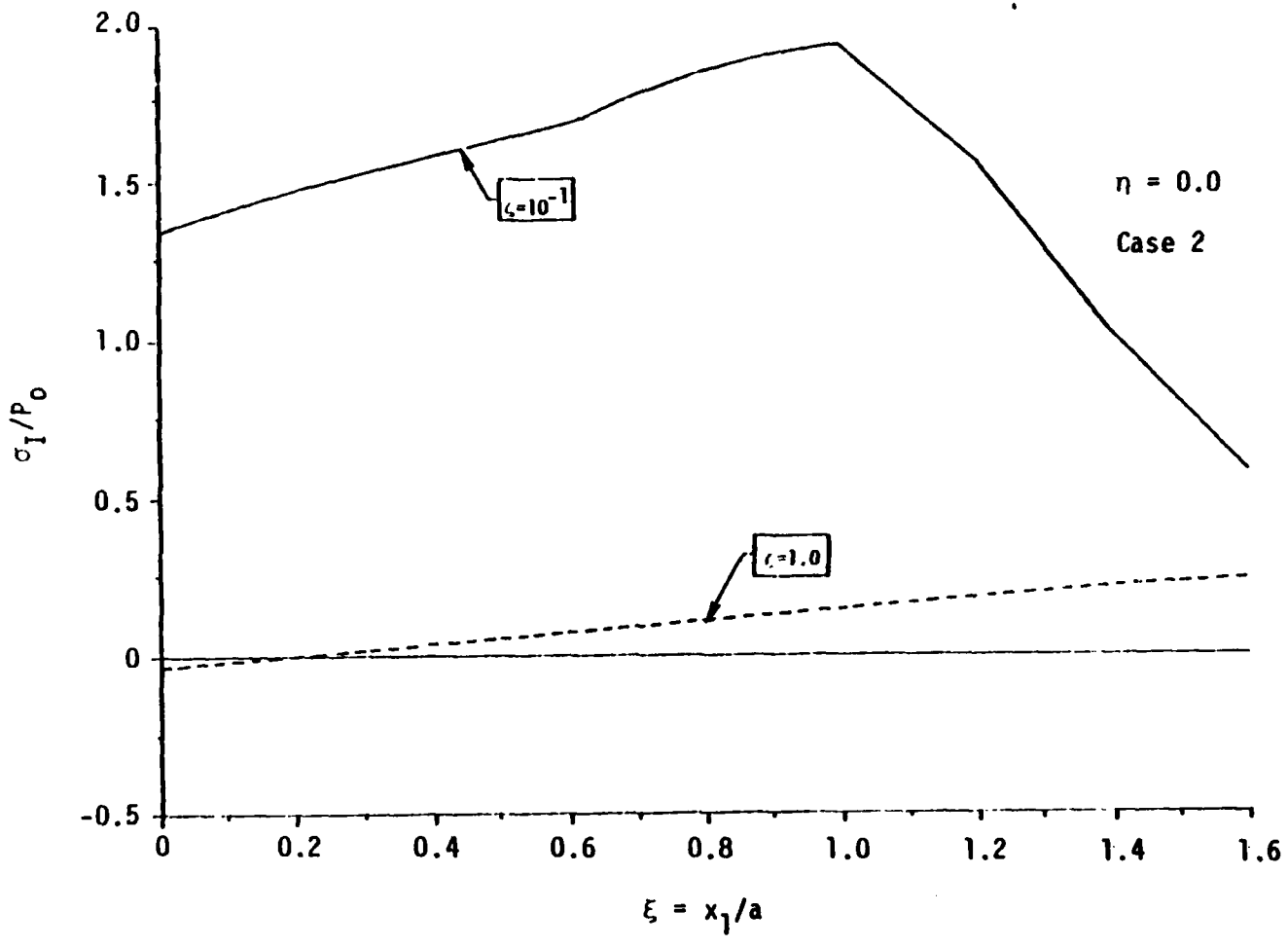

Figure 3.12. Maximum combined thermomechanical principal stress field (Case 2).

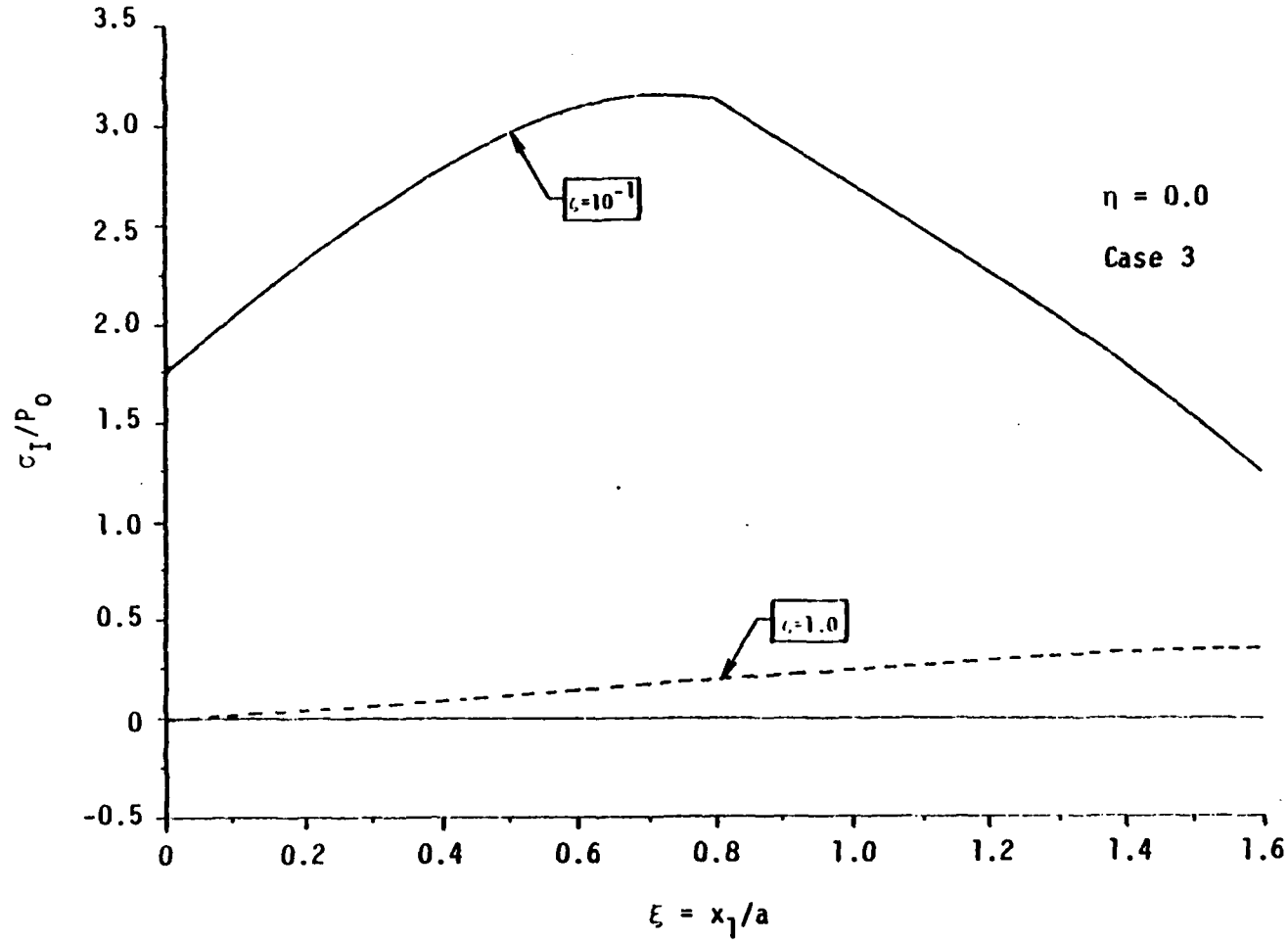

Figure 3.13. Maximum combined thermomechanical principal stress field (Case 3).

initiate cracks can be predicted. For an asperity with a size of 0.5 mm (0.02 in.), a velocity of 15 m/s (600 ips) and a coefficient of friction μ_f = 0.5, the maximum principal stress for Cases 1, 2, and 3 reaches the ultimate strengh at critical pressures of 353 MPa (51,253 psi), 318 MPa (46,083 psi), 196 MPa (28,400 psi), respectively. In all cases, heat checking by the mechanisms postulated may occur on the trailing side at a depth of 0.025 mm (0.001 in.) from the surface.

CHAPTER 4

A THREE-DIMENSIONAL MODEL OF PERIODIC MOVING ASPERITIES

4.1 Mathematical Model

The established three-dimensional theory of a single moving asperity in Chapter 3.0 is expanded to incorporate the more realistic checking failure in a friction loaded medium shown in Figure 4.1. As demonstrated by Burton [7], the hot spot at the interface between a stationary and a rotating contacting surface precesses at a regular rate. With reference to a region on the surface, the hot spot is indeed moving over the surface at a periodic regularity. Under a single severe asperity, the seal may initiate a crack. With repeated moving friction loads, the crack may be initiated at a much lower friction load and may be associated with a different fracture configuration. The geometries of the contact area and loading profiles under consideration will be classified into Cases 1, 2, and 3, which are the same as those cases in Chapter 3. Moving coordinates fixed to the center of the first moving asperity and a time coordinate, $(x_1 - x_2 - x_3, t)$, are used throughout the analysis. It is assumed that the repeated asperities occur with a period of τ and move with the same velocity (V). Therefore, the center distance between asperities ($\lambda' = V\tau/a$) will later play an important role in illustrating the cumulative effects.

The period τ is an important parameter because of the following arguments:

I. If the period is so large that the thermomechanical effect resulting from the first asperity has already died out at the time the

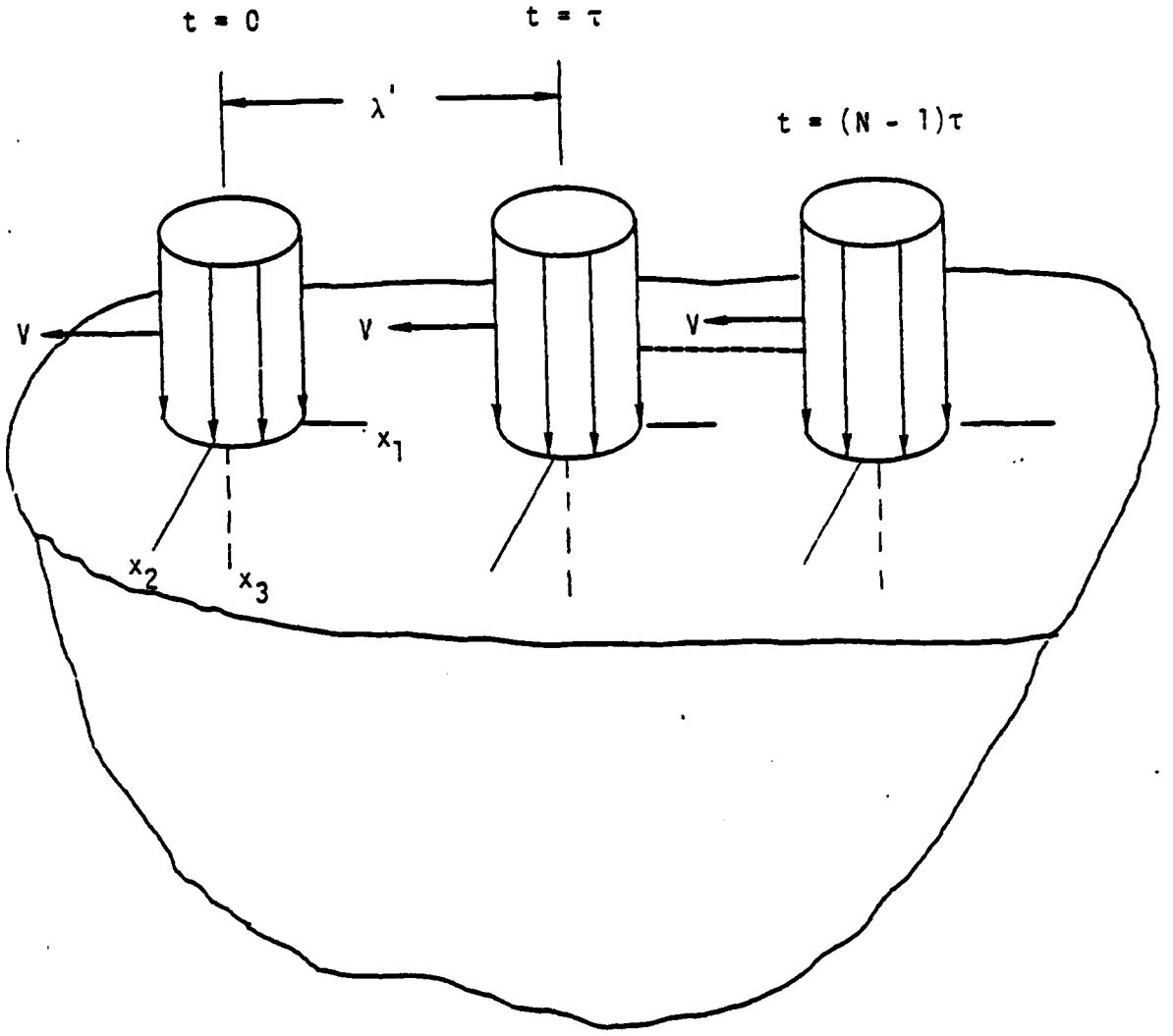

Figure 4.1. Three-dimensional model of N periodic moving asperities.

second asperity appears, then the physical and mathematical models will be those of the single moving asperity.

II. If the period is shortened so that the mechanical effect of the first asperity has dissipated, then the thermal effect, which diffuses at a slower rate, remains to affect the thermomechanical response to the following asperity.

III. If the period is very short (high frequency), then both the mechanical and the thermal responses of the first asperity could interact with the following one.

The results in Chapter 3.0 are therefore applicable to the long period excitations. Category III applies to loads traveling at wave speed. For the problem under consideration, such speeds do appear in realistic situations. Consequently, it is important to consider Category II for the present problem. It is significant to investigate first whether a bounded steady state solution exists. If it does, the thermal stress field after long term operation would also reach a steady state solution which will be obtained analytically by Fourier transform. General solutions of different cases for the mechanical, temperature, and thermal stress fields will be given in Sections 2 to 4 and numerical results will be shown in Section 5. The variables used throughout this chapter will be the same as those in previous chapters unless specified otherwise.

4.2 Mechanical Stress Field

In the Category II problem, there is no interaction between mechanical responses. The governing equations and the method of

approach for the mechanical stresses are exactly the same as those of a single asperity in Section 3.2. However, it should be mentioned that the boundary conditions for the current periodic loading problem are modified to be

$$\sigma_{3i}^{M} = -R_i \quad \text{at} \quad x_3 = 0$$

and

$$u_i \, , \; \sigma_{ij}^{M} \to 0 \quad \text{as} \quad (x_i x_i)^{1/2} \to \infty \tag{4.1}$$

where

$$R_3 = \begin{cases} P(x_1,x_2) \, , & B_j\text{: contact regions, } j = 1,\ldots,N \\ 0 \, , & \text{elsewhere} \end{cases}$$

$$R_1 = -\mu_f R_3 \, , \quad R_2 = 0$$

where P is the normal pressure distribution prescribed over the contact regions, which is quite general at this stage. N is the total number of existing moving asperities.

Following the same approach and using the same notation, the solutions subject to the boundary condition (4.1) are obtained as follows.

$$2\mu F\,\overline{\sigma}_{11}^{M} = \overline{D}\big[(s^2 - n_1^2)\,\lambda + 2\mu\,\overline{x}_1^2\big]\, e^{-n_1 x_3}$$

$$- 2\mu\big[\overline{x}_1^2 n_1 n_2 \overline{R}_3 + i\overline{x}_1(\overline{x}_2^2 N_2 + n_2 n_3)\,\overline{R}_1\big]\, e^{-n_2 x_3} \, ,$$

$$2\mu F\,\overline{\sigma}_{22}^{M} = \overline{D}\big[(s^2 - n_1^2)\,\lambda + 2\mu\,\overline{x}_2^2\big]\, e^{-n_1 x_3}$$

$$- 2\mu\big[\overline{x}_2^2 n_1 n_2 \overline{R}_3 - i\overline{x}_1\overline{x}_2^2 N_2 \overline{R}_1\big]\, e^{-n_2 x_3}$$

$$2\mu F\,\bar{\sigma}^{M}_{33} = \bar{D}[(s^2 - n_1^2)\,\lambda - 2\mu\, n_1^2]\, e^{-n_1 x_3}$$

$$+ 2\mu\, n_2(s^2 n_1 \bar{R}_3 + i n_3 \bar{x}_1 \bar{R}_1]\, e^{-n_2 x_3}\ ,$$

$$2\mu F\,\bar{\sigma}^{M}_{12} = 2\mu\, \bar{x}_1 \bar{x}_2\, \bar{D}\, e^{-n_1 x_3} - 2\mu\{\bar{x}_1 \bar{x}_2 n_1 n_2 \bar{R}_3 + \tfrac{i}{2}\, \bar{x}_2[n_2 n_3$$

$$- (\bar{x}_1^2 - \bar{x}_2^2)\, N_2]\, \bar{R}_1\}\, e^{-n_2 x_3}\ ,$$

$$2\mu F\,\bar{\sigma}^{M}_{23} = -2\mu i\, \bar{x}_2 n_1\, \bar{D}\, e^{-n_1 x_3} + \mu\{i\bar{x}_2 n_1 (s^2 + n_2^2)\, \bar{R}_3$$

$$- 2\bar{x}_1 \bar{x}_2 n_1 n_2 \bar{R}_1\}\, e^{-n_2 x_3}\ ,$$

$$2\mu F\,\bar{\sigma}^{M}_{31} = -2\mu i\, \bar{x}_1 n_1\, \bar{D}\, e^{-n_1 x_3} + \mu\{i\bar{x}_1 n_1 (s^2 + n_2^2)\, \bar{R}_3$$

$$- [\bar{x}_2^2 N_1 + n_3(n_2^2 + \bar{x}_1^2)]\, \bar{R}_1\}\, e^{-n_2 x_3} \qquad (4.2)$$

where $\bar{D} = n_3 \bar{R}_3 + i n_2 \bar{x}_1 \bar{R}_1$, the remaining coefficients are defined as in Chapter 3.0.

4.3 Temperature Field

It is assumed that the temperature field has a slow dissipation rate and remains at an appreciable magnitude during the passage of the second moving asperity. In other words, at every traverse of an asperity, the corresponding initial temperature is modified after the passage of the preceding asperity. The analysis therefore proceeds with a

time sequence, at the period of the asperity occurrence (τ), to solve the transient temperature field of each asperity in accordance with the initial condition resulting from the previous response. Let T_α *denote the transient solution due to the* α*th moving asperity appearing* at the instant $t = (\alpha - 1)\,\tau$. The governing equation for unsteady heat condition in terms of the coordinate system $(x_1 - x_2 - x_2, t)$ has the form

$$\partial_{ii}T_\alpha = \frac{1}{\kappa}\,(\partial_t T_\alpha + V\partial_1 T_\alpha)\ , \qquad t \geq (\alpha - 1)\,\tau\ . \tag{4.3}$$

The solution of Equation (4.3) must satisfy the following initial and boundary conditions

$$T_\alpha = U_\alpha \quad \text{when} \quad t = (\alpha - 1)\,\tau \tag{4.4}$$

where U_α is the initial temperature resulting from the preceding asperities,

$$k\partial_3 T_\alpha = Q_\alpha = -\mu_f V \begin{cases} P(x_1,x_2),\ B_j\text{: contact regions, } j = 1,2,\ldots,\alpha \\ 0 \qquad\quad ,\ \text{elsewhere} \end{cases} . \tag{4.5}$$

At $x_3 = 0$,

$$T_\alpha \to 0 \quad \text{as} \quad x_3 \to \infty$$

where $\alpha = 1,2,\ldots,N$.

Equations (4.3) to (4.5) can be solved by Green's function approach. First, consider $\alpha = 1$ and denote T_1 as the temperature above the traction-free ambient. Then, setting

$$T_1 = \omega_1 \exp[\tfrac{V}{2\kappa}\,(x_1 - \tfrac{V}{2}\,t)]\ ,$$

we have

$$\partial_{ii}\omega_1 = \frac{1}{\kappa}\,\partial_t\omega_1 \ ,$$

$$\omega_1 = 0 \quad \text{at} \quad t = 0 \ ,$$

$$k\partial_3\omega_1 = Q_1 \cdot \exp[-\frac{V}{2\kappa}\,(x_1 - \frac{V}{2}\,t)] \ ,$$

for which the Green's function solution can be expressed as

$$G(x_1',x_2',t') = \frac{1}{4\rho c[\pi\kappa(t - t')]^{3/2}} \exp\left\{-\frac{[(x_1 - x_1')^2 + (x_2 - x_2')^2 + x_3^2]}{4\kappa(t - t')}\right\}$$

and hence,

$$\omega_1 = \mu_f V \int_0^t \int_{B_1} P(x_1',x_2') \cdot \exp[-\frac{V}{2\kappa}\,(x_1' - \frac{V}{2}\,t')]\, G(x_1',x_2',t)\, dx_1'\, dx_2'\, dt'$$

and

$$T_1 = \mu_f V \int_0^t \int_{B_1} P(x_1',x_2') \cdot g(x_1 - x_1',x_2 - x_2',x_3,t - t')\, dx_1'\, dx_2'\, dt' \qquad (4.6)$$

where

$$g(x_1,x_2,x_3,t) = \frac{1}{4\rho c(\pi\kappa t)^{3/2}} \exp\left\{-\frac{(x_1 - Vt)^2 + x_2^2 + x_3^2}{4\kappa t}\right\} \qquad (4.7)$$

which is essentially the Green's function solution for Equations (4.3) and (4.5).

Now, considering $\alpha = 2$, we have

$$\partial_{ii}T_2 = \frac{1}{\kappa}\,(\partial_t T_2 + V\partial_1 T_2) \ , \qquad t \geq \tau$$

$$T_2 = U_2 \quad \text{at} \quad t = \tau \tag{4.8}$$

and

$$k\partial_3 T_2 = Q_2 = -\mu_f V \begin{cases} P(x_1,x_2) , & B_1 \text{ and } B_2 \\ 0 , & \text{elsewhere} \end{cases} \quad \text{at} \quad x_3 = 0 .$$

Note that the initial temperature can be written as $U_2 = T_1(x_1,x_2,x_3,\tau)$, where T_1 is given in Equation (4.6).

The solution of Equation (4.8) can be readily determined, which is

$$T_2 = \rho c \int_{-\infty}^{\infty}\int_{-\infty}^{\infty}\int_0^{\infty} T_1(x_1',x_2',x_3',\tau) \cdot g(x_1 - x_1',x_2 - x_2',x_3 - x_3',t)$$

$$dx_3' \, dx_2' \, dx_1' + \mu_f V \sum_{j=1}^{2} \int_\tau^t \int_{B_j} P(x_1',x_2') \cdot g(x_1 - x_1',x_2 - x_2',x_3,t - t')$$

$$dx_1' \, dx_2' \, dt' . \tag{4.9}$$

Similarly, the recurrence formula can be obtained for subsequent temperature fields. Therefore, the transient solution for the time after $(N - 1)\,\tau$ has the following form

$$T_N = \rho c \int_{-\infty}^{\infty}\int_{-\infty}^{\infty}\int_0^{\infty} T_{N-1}(x_1',x_2',x_3',(N - 1)\,\tau) \cdot$$

$$\cdot g(x_1 - x_1',x_2 - x_2',x_3 - x_3',t) \, dx_3' \, dx_2' \, dx_1' + \mu_f V \sum_{j=1}^{N} \int_{(N-1)\tau}^{t} \int_{B_j}$$

$$\cdot P(x_1',x_2') \cdot g(x_1 - x_1',x_2 - x_2',x_3,t - t') \, dx_1' \, dx_2' \, dt' \tag{4.10}$$

We observe that the first term of Equation (4.10) converges uniformly to zero as t approaches infinity. Hence, for the steady state solution, Equation (4.10) yields

$$T = \mu_f V \lim_{t\to\infty} \left[\sum_{j=1}^{N} \int_{(N-1)\tau}^{t} \int_{B_j} P(x_1', x_2') \cdot g(x_1 - x_1', x_2 - x_2', x_3, t - t') \cdot dx_1' \, dx_2' \, dt' \right] \tag{4.11}$$

Making use of the succeeding result

$$\lim_{t\to\infty} \int_{(N-1)\tau}^{t} g(x_1 - x_1', x_2 - x_2', x_3, t - t') \, dt'$$

$$= \frac{e^{V(x_1 - x_1')/2\kappa}}{\pi^{3/2} kR} \lim_{t\to\infty} \int_{R/2\sqrt{t-(N-1)\tau}}^{\infty} \exp\left[- \left(y^2 + \frac{V^2 R^2}{16\kappa^2 y^2} \right) \right] dy$$

$$= \frac{1}{2\pi kR} \exp\{ - V[R - (x_1 - x_1')]/2\kappa \} ,$$

in Equation (4.11), we can rewrite the steady state solution as

$$T = \frac{\mu_f V}{2\pi k} \sum_{j=1}^{N} \int_{B_j} P(x_1', x_2') \cdot \frac{\exp\{ - V[R - (x_1 - x_1')]/2\kappa \}}{R} \, dx_1' \, dx_2' . \tag{4.12}$$

The expression above, while leading to the solution of the temperature field, cannot be applied readily in solving the thermal stress field. An alternative method with double Fourier transform is then used. We start by taking the transform of the heat equation, using the corresponding initial and boundary conditions for T_N, and then simplifying the result by the relation

$$\bar{T}_N = \bar{\phi}_N \, e^{-\kappa(s^2+in)\, t} \tag{4.13}$$

results in:

$$D^2 \bar{\phi}_N = \frac{1}{\kappa} \partial_t \bar{\phi}_N \, , \qquad t \geq (N-1)\,\tau \, , \quad 0 \leq x_3 < \infty$$

$$\bar{\phi}_N = \bar{U}_N \, , \qquad t = (N-1)\,\tau$$

$$kD \, \bar{\phi}_N = \bar{Q}_N \cdot e^{\kappa(s^2+in)t} \tag{4.14}$$

where

$$\bar{U}_N = \bar{T}_{N-1}(\bar{x}_1, \bar{x}_2, x_3, (N-1)\,\tau) \, .$$

Equation (4.14) leads to the solution

$$\bar{\phi}_N = \rho c \int_0^\infty \bar{T}_{N-1}(\bar{x}_1, \bar{x}_2, x_3', (N-1)\,\tau) \cdot g_1(x_3 - x_3', t)\, dx_3'$$

$$- \bar{Q}_N(\bar{x}_1, \bar{x}_2) \int_{(N-1)\tau}^{t} e^{\kappa(s^2+in)t'} \cdot g_1(x_3, t - t')\, dt' \tag{4.15}$$

where

$$g_1(x_3, t) = \frac{1}{\rho c (\pi \kappa t)^{1/2}} \, e^{-\frac{x_3^2}{4\kappa t}} \, . \tag{4.16}$$

Equations (4.13), (4.15), and (4.16) lead to

$$\bar{T}_N = \frac{\rho c e^{-\kappa(s^2+in)\,t}}{(\pi\kappa t)^{1/2}} \int_0^{\infty} \bar{T}_{N-1}(\bar{x}_1, \bar{x}_2, x_3', (N-1)\,\tau) \cdot e^{-\frac{(x_3 - x_3')^2}{4\kappa t}}\, dx_3'$$

$$- \frac{\bar{Q}_N(\bar{x}_1, \bar{x}_2)}{\rho c(\pi\kappa)^{1/2}} \int_{(N-1)\tau}^{t} \frac{\exp\{-[\kappa(s^2 + in)(t - t') + x_3^2/4\kappa(t - t')]\}}{(t - t')^{1/2}}\, dt' \quad . \tag{4-17}$$

Introduce the change of variable as follows

$$z = (t - t')^{1/2} \ ,$$

then transform the last term of Equation (4.17) into the form

$$- \frac{2\bar{Q}_N(\bar{x}_1, \bar{x}_2)}{\rho c(\pi\kappa)^{1/2}} \int_0^{[t-(N-1)\tau]^{1/2}} e^{-[\kappa(s^2+in)z^2 + x_3^2/4\kappa z^2]}\, dz \ . \tag{4.18}$$

By letting $t \to \infty$, the first term of Equation (4.17) vanishes. In connection with the expression (4.18), it follows that the steady state solution can be written as

$$\bar{T} = \frac{-2\bar{Q}_N(\bar{x}_1, \bar{x}_2)}{\rho c(\pi\kappa)^{1/2}} \int_0^{\infty} e^{-[\kappa(s^2+in)z^2 + x_3^2/4\kappa z^2]}\, dz \ . \tag{4.19}$$

Note that

$$\int_0^{\infty} x^{\nu-1} \exp(-\beta x^u - \gamma x^{-u})\, dx = \frac{2}{u} \left(\frac{\gamma}{\beta}\right)^{\frac{\nu}{2u}} K_{\frac{\nu}{u}}(2\sqrt{\beta\gamma})$$

where $K_{\frac{\nu}{u}}$ is the modified Bessel function of the second kind of order $\frac{\nu}{u}$. Therefore, Equation (4.19) becomes

$$\bar{T} = \frac{-2\bar{Q}_N(\bar{x}_1,\bar{x}_2)}{\rho c(\pi\kappa)^{1/2}} \cdot \left[\frac{x_3^2}{4\kappa^2(s + in)}\right]^{1/4} K_{\frac{1}{2}}[x_3(s^2 + in)^{1/2}] .$$

Further simplification can be made by using the identity

$$K_{\frac{1}{2}}(z) = (\frac{\pi}{2z})^{1/2} e^{-z} .$$

By the same notations as in Section (3.2),

$$\bar{T} = \frac{\bar{Q}_N}{k} e^{-\omega x_3} [C_1 \cos(\theta x_3) + C_2 \sin(\theta x_3)] \qquad (4.20)$$

which is the steady state temperature field due to N periodic moving asperities and will be used to derive the corresponding thermal stress field in the following section.

4.4 Thermal Stress Field

The governing equations and boundary conditions are the same as given in Equations (3.38) to (3.41), their transformed expressions are also the same as Equations (3.42) to (3.52). In view of the temperature expression (4.20) which is similar to the temperature Equation (3.31) for a single moving asperity, the solution approach in Section 3.2 can be applied. However, a different method of Inverse Differential Operator is presented here so that we can check the solutions from both methods.

Equations (3.42) through (3.44) form a system of three simultaneous linear differential equations. The dependent variables $\bar{u}_i$ are to be solved. The system can be rewritten as

$$\Delta\bar{u}_i = \Delta_i \ , \qquad i = 1,2,3 \tag{4.21}$$

where Δ is the determinant of the system,

$$\Delta = \begin{vmatrix} D^2 - (a_1\bar{x}_1^2 + \bar{x}_2^2) & -a_2\bar{x}_1\bar{x}_2 & -ia_2\bar{x}_1 D \\ -a_2\bar{x}_1\bar{x}_2 & D^2 - (a_1\bar{x}_2^2 + \bar{x}_1^2) & -ia_2\bar{x}_2 D \\ -ia_2\bar{x}_1 D & -ia_2\bar{x}_2 D & a_1 D^2 - s^2 \end{vmatrix}$$

$$= a_1(D^2 - s^2)^3$$

and Δ_i's are

$$\Delta_1 = \begin{vmatrix} -ia_3\bar{x}_1\bar{T} & -a_2\bar{x}_1\bar{x}_2 & -ia_2\bar{x}_1 D \\ -ia_3\bar{x}_2\bar{T} & D^2 - (a_1\bar{x}_2^2 + \bar{x}_1^2) & -ia_2\bar{x}_2 D \\ a_3 D\bar{T} & -ia_2\bar{x}_2 D & a_1 D^2 - s^2 \end{vmatrix}$$

$$= -ia_3\bar{x}_1(D^2 - s^2)^2\,\bar{T} \ ,$$

$$\Delta_2 = \begin{vmatrix} D^2 - (a_1\bar{x}_1^2 + \bar{x}_2^2) & -ia_3\bar{x}_1\bar{T} & -ia_2\bar{x}_1 D \\ -a_2\bar{x}_1\bar{x}_2 & -ia_3\bar{x}_2\bar{T} & -ia_2\bar{x}_2 D \\ -ia_2\bar{x}_1 D & a_3 D\bar{T} & a_1 D^2 - s^2 \end{vmatrix}$$

$$= -ia_3\bar{x}_2(D^2 - s^2)^2\,\bar{T}\,,$$

$$\Delta_3 = \begin{vmatrix} D^2 - (a_1\bar{x}_1^2 + \bar{x}_2^2) & -a_2\bar{x}_1\bar{x}_2 & -ia_3\bar{x}_1\bar{T} \\ -a_2\bar{x}_1\bar{x}_2 & D^2 - (a_1\bar{x}_2^2 + \bar{x}_1^2) & -ia_3\bar{x}_2\bar{T} \\ -ia_2\bar{x}_1 D & -ia_2\bar{x}_2 D & a_3 D\bar{T} \end{vmatrix}$$

$$= a_3 D(D^2 - s^2)^2\,\bar{T}\,.$$

Thus the particular solutions $\bar{u}_i^p$ will be determined by the application of Cramer's rule.

$$\bar{u}_1^p = \frac{\Delta_1}{\Delta} = \frac{-ia_3\bar{x}_1}{a_1} \cdot (D^2 - s^2)^{-1}\,\bar{T}\,,$$

$$\bar{u}_2^p = \frac{\Delta_2}{\Delta} = \frac{-ia_3\bar{x}_2}{a_1} \cdot (D^2 - s^2)^{-1}\,\bar{T}\,,$$

$$\bar{u}_3^p = \frac{\Delta_3}{\Delta} = \frac{a_3}{a_1} \cdot D(D^2 - s^2)^{-1}\,\bar{T}\,. \qquad (4.22)$$

Rewrite Equation (4.20) and its derivative with respect to x_3 as

$$T = e^{-\omega x_3}[F' \cos(\theta x_3) + G' \sin(\theta x_3)]$$

and

$$D\overline{T} = e^{-\omega x_3}[F_1' \cos(\theta x_3) + G_1' \sin(\theta x_3)] \qquad (4.23)$$

respectively, where

$$F' = \frac{\overline{Q}_N}{k} C_1 , \qquad G' = \frac{\overline{Q}_N}{k} C_2 ,$$

$$F_1' = \theta G - \omega F , \qquad G_1' = -(\omega G + \theta F) .$$

In accordance with Equation (4.23), we solve Equation (4.22) as follows.

$$\overline{u}_1^p = \frac{-ia_3\overline{x}_1}{a_1} \cdot (D^2 - s^2)^{-1} \left\{e^{-\omega x_3} [F' \cos(\theta x_3) + G' \sin(\theta x_3)]\right\}$$

$$= \frac{-ia_3\overline{x}_1}{a_1} e^{-\omega x_3} \cdot (D^2 - 2\omega D + \theta^2)^{-1} [F' \cos(\theta x_3) + G' \sin(\theta x_3)]$$

$$= \frac{ia_3\overline{x}_1}{2a_1\omega} e^{-\omega x_3} \cdot D^{-1} [F' \cos(\theta x_3) + G' \sin(\theta x_3)]$$

$$= \frac{-ia_3\overline{x}_1}{2a_1\omega\theta} [G' \cos(\theta x_3) - F' \sin(\theta x_3)] . \qquad (4.24)$$

Note that use has been made of the fact that

$$\omega^2 = s^2 + \vartheta^2 .$$

In a similar fashion we obtain

$$\bar{u}_2^p = \frac{-ia_3\bar{x}_2}{2a_1\omega\theta}\,[G' \cos(\theta x_3) - F' \sin(\theta x_3)]\,, \tag{4.25}$$

$$\bar{u}_3^p = \frac{a_3}{a_1} \cdot (D^2 - s^2)^{-1}\, e^{-\omega x_3}\,[F_1' \cos(\theta x_3) + G_1' \sin(\theta x_3)]$$

$$= \frac{a_3}{2a_1\omega\theta}\, e^{-\omega x_3}\,[G_1' \cos(\theta x_3) - F_1' \sin(\theta x_3)]\,. \tag{4.26}$$

The complementary solution is determined by $\Delta\bar{u}_i = 0$ which is equivalent to

$$(D^2 - s^2)^3\,(\bar{u}_1^C, \bar{u}_2^C, \bar{u}_3^C) = 0$$

of which the solutions, with the consideration of the regularity condition, are

$$\bar{u}_i^C = (A_i' + B_i' x_3)\, e^{-sx_3}\,, \qquad i = 1,2,3 \tag{4.27}$$

where A_i''s are unknown constants which are to be determined by boundary conditions. B_i''s are expressed in terms of A_i''s as shown below.

$$B_1' = -\frac{a_2}{a_2 + 2} \cdot \frac{\bar{x}_1}{s}\,(\bar{x}_1 A_1' + \bar{x}_2 A_2' - isA_3')\,,$$

$$B_2' = -\frac{a_2}{a_2 + 2} \cdot \frac{\bar{x}_2}{s}\,(\bar{x}_1 A_1' + \bar{x}_2 A_2' - isA_3')\,,$$

$$B_3' = i\,\frac{a_2}{a_2 + 2}\,(\bar{x}_1 A_1' + \bar{x}_2 A_2' - isA_3')\,. \tag{4.28}$$

According to Equations (4.24) to (4.27), the general solutions, $\bar{u}_i = \bar{u}_i^C + \bar{u}_i^P$, have the form

$$\bar{u}_i = (A_i' + B_i' x_3)\, e^{-sx_3} + [C_i' \cos(\theta x_3) + D_i' \sin(\theta x_3)]\, e^{-\omega x_3} \quad (4.29)$$

in which

$$C_r' = \frac{-ia_3\bar{x}_r}{2a_1\omega\theta} G' , \qquad D_r' = \frac{ia_3\bar{x}_r}{2a_1\omega\theta} F' , \qquad r = 1,2$$

$$C_3' = \frac{a_3}{2a_1\omega\theta} G_1' , \qquad D_3' = \frac{-a_3}{2a_1\omega\theta} F_1'$$

In view of Equations (3.47), (3.49), and (3.50) and taking account of traction-free boundary conditions leads to a system of three simultaneous equations

$$D\bar{u}_1 - i\bar{x}_1\bar{u}_3 = 0 ,$$

$$D\bar{u}_2 - i\bar{x}_2\bar{u}_3 = 0 ,$$

$$-ia_4(\bar{x}_1\bar{u}_1 + \bar{x}_2\bar{u}_2) + a_1 D\bar{u}_3 - a_3\bar{T} = 0 . \quad (4.30)$$

Substituting expression of $\bar{T}$ (4.23) and $\bar{u}_i$ (4.28) into Equations (4.29) to solve three unknowns A_i''s, we have

$$A_1' = \frac{ia_3\bar{x}_1}{2a_1a_2ks\omega\theta} [(a_1\omega - s)\, C_2 + a_1\theta\, C_1] ,$$

$$A_2' = \frac{ia_3\bar{x}_2}{2a_1a_2ks\omega\theta}\left[(a_1\omega - s)\,C_2 + a_1\,\theta\,C_1\right],$$

$$A_3' = \frac{a_3}{2a_1a_2k\omega\theta}\left[(a_1 s - \omega)\,C_2 - \theta\,C_1\right]. \qquad (4.31)$$

Following the substitution of $\bar{u}_i$ (4.29) with the aid of Equations (4.23), (4.28), and (4.31) into Equations (3.45) through (3.50), we finally obtain the thermal stress field as follows.

$$\frac{\bar{\sigma}^T_{11}}{\mu} = \frac{\bar{Q}_N}{k}\left[(b_1c_1 + b_2c_2)\,e^{-\omega x_3} + (b_3c_1 + b_4c_2)\,e^{-sx_3}\right],$$

$$\frac{\bar{\sigma}^T_{22}}{\mu} = \frac{\bar{Q}_N}{k}\left[(b_5c_1 + b_6c_2)\,e^{-\omega x_3} + (b_7c_1 + b_8c_2)\,e^{-sx_3}\right],$$

$$\frac{\bar{\sigma}^T_{33}}{\mu} = \frac{\bar{Q}_N}{k}\left[(b_9c_1 + b_{10}c_2)\,e^{-\omega x_3} - (b_{11}c_1 + b_{12}c_2)\,e^{-sx_3}\right],$$

$$\frac{\bar{\sigma}^T_{12}}{\mu} = \frac{\bar{Q}_N}{k}\bar{x}_1\bar{x}_2\left[(b_{13}c_1 + b_{14}c_2)\,e^{-\omega x_3} + (b_{15}c_1 + b_{16}c_2)\,e^{-sx_3}\right],$$

$$\frac{\bar{\sigma}^T_{23}}{\mu} = \frac{-i\bar{Q}_N}{k}\bar{x}_2\left[(b_{17}c_1 + b_{18}c_2)\,e^{-\omega x_3} - (b_{19}c_1 + b_{20}c_2)\,e^{-sx_3}\right],$$

$$\frac{\bar{\sigma}^T_{31}}{\mu} = \frac{-i\bar{Q}_N}{k}\bar{x}_1\left[(b_{17}c_1 + b_{18}c_2)\,e^{-\omega x_3} - (b_{19}c_1 + b_{20}c_2)\,e^{-sx_3}\right], \qquad (4.32)$$

It can be shown that, for a single moving asperity, i.e., N = 1, Equations (4.32) check with the Equations (3.67) for the case $\bar{P}_2 = 0$.

4.5 Numerical Results

As in Chapter 3.0 the mechanical, the temperature, and the thermal solutions are all expressed in the Fourier transformed expressions. Inverse Fourier transform will be applied accordingly. Numerical evaluation of the integrals and corresponding graphical results for Cases 1, 2, and 3 will be presented.

4.5.1 Rectangular Contact Area with Uniform Pressure (Case 1)

Mechanical Stress Field

In view of Equation (4.1), the transformed boundary conditions are

$$\bar{R}_3 = \frac{P_o}{2\pi}\int_{-b}^{b} e^{i\bar{x}_2 x_2}\, dx_2 \cdot \sum_{j=1}^{N}\int_{\lambda'(j-1)-a}^{\lambda'(j-1)+a} e^{i\bar{x}_1 x_1}\, dx_1$$

$$= \frac{2P_o}{\pi\bar{x}_1\bar{x}_2}\sin(\bar{x}_1 a)\,\sin(\bar{x}_2 b)\cdot\sum_{j=1}^{N} e^{i\bar{x}_1\lambda'(j-1)}\,,$$

$$\bar{R}_1 = -\mu_f\,\bar{R}_3\,. \tag{4.33}$$

Substituting the expressions above into Equations (4.2), applying the inverse transform, and going through the same simplification as shown in Section (3.5.1), leads to the following expression.

$$\sigma_{11}^{n} = \frac{P_o}{4\pi^2}\sum_{j=1}^{N}\int_0^{\pi}\frac{\cot\phi}{H}\left[\gamma_3\left(1+\frac{1}{2}M_2^2-M_1^2\right)E_1-\gamma_1\gamma_2 E_2\right]d\phi\,,$$

$$\sigma_{22}^{n} = \frac{P_o}{2\pi^2} \sum_{j=1}^{N} \int_0^{\pi} \frac{1}{H \sin 2\phi} \{[\gamma_3(\tfrac{1}{2}\beta^2 - 1) M_1^2 \cos^2\phi + \sin^2\phi] E_1$$

$$- \gamma_1\gamma_2 \sin^2\phi E_2\} d\phi ,$$

$$\sigma_{33}^{n} = \frac{-P_o}{2\pi^2} \sum_{j=1}^{N} \int_0^{\pi} \frac{1}{H \sin 2\phi} [\gamma_3^2 E_1 - \gamma_1\gamma_2 E_2] d\phi ,$$

$$\sigma_{12}^{n} = \frac{P_o}{4\pi^2} \sum_{j=1}^{N} \int_0^{\pi} \frac{1}{H} [\gamma_3 E_1 - \gamma_1\gamma_2 E_2] d\phi ,$$

$$\sigma_{23}^{n} = \frac{-P_o}{2\pi^2} \sum_{j=1}^{N} \int_0^{\pi} \frac{\gamma_1\gamma_3}{H \cos\phi} [I_1 - I_2] d\phi ,$$

$$\sigma_{31}^{n} = \frac{-P_o}{2\pi^2} \sum_{j=1}^{N} \int_0^{\pi} \frac{\gamma_1\gamma_3}{H \sin\phi} [I_1 - I_2] d\phi ,$$

$$\sigma_{11}^{f} = \frac{-u_f P_o}{2\pi^2} \sum_{j=1}^{N} \int_0^{\pi} \frac{1}{H \sin\phi} \Bigg\{\gamma_2 \cos^2\phi(1 + \tfrac{1}{2} M_2^2 - M_1^2) I_1$$

$$- \left[\frac{(\gamma_3 - 2\gamma_1\gamma_2)}{\gamma_2} \sin^2\phi + \gamma_2\gamma_3\right] I_2 \Bigg\} d\phi ,$$

$$\sigma_{22}^{f} = \frac{-u_f P_o}{2\pi^2} \sum_{j=1}^{N} \int_0^{\pi} \frac{1}{H \sin\phi} \Bigg\{\gamma_2[(\tfrac{1}{2}\beta^2 - 1) M_1^2 \cos^2\phi + \sin^2\phi] I_1$$

$$+ \left[\frac{(\gamma_3 - 2\gamma_1\gamma_2)}{\gamma_2} \sin^2\phi\right] I_2 \Bigg\} d\phi ,$$

$$\sigma_{33}^{f} = \frac{-u_f P_o}{2\pi^2} \sum_{j=1}^{N} \int_0^{\pi} \frac{\gamma_2}{H \sin\phi} \{[(\tfrac{1}{2}\beta^2 - 1) M_1^2 \cos^2\phi - \gamma_1^2] I_1 + \gamma_3 I_2\} d\phi$$

$$\sigma_{12}^f = \frac{-\mu_f P_o}{2\pi^2} \sum_{j=1}^{N} \int_0^{\pi} \frac{\gamma_2}{H \cos\phi} \left\{ \cos^2\phi \, I_1 - \frac{1}{2} \left[\frac{(\gamma_3 - 2\gamma_1\gamma_2)}{\gamma_2^2} \right.\right.$$

$$\left.\left. \cdot (\sin^2\phi - \cos^2\phi) + \gamma_3 \right] I_2 \right\} d\phi \, ,$$

$$\sigma_{23}^f = \frac{-\mu_f P_o}{4\pi^2} \sum_{j=1}^{N} \int_0^{\pi} \frac{\gamma_1\gamma_2}{H} [E_1 - E_2] \, d\phi \, ,$$

$$\sigma_{31}^f = \frac{-\mu_f P_o}{2\pi^2} \sum_{j=1}^{N} \int_0^{\pi} \frac{1}{H \sin^2\phi} [\gamma_1\gamma_2 \cos^2\phi E_1 - (\gamma_3^2 - \gamma_1\gamma_2 \sin^2\phi) E_2] \, d\phi$$

(4.34)

where

$$E_t = \ln \frac{\{[a \cos\phi + b \sin\phi + \gamma \cos(\theta - \phi) - \lambda'(j - 1) \cos\phi]^2 + \gamma_t^2 x_3^2\}}{\{[a \cos\phi - b \sin\phi - \gamma \cos(\theta - \phi) + \lambda'(j - 1) \cos\phi]^2 + \gamma_t^2 x_3^2\}}$$

$$+ \ln \frac{\{[a \cos\phi + b \sin\phi - \gamma \cos(\theta - \phi) + \lambda'(j - 1) \cos\phi]^2 + \gamma_t^2 x_3^2\}}{\{[a \cos\phi - b \sin\phi + \gamma \cos(\theta - \phi) - \lambda'(j - 1) \cos\phi]^2 + \gamma_t^2 x_3^2\}}$$

$$I_t = \tan^{-1} \frac{a \cos\phi - b \sin\phi + \gamma \cos(\theta - \phi) - \lambda'(j - 1) \cos\phi}{\gamma_t x_3}$$

$$+ \tan^{-1} \frac{a \cos\phi + b \sin\phi - \gamma \cos(\theta - \phi) + \lambda'(j - 1) \cos\phi}{\gamma_t x_3}$$

$$- \tan^{-1} \frac{a \cos\phi - b \sin\phi - \gamma \cos(\theta - \phi) + \lambda'(j - 1) \cos\phi}{\gamma_t x_3}$$

$$- \tan^{-1} \frac{a \cos\phi + b \sin\phi + \gamma \cos(\theta - \phi) + \lambda'(j - 1) \cos\phi}{\gamma_t x_3} \, ,$$

$t = 1,2$.

Temperature Field. The expression of $\bar{Q}_N$ in Equation (4.20) is equivalent to $-\mu_f V \bar{R}_3$, i.e.,

$$\bar{Q}_N = \frac{-2\mu_f P_o V}{\pi \bar{x}_1 \bar{x}_2} \sin(\bar{x}_1 a) \sin(\bar{x}_2 b) \cdot \sum_{j=1}^{N} e^{i\bar{x}_1 \lambda'(j-1)} . \qquad (4.35)$$

Substituting Equation (4.35) into (4.20) and taking the inverse transform leads to

$$T = \frac{-4\mu_f P_o V}{\pi^2 k} \sum_{j=1}^{N} \int_0^\infty \int_0^\infty f_1 \cos(\bar{x}_2 x_2) e^{-\omega x_3}$$

$$\cdot [M_1' \cos(\theta x_3) + M_2' \sin(\theta x_3)] \, d\bar{x}_1 \, d\bar{x}_2 \qquad (4.36)$$

where

$$M_1' = -\frac{1}{\omega^2 + \theta^2} \left\{ \omega \cos \bar{x}_1[x_1 - \lambda'(j-1)] - \frac{n}{2\omega} \sin \bar{x}_1[x_1 - \lambda'(j-1)] \right\} ,$$

$$M_2' = \frac{1}{\omega^2 + \theta^2} \left\{ \theta \cos \bar{x}_1[x_1 - \lambda'(j-1)] + \frac{n}{2\theta} \sin \bar{x}_1[x_1 - \lambda'(j-1)] \right\} ,$$

By analogy with Equation (3.72), the temperature field from Green's function approach is

$$T = \frac{\mu_f V P_o}{4\sqrt{2\pi k}} \sum_{j=1}^{N} \int_0^\infty \frac{\exp\left(-\frac{x_3^2}{2y}\right)}{\sqrt{y}} \left[\operatorname{erf}\left(\frac{x_2 + b}{\sqrt{2y}}\right) - \operatorname{erf}\left(\frac{x_2 - b}{\sqrt{2y}}\right) \right]$$

$$\cdot \left\{ \operatorname{erf}\left[\frac{x_1 + a - \frac{V}{2\kappa} y - \lambda'(j-1)}{\sqrt{2y}} \right] - \operatorname{erf}\left[\frac{x_1 - a - \frac{V}{2\kappa} y - \lambda'(j-1)}{\sqrt{2y}} \right] \right\} dy . \qquad (4.37)$$

Thermal Stress Field. After substituting the expression $\bar{Q}_N$ into Equation (4.32) and applying the inverse transform, we find

$$\frac{\sigma_{11}^T}{\mu} = \frac{-4\mu_f P_o V}{\pi^2 k} \sum_{j=1}^{N} \int_0^\infty \int_0^\infty f_1 \cos(\bar{x}_2 x_2) \left[e^{-\omega x_3} (b_1 M_1' + b_2 M_2') \right.$$

$$\left. + e^{-sx_3} (b_3 M_1' + b_4 M_2') \right] d\bar{x}_1 \, d\bar{x}_2 ,$$

$$\frac{\sigma_{22}^T}{\mu} = \frac{-4\mu_f P_o V}{\pi^2 k} \sum_{j=1}^{N} \int_0^\infty \int_0^\infty f_1 \cos(\bar{x}_2 x_2) \left[e^{-\omega x_3} (b_5 M_1' + b_6 M_2') \right.$$

$$\left. + e^{-sx_3} (b_7 M_1' + b_8 M_2') \right] d\bar{x}_1 \, d\bar{x}_2 ,$$

$$\frac{\sigma_{33}^T}{\mu} = \frac{-4\mu_f P_o V}{\pi^2 k} \sum_{j=1}^{N} \int_0^\infty \int_0^\infty f_1 \cos(\bar{x}_2 x_2) \left[e^{-\omega x_3} (b_9 M_1' + b_{10} M_2') \right.$$

$$\left. - e^{-sx_3} (b_{11} M_1' + b_{12} M_2') \right] d\bar{x}_1 \, d\bar{x}_2 ,$$

$$\frac{\sigma_{12}^T}{\mu} = \frac{-4\mu_f P_o V}{\pi^2 k} \sum_{j=1}^{N} \int_0^\infty \int_0^\infty \bar{x}_1 \bar{x}_2 f_1 \sin(\bar{x}_2 x_2) \left[e^{-\omega x_3} (-b_{13} M_3' - b_{14} M_4') \right.$$

$$\left. - e^{-sx_3} (b_{15} M_3' + b_{16} M_4') \right] d\bar{x}_1 \, d\bar{x}_2 ,$$

$$\frac{\sigma_{23}^{T}}{\mu} = \frac{-4\mu_f P_o V}{\pi^2 k} \sum_{j=1}^{N} \int_0^{\infty} \int_0^{\infty} \bar{x}_2 f_1 \sin(\bar{x}_2 x_2) \left[e^{-\omega x_3} (b_{17} M_5' + b_{18} M_6') \right.$$

$$\left. - e^{-sx_3} (b_{19} M_5' + b_{20} M_6') \right] d\bar{x}_1 \, d\bar{x}_2 \, ,$$

$$\frac{\sigma_{31}^{T}}{\mu} = \frac{-4\mu_f P_o V}{\pi^2 k} \sum_{j=1}^{N} \int_0^{\infty} \int_0^{\infty} \bar{x}_1 f_1 \cos(\bar{x}_2 x_2) \left[e^{-\omega x_3} (b_{17} M_7' + b_{18} M_8') \right.$$

$$\left. - e^{-sx_3} (b_{19} M_7' + b_{20} M_8') \right] d\bar{x}_1 \, d\bar{x}_2 \, , \qquad (4.38)$$

where

$$M_3' = - \frac{1}{\omega^2 + \theta^2} \{ \omega \sin \bar{x}_1 [x_1 - \lambda'(j-1)] + \frac{n}{2\omega} \cos \bar{x}_1 [x_1 - \lambda'(j-1)] \} \, ,$$

$$M_4' = \frac{1}{\omega^2 + \theta^2} \{ \theta \sin \bar{x}_1 [x_1 - \lambda'(j-1)] - \frac{n}{2\theta} \cos \bar{x}_1 [x_1 - \lambda'(j-1)] \} \, ,$$

$$M_5' = \frac{1}{\omega^2 + \theta^2} \{ - \frac{n}{2\omega} \sin \bar{x}_1 [x_1 - \lambda'(j-1)] + \omega \cos \bar{x}_1 [x_1 - \lambda'(j-1)] \} \, ,$$

$$M_6' = - \frac{1}{\omega^2 + \theta^2} \{ \frac{n}{2\theta} \sin \bar{x}_1 [x_1 - \lambda'(j-1)] + \theta \cos \bar{x}_1 [x_1 - \lambda'(j-1)] \} \, ,$$

$$M_7' = \frac{1}{\omega^2 + \theta^2} \{ \frac{n}{2\omega} \cos \bar{x}_1 [x_1 - \lambda'(j-1)] + \omega \sin \bar{x}_1 [x_1 - \lambda'(j-1)] \} \, ,$$

$$M_8' = \frac{1}{\omega^2 + \theta^2} \{ \frac{n}{2\theta} \cos \bar{x}_1 [x_1 - \lambda'(j-1)] - \theta \sin \bar{x}_1 [x_1 - \lambda'(j-1)] \} \, .$$

4.5.2 Disk Contact Area with Uniform Pressure (Case 2)

Mechanical Stress Field. In this case the transformed boundary conditions are

$$\bar{R}_3 = \frac{P_o}{2\pi}\int_{-a}^{a}\sum_{j=1}^{N}\left[\int_{-\{a^2-[x_1-\lambda'(j-1)]\}}^{\{a^2-[x_1-\lambda'(j-1)]\}} e^{i(\bar{x}_1x_1+\bar{x}_2x_2)}\,dx_2\right]dx_1$$

$$= \frac{aP_o}{s}J_1(sa)\sum_{j=1}^{N} e^{i\bar{x}_1\lambda'(j-1)} ,$$

$$\bar{R}_1 = -\mu_f\bar{R}_3 . \qquad (4.39)$$

With the expressions (4.39) in (4.2) and by taking inverse transform, the solution for the mechanical stress field becomes

$$\sigma_{11}^n = \frac{aP_o}{\pi}\sum_{j=1}^{N}\int_0^{\pi}\frac{\cos^2\phi}{H}\left[\gamma_3\left(1+\frac{1}{2}M_2^2-M_1^2\right)E_1' - \gamma_1\gamma_2E_2'\right]d\phi ,$$

$$\sigma_{22}^n = \frac{aP_o}{\pi}\sum_{j=1}^{N}\int_0^{\pi}\frac{1}{H}\left\{\gamma_3\left(\frac{1}{2}\beta^2-1\right)M_1^2\cos^2\phi + \sin^2\phi\right]E_1' - \gamma_1\gamma_2\sin^2\phi\,E_2'\right\}d\phi ,$$

$$\sigma_{33}^n = \frac{-aP_o}{\pi}\sum_{j=1}^{N}\int_0^{\pi}\frac{1}{H}\left[\gamma_3^2E_1' - \gamma_1\gamma_2E_2'\right]d\phi ,$$

$$\sigma_{12}^n = \frac{aP_o}{2\pi}\sum_{j=1}^{N}\int_0^{\pi}\frac{\sin 2\phi}{H}\left[\gamma_3E_1' - \gamma_1\gamma_2E_2'\right]d\phi ,$$

$$\sigma_{23}^{n} = \frac{-aP_o}{\pi} \sum_{j=1}^{N} \int_0^{\pi} \frac{\gamma_1\gamma_2 \sin\phi}{H} (I_1' - I_2') \, d\phi ,$$

$$\sigma_{31}^{n} = \frac{-aP_o}{\pi} \sum_{j=1}^{N} \int_0^{\pi} \frac{\gamma_1\gamma_3 \cos\phi}{H} (I_1' - I_2') \, d\phi ,$$

$$\sigma_{11}^{f} = \frac{-a\mu_f P_o}{\pi} \sum_{j=1}^{N} \int_0^{\pi} \frac{\cos\phi}{H} \left\{ \gamma_2 \cos^2\phi (1 + M_2^2 - M_1^2) I_1' \right.$$

$$\left. - \left[\frac{(\gamma_3 - 2\gamma_1\gamma_2)}{\gamma_2} \sin^2\phi + \gamma_2\gamma_3 \right] I_2' \right\} d\phi ,$$

$$\sigma_{22}^{f} = \frac{-a\mu_f P_o}{\pi} \sum_{j=1}^{N} \int_0^{\pi} \frac{\cos\phi}{H} \left\{ \gamma_2 [(\tfrac{1}{2}\beta^2 - 1) M_1^2 \cos^2\phi + \sin^2\phi] I_1' \right.$$

$$\left. + \left[\frac{(\gamma_3 - 2\gamma_1\gamma_2)}{\gamma_2} \sin^2\phi \right] I_2' \right\} d\phi ,$$

$$\sigma_{33}^{f} = \frac{-a\mu_f P_o}{\pi} \sum_{j=1}^{N} \int_0^{\pi} \frac{\gamma_2 \cos\phi}{H} \left\{ [(\tfrac{1}{2}\beta^2 - 1) M_1^2 \cos^2\phi \right.$$

$$\left. - \gamma_1^2] I_1' + \gamma_3 I_2' \right\} d\phi ,$$

$$\sigma_{12}^{f} = \frac{-a\mu_f P_o}{\pi} \sum_{j=1}^{N} \int_0^{\pi} \frac{\gamma_2 \sin\phi}{H} \left\{ \cos^2\phi I_1' - \frac{1}{2} \left[\frac{(\gamma_3 - 2\gamma_1\gamma_2)}{\gamma_2^2} (\sin^2\phi \right. \right.$$

$$\left. \left. - \cos^2\phi) + \gamma_3 \right] I_2' \right\} d\phi ,$$

$$\sigma_{23}^{f} = \frac{-a\mu_f P_o}{2\pi} \sum_{j=1}^{N} \int_0^{\pi} \frac{\sin 2\phi}{H} \gamma_1\gamma_2(E_1' - E_2') \, d\phi \, ,$$

$$\sigma_{31}^{f} = \frac{-a\mu_f P_o}{\pi} \sum_{j=1}^{N} \int_0^{\pi} \frac{1}{H} [\gamma_1\gamma_2 \cos^2\phi \, E_1' - (\gamma_3^2 - \gamma_1\gamma_2 \sin^2\phi) \, E_2'] \, , \quad (4.40)$$

where

$$E_t' = \int_0^{\infty} J_1(sa) \cos\{s[\gamma \cos(\theta - \phi) - \lambda'(j-1) \cos\phi]\} \, e^{-s\gamma_t x_3} \, ds \, ,$$

$$I_t' = \int_0^{\infty} J_1(sa) \sin\{s[\gamma \cos(\theta - \phi) - \lambda'(j-1) \cos\phi]\} \, e^{-s\gamma_t x_3} \, ds \, ,$$

$t = 1,2$.

Temperature Field. With the expression of $\bar{Q}_N$ given by

$$\bar{Q}_N = \frac{-a\mu_f P_o V}{s} J_1(sa) \sum_{j=1}^{N} e^{i\bar{x}_1\lambda'(j-1)} \quad (4.41)$$

the temperature solution can be readily obtained as

$$T = \frac{-2\mu_f P_o V}{\pi k} \sum_{j=1}^{N} \int_0^{\infty} \int_0^{\infty} f_2 \cos(\bar{x}_2 x_2) \, e^{-\omega x_3} \, [M_1' \cos(\theta x_3)$$

$$+ M_2' \sin(\theta x_3)] \, d\bar{x}_1 \, d\bar{x}_2 \, . \quad (4.42)$$

In view of Equation (4.12), the Green's function solution is

$$T = \frac{\mu_f P_o V}{2\pi k} \sum_{j=1}^{N} \int_{-a}^{a} \int_{-\{a^2-[x_1'-\lambda'(j-1)]\}}^{\{a^2-[x_1'-\lambda'(j-1)]\}} \frac{\exp\{-V[R - (x_1 - x_1')]/2\kappa\}}{R} \, dx_2' \, dx_1' \, .$$

(4.43)

Thermal Stress Field. The expressions are

$$\frac{\sigma_{11}^T}{\mu} = \frac{-2\mu_f P_o V}{\pi k} \sum_{j=1}^{N} \int_0^\infty \int_0^\infty f_2 \cos(\bar{x}_2 x_2) \left[e^{-\omega x_3} (b_1 M_1' + b_2 M_2') \right.$$

$$\left. + e^{-sx_3} (b_3 M_1' + b_4 M_2') \right] d\bar{x}_1 \, d\bar{x}_2 ,$$

$$\frac{\sigma_{22}^T}{\mu} = \frac{-2\mu_f P_o V}{\pi k} \sum_{j=1}^{N} \int_0^\infty \int_0^\infty f_2 \cos(\bar{x}_2 x_2) \left[e^{-\omega x_3} (b_5 M_1' + b_6 M_2') \right.$$

$$\left. + e^{-sx_3} (b_7 M_1' + b_8 M_2') \right] d\bar{x}_1 \, d\bar{x}_2 ,$$

$$\frac{\sigma_{33}^T}{\mu} = \frac{-2\mu_f P_o V}{\pi k} \sum_{j=1}^{N} \int_0^\infty \int_0^\infty f_2 \cos(\bar{x}_2 x_2) \left[e^{-\omega x_3} (b_9 M_1' + b_{10} M_2') \right.$$

$$\left. - e^{-sx_3} (b_{11} M_1' + b_{12} M_2') \right] d\bar{x}_1 \, d\bar{x}_2 ,$$

$$\frac{\sigma_{12}^T}{\mu} = \frac{-2\mu_f P_o V}{\pi k} \sum_{j=1}^{N} \int_0^\infty \int_0^\infty \bar{x}_1 \bar{x}_2 f_2 \sin(\bar{x}_2 x_2) \left[e^{-\omega x_3} (-b_{13} M_3' - b_{14} M_4') \right.$$

$$\left. - e^{-sx_3} (b_{15} M_3' + b_{16} M_4') \right] d\bar{x}_1 \, d\bar{x}_2 ,$$

$$\frac{\sigma_{23}^T}{\mu} = \frac{-2\mu_f P_o V}{\pi k} \sum_{j=1}^{N} \int_0^\infty \int_0^\infty \bar{x}_2 f_2 \sin(\bar{x}_2 x_2) \left[e^{-\omega x_3} (b_{17} M_5' + b_{18} M_6') \right.$$

$$\left. - e^{-sx_3} (b_{19} M_5' + b_{20} M_6') \right] d\bar{x}_1 \, d\bar{x}_2 ,$$

$$\frac{\sigma_{31}^{T}}{\mu} = \frac{-2\mu_f P_o V}{\pi k} \sum_{j=1}^{N} \int_0^{\infty} \int_0^{\infty} \bar{x}_1 f_2 \cos(\bar{x}_2 x_2) \left[e^{-\omega x_3} (b_{17} M_7' + b_{18} M_8') \right.$$

$$\left. - e^{-sx_3} (b_{19} M_7' + b_{20} M_8') \right] d\bar{x}_1 \, d\bar{x}_2 \, . \qquad (4.44)$$

4.5.3 Disk Contact Area with Paraboloidal Distribution of Pressure (Case 3)

Mechanical Stress Field. Similarly, we can obtain the transformed expressions of boundary conditions in Equation (4.1). This is given by

$$\bar{R}_3 = \frac{P_o}{\pi} \int_{-a}^{a} \sum_{j=1}^{N} \left[\int_{-\{a^2-[x_1-\lambda'(j-1)]^2\}}^{\{a^2-[x_1-\lambda'(j-1)]^2\}} \left\{ 1 - \frac{[x_1 - \lambda'(j-1)]^2 + x_2^2}{a^2} \right\} \right.$$

$$\left. \cdot \, e^{i(\bar{x}_1 x_1 + \bar{x}_2 x_2)} \, dx_2 \right] dx_1$$

$$= \frac{4P_o}{s^2} J_2(sa) \sum_{j=1}^{N} e^{i\bar{x}_1 \lambda'(j-1)} \, ,$$

$$\bar{R}_1 = -\mu_f \bar{R}_3 \, . \qquad (4.45)$$

The mechanical stresses are analogous to those outlined in Equations (4.40) except E_t' and I_t' are replaced by E_t'' and I_t'', respectively. Their forms are

$$E_t'' = \frac{4}{a} \int_0^{\infty} \frac{J_2(sa)}{s} \cos\{s[\gamma \cos(\theta - \phi) - \lambda'(j-1) \cos \phi]\} \, e^{-s\gamma_t x_3} \, ds \, ,$$

$$I_t'' = \frac{4}{a}\int_0^\infty \frac{J_2(sa)}{s} \sin\{s[\gamma \cos(\theta - \phi) - \lambda'(j-1)\cos\phi]\}\, e^{-s\gamma_t x_3}\, ds\,,$$

$t = 1,2$.

Temperature Field. According to Equation (4.45), we have

$$\bar{Q}_N = \frac{-4\mu_f P_o V}{s^2} J_2(sa) \sum_{j=1}^{N} e^{i\bar{x}_1\lambda'(j-1)} \,. \tag{4.46}$$

Thus the temperature field with the aid of the above equation after the inverse transform is

$$T = \frac{-2\mu_f P_o V}{\pi k} \sum_{j=1}^{N} \int_0^\infty \int_0^\infty f_3 \cos(\bar{x}_2 x_2)\, [M_1' \cos(\theta x_3) + M_2' \sin(\theta x_3)]\, d\bar{x}_1\, d\bar{x}_2 \,. \tag{4.47}$$

The Green's function solution is

$$T = \frac{\mu_f P_o V}{2\pi k} \sum_{j=1}^{N} \int_{-a}^{a} \int_{-\{a^2-[x_1'-\lambda'(j-1)]\}}^{\{a^2-[x_1'-\lambda'(j-1)]\}} \left\{1 - \frac{[x_1' - \lambda'(j-1)]^2 + x_2'^2}{a}\right\} \cdot \frac{\exp\{-V[R - (x_1 - x_1')]/2\kappa\}}{R}\, dx_2'\, dx_1' \,. \tag{4.48}$$

Thermal Stress Field. Replacing f_2 in Equation (4.44) with f_3 leads to the solution accordingly.

As above, the temperature and the thermal stress fields for three cases have the form of the summation for the index j from 1 to N before double integrals, which would increase computing time and cost for large N. This inefficiency can be overcome by using the fact that

$$\sum_{j=1}^{N} e^{i\bar{x}_1\lambda'(j-1)} = \frac{\sin\left(\frac{1}{2} N\lambda'\bar{x}_1\right)}{\sin\left(\frac{1}{2}\lambda'\bar{x}_1\right)} e^{i\tau_N}$$

where $\tau_N = 1/2\ \lambda'(N-1)\ \bar{x}_1$. Thus the expressions (4.35), (4.41), and (4.46) for $\bar{Q}_N$ can be modified. As a result, the temperature and the thermal stress fields can be rewritten as

$$T_r = \frac{-2\mu_f P_o V}{\pi k}\int_0^\infty\int_0^\infty \Omega_r \cos(\bar{x}_2 x_2)\ [N_1' \cos(\theta x_3) + N_2' \sin(\theta x_3)]$$

$$\cdot\ e^{-\omega x_3}\ d\bar{x}_1\ d\bar{x}_2 \qquad (4.49)$$

and

$$\left(\frac{\sigma_{11}^T}{\mu}\right)_r = \frac{-2\mu_f P_o V}{\pi k}\int_0^\infty\int_0^\infty \Omega_r \cos(\bar{x}_2 x_2)\left[e^{-\omega x_3}(b_1 N_1' + b_2 N_2')\right.$$

$$\left. + e^{-sx_3}(b_3 N_1' + b_4 N_2')\right] d\bar{x}_1\ d\bar{x}_2\ ,$$

$$\left(\frac{\sigma_{22}^T}{\mu}\right)_r = \frac{-2\mu_f P_o V}{\pi k}\int_0^\infty\int_0^\infty \Omega_r \cos(\bar{x}_2 x_2)\left[e^{-\omega x_3}(b_5 N_1' + b_6 N_2')\right.$$

$$\left. + e^{-sx_3}(b_7 N_1' + b_8 N_2')\right] d\bar{x}_1\ d\bar{x}_2\ ,$$

$$\left(\frac{\sigma_{33}^T}{\mu}\right)_r = \frac{-2\mu_f P_o V}{\pi k}\int_0^\infty\int_0^\infty \Omega_r \cos(\bar{x}_2 x_2)\left[e^{-\omega x_3}(b_9 N_1' + b_{10}N_2')\right.$$

$$\left. - e^{-sx_3}(b_{11}N_1' + b_{12}N_2')\right] d\bar{x}_1\, d\bar{x}_2 ,$$

$$\left(\frac{\sigma_{12}^T}{\mu}\right)_r = \frac{-2\mu_f P_o V}{\pi k}\int_0^\infty\int_0^\infty \Omega_r\, \bar{x}_1\bar{x}_2 \sin(\bar{x}_2 x_2)\left[e^{-\omega x_3}(-b_{13}N_3' - b_{14}N_4')\right.$$

$$\left. + e^{-sx_3}(-b_{15}N_3' - b_{16}N_4')\right] d\bar{x}_1\, d\bar{x}_2 ,$$

$$\left(\frac{\sigma_{23}^T}{\mu}\right)_r = \frac{-2\mu_f P_o V}{\pi k}\int_0^\infty\int_0^\infty \Omega_r\, \bar{x}_2 \sin(\bar{x}_2 x_2)\left[e^{-\omega x_3}(b_{17}N_5' + b_{18}N_6')\right.$$

$$\left. - e^{-sx_3}(b_{19}N_5' + b_{20}N_6')\right] d\bar{x}_1\, d\bar{x}_2 ,$$

$$\left(\frac{\sigma_{31}^T}{\mu}\right)_r = \frac{-2\mu_f P_o V}{\pi k}\int_0^\infty\int_0^\infty \Omega_r\, \bar{x}_1 \cos(\bar{x}_2 x_2)\left[e^{-\omega x_3}(b_{17}N_7' + b_{18}N_8')\right.$$

$$\left. - e^{-sx_3}(b_{19}N_7' + b_{20}N_8')\right] d\bar{x}_1\, d\bar{x}_2 . \qquad (4.50)$$

where r = 1, 2, and 3 for Cases 1, 2, and 3, respectively. And

$$\Omega_1 = \frac{2}{\pi}\cdot\frac{\sin(\bar{x}_1 a)\,\sin(\bar{x}_2 b)}{\bar{x}_1\bar{x}_2}\cdot\frac{\sin\left(\frac{1}{2}N\lambda'\bar{x}_1\right)}{\sin\left(\frac{1}{2}\lambda'\bar{x}_1\right)} ,$$

$$\Omega_2 = \frac{a}{s} \cdot \frac{\sin(\frac{1}{2} N\lambda' \bar{x}_1)}{\sin(\frac{1}{2} \lambda' \bar{x}_1)} J_1(sa) ,$$

$$\Omega_3 = \frac{4}{s^2} \cdot \frac{\sin(\frac{1}{2} N\lambda' \bar{x}_1)}{\sin(\frac{1}{2} \lambda' \bar{x}_1)} J_2(sa) ,$$

$$N_1' = -\frac{1}{\omega^2 + \theta^2} \{\omega \cos[\bar{x}_1(x_1 - \tau_N)] - \frac{n}{2\omega} \sin[\bar{x}_1(x_1 - \tau_N)]\} ,$$

$$N_2' = \frac{1}{\omega^2 + \theta^2} \{\theta \cos[\bar{x}_1(x_1 - \tau_N)] + \frac{n}{2\theta} \sin[\bar{x}_1(x_1 - \tau_N)]\} ,$$

$$N_3' = -\frac{1}{\omega^2 + \theta^2} \{\omega \sin[\bar{x}_1(x_1 - \tau_N)] + \frac{n}{2\omega} \cos[\bar{x}_1(x_1 - \tau_N)]\} ,$$

$$N_4' = \frac{1}{\omega^2 + \theta^2} \{\theta \sin[\bar{x}_1(x_1 - \tau_N)] - \frac{n}{2\theta} \cos[\bar{x}_1(x_1 - \tau_N)]\} ,$$

$$N_5' = \frac{1}{\omega^2 + \theta^2} \{-\frac{n}{2\omega} \sin[\bar{x}_1(x_1 - \tau_N)] + \omega \cos[\bar{x}_1(x_1 - \tau_N)]\} ,$$

$$N_6' = -\frac{1}{\omega^2 + \theta^2} \{\frac{n}{2\theta} \sin[\bar{x}_1(x_1 - \tau_N)] + \theta \cos[\bar{x}_1(x_1 - \tau_N)]\} ,$$

$$N_7' = \frac{1}{\omega^2 + \theta^2} \{\frac{n}{2\omega} \cos[\bar{x}_1(x_1 - \tau_N)] + \omega \sin[\bar{x}_1(x_1 - \tau_N)]\} ,$$

$$N_8' = \frac{1}{\omega^2 + \theta^2} \{\frac{n}{2\theta} \cos[\bar{x}_1(x_1 - \tau_N)] - \theta \sin[\bar{x}_1(x_1 - \tau_N)]\} .$$

For the numerical results which follow it is considered that contact is in the form of a sequence of three asperities with centers separated by a distance $\lambda' = 12$. The values used for the moving velocity of asperities, the dimension of contact areas, and the coefficient of friction are the same as in previous chapters, i.e., V = 15 m/s (600 ips), a = 0.25 mm (0.01 in.), and $\mu_f = 0.5$, respectively. Figure 4.2 shows the mechanical principal stress fields for three cases at the depth $\zeta = 10^{-1}$, which is of interest here. It can be seen that the tensile stresses occur on the trailing side and the compressive stresses on the leading side of each moving asperity. In each case the corresponding value at the corresponding location beneath each asperity has the same order of magnitude, which justifies that the cumulative mechanical effect is negligible as expected. In Figure 4.3 is shown the temperature field for Case 1 in the surface layer. It is noted that the temperature is high near the surface, however, its magnitude drops rapidly with respect to the depth. The temperature gradient, which affects the thermal stress field, attains its maximum at $\zeta = 10^{-1}$. Consequently, high tensile stresses are again expected at this depth. The temperature rise underneath the second and third asperities is due to the cumulative effect from the previous asperity. For comparison, the temperature fields for three cases are presented in Figure 4.4. It shows that Case 3 for the non-uniform heating has higher temperature than Cases 1 and 2 for the uniform heating. In all cases, the temperature rises at the corresponding location for each asperity. As a result, large tensile stresses occur near the first

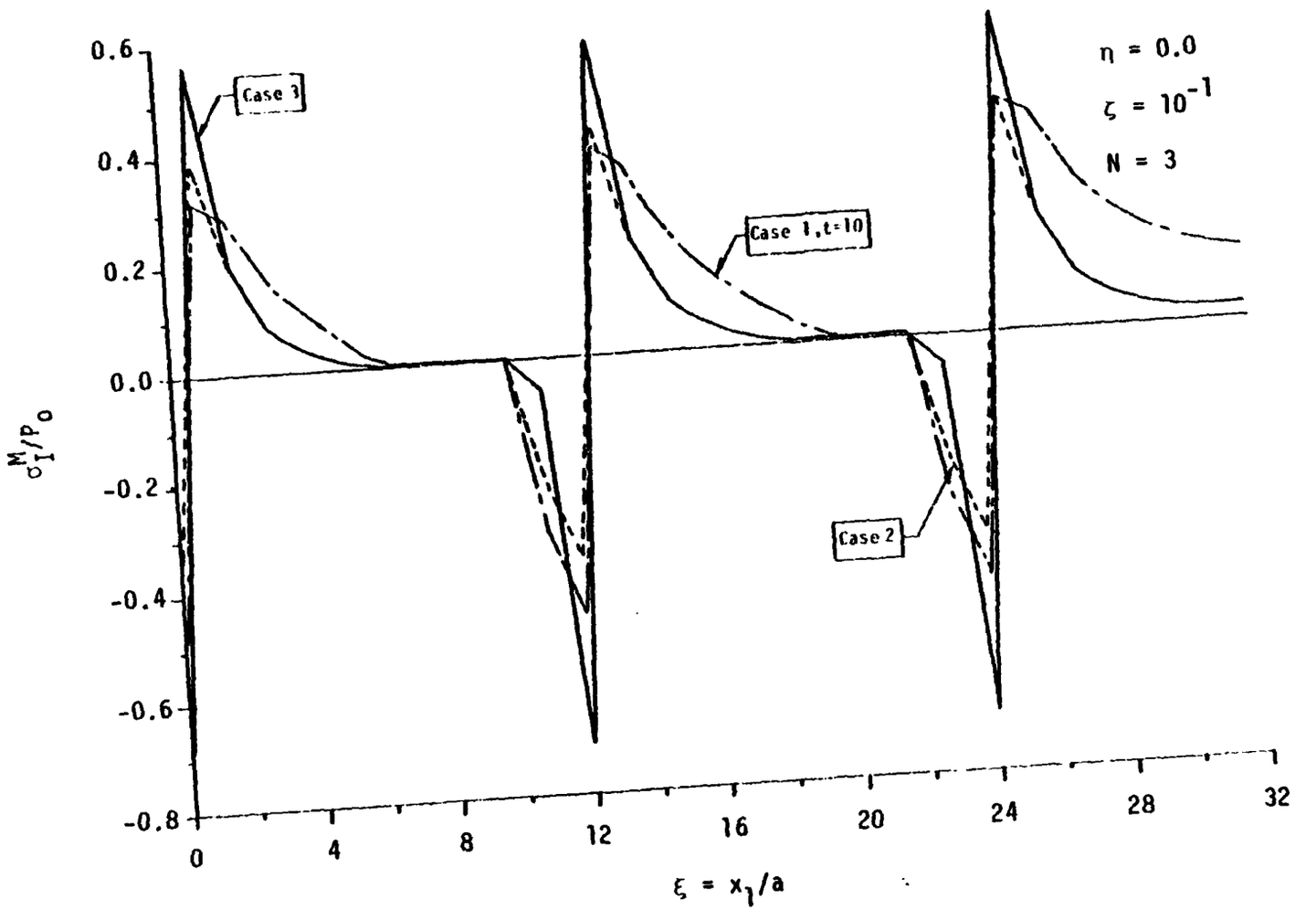

Figure 4.2. Maximum mechanical principal stress fields from periodic excitation.

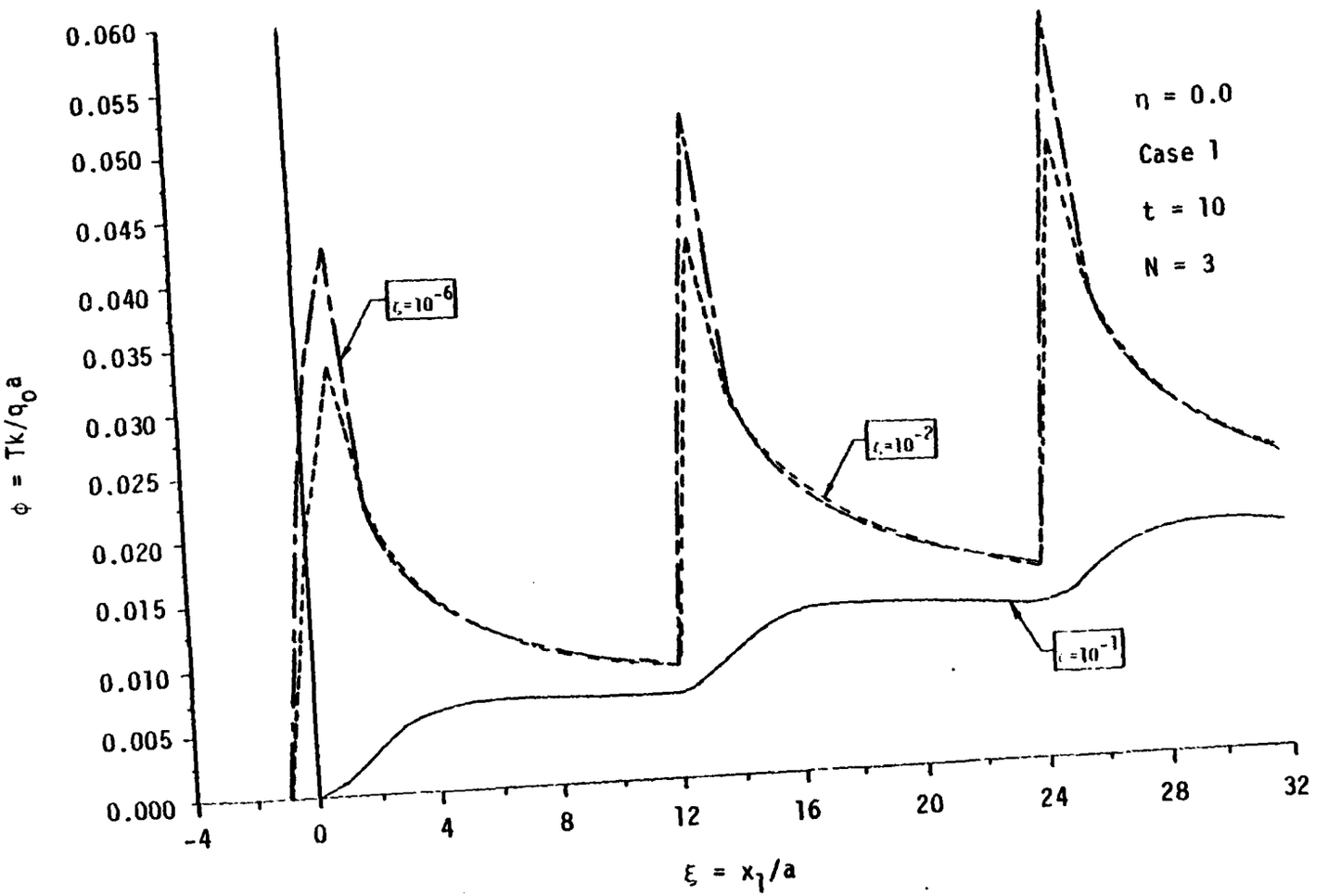

Figure 4.3. Temperature fields in the surface layer from periodic excitation.

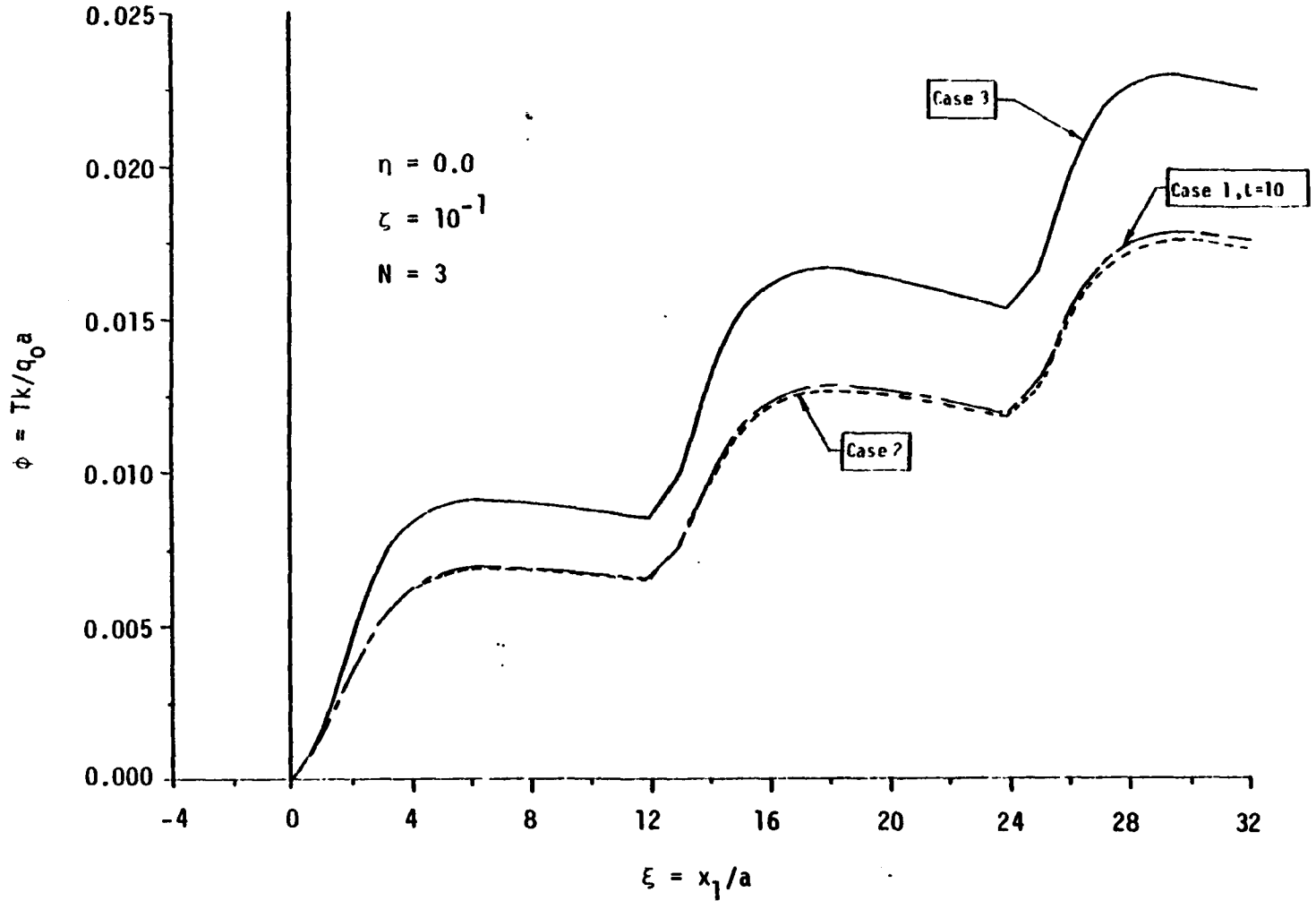

Figure 4.4. Temperature fields from periodic excitation.

asperity and become smaller when ξ is large (see Figure 4.5). The combined effects from mechanical and thermal stress fields for three cases are shown in Figure 4.6. Accordingly, the maximum principal stress for Cases 1, 2, and 3 would reach the ultimate strength at critical pressures of 119 MPa (17,245 psi), 104 MPa (15,091 psi), and 88 MPa (12,700 psi), respectively.

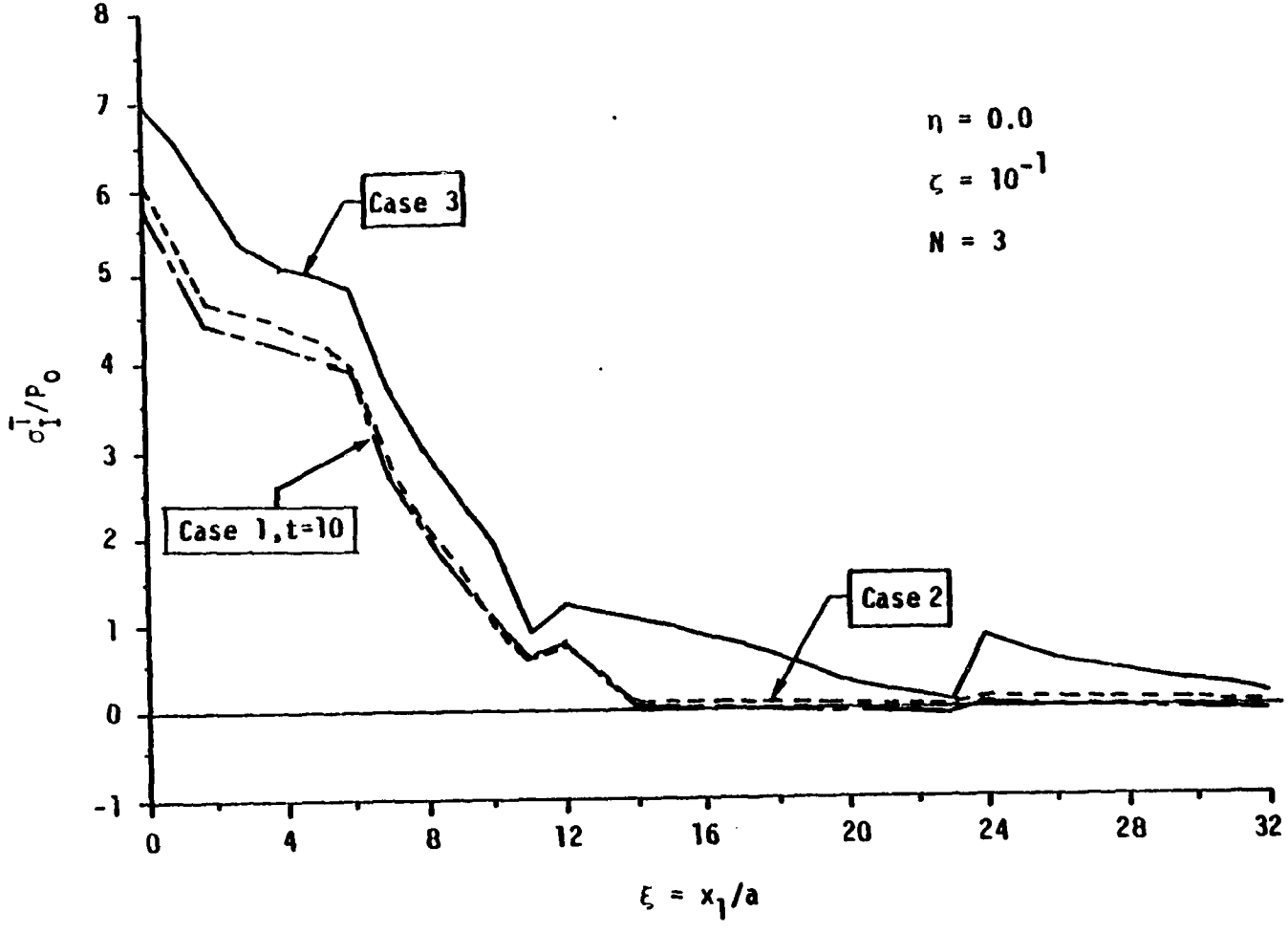

Figure 4.5. Maximum thermal principal stress fields from periodic excitation.

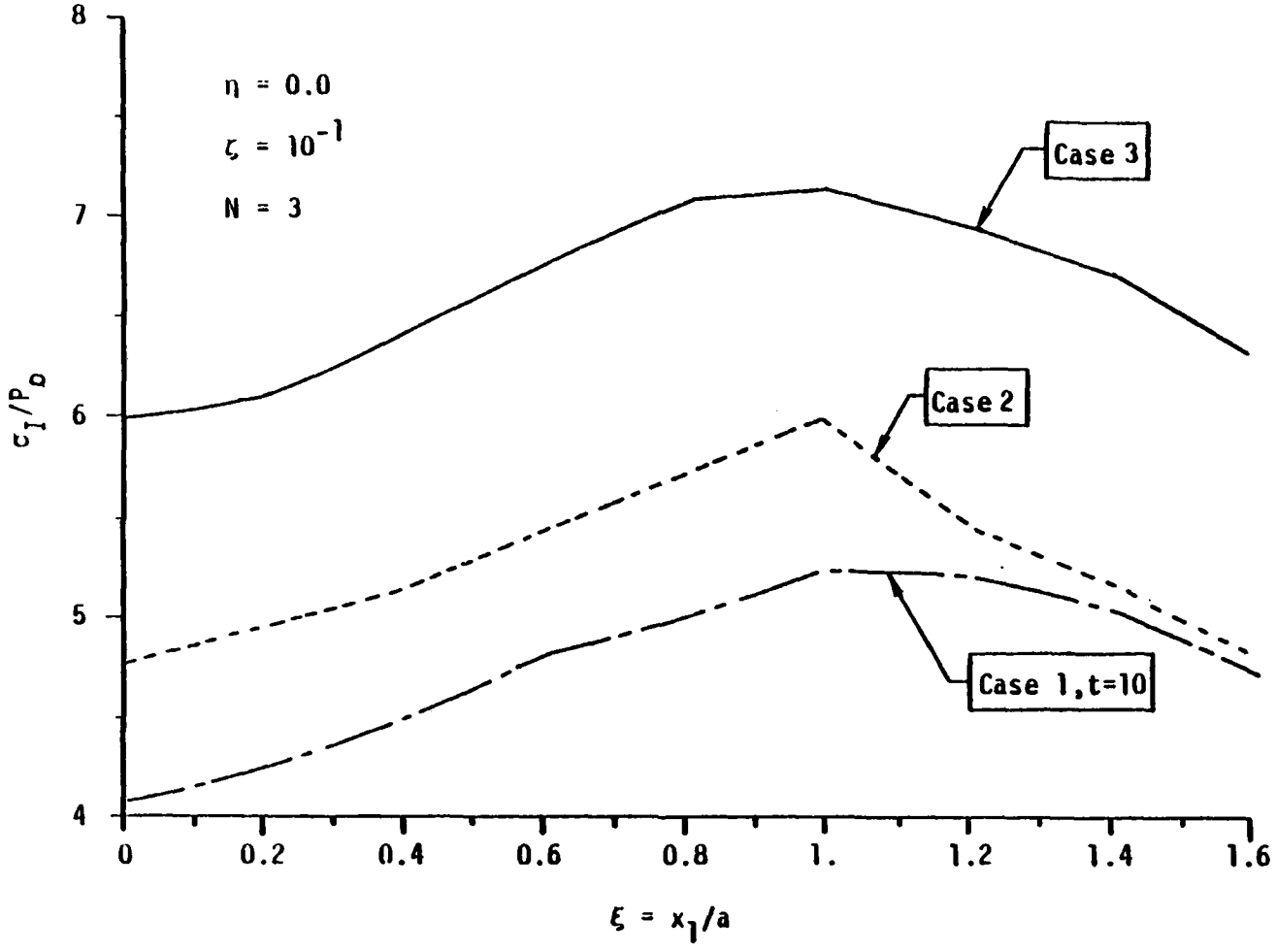

Figure 4.6. Maximum combined thermomechanical principal stress fields from periodic excitation.

CHAPTER 5

DISCUSSIONS AND CONCLUSIONS

5.1 Asperity-Size, Shape of Contact Area, Load Distribution

Of interest here are the effects of different sizes, shapes of contact areas, and load distributions of a moving asperity in addition to what we have discussed in Section 2.5 (see Figure 2.8 and 2.9). In three-dimensional analysis, we recall that the pressure distribution is non-uniform for Case 3 and uniform for Cases 1 and 2; while the shape of the contact area is rectangular for Case 1 and circular for Cases 2 and 3. For a comparison among the three cases, Figures 5.1 and 5.3 show maximum mechanical and thermal principal stress fields, respectively. Moreover, temperature fields are presented in Figure 5.2 and maximum combined thermomechanical principal stress fields in Figure 5.4. Accordingly, we observe that the order of magnitude of the solutions from Case 2 is close to (a little higher than) that from Case 1; while the solutions from Case 3 have much higher order of magnitude compared with Cases 1 and 2. Consequently, it can be argued that the shape of contact area is less of a deciding factor than the pressure distribution over the contact area. Since the inevitable irregularities in the contact surfaces will cause the load distribution to be non-uniform when two sliding solids are nominally in contact over some small areas, this result is of great significance to account for the strong tendency of the crack onset in actual practice. In order to show the asperity size effect, temperature and maximum combined thermomechanical principal stress fields from three different sizes are

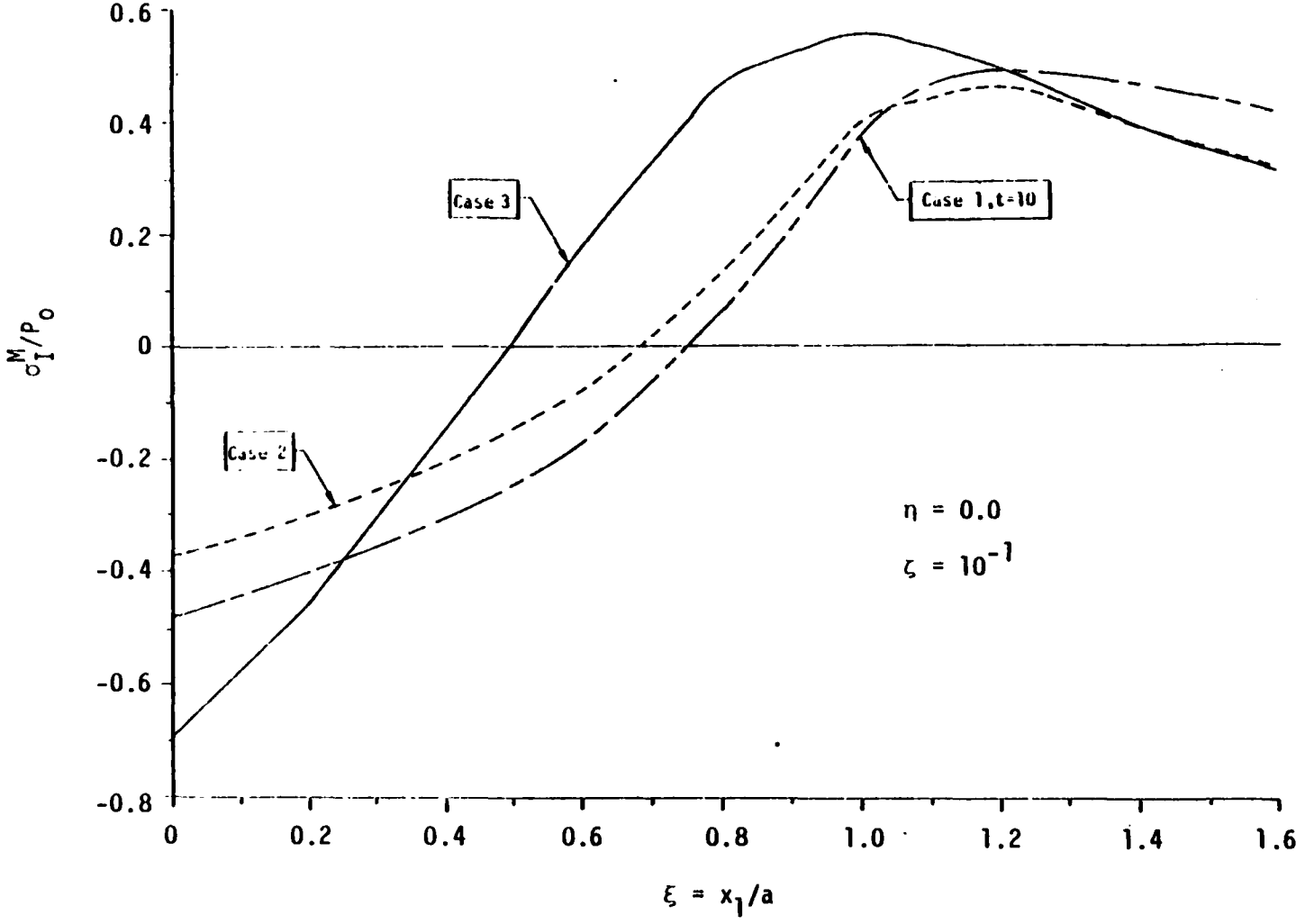

Figure 5.1. Maximum mechanical principal stress fields for three cases.

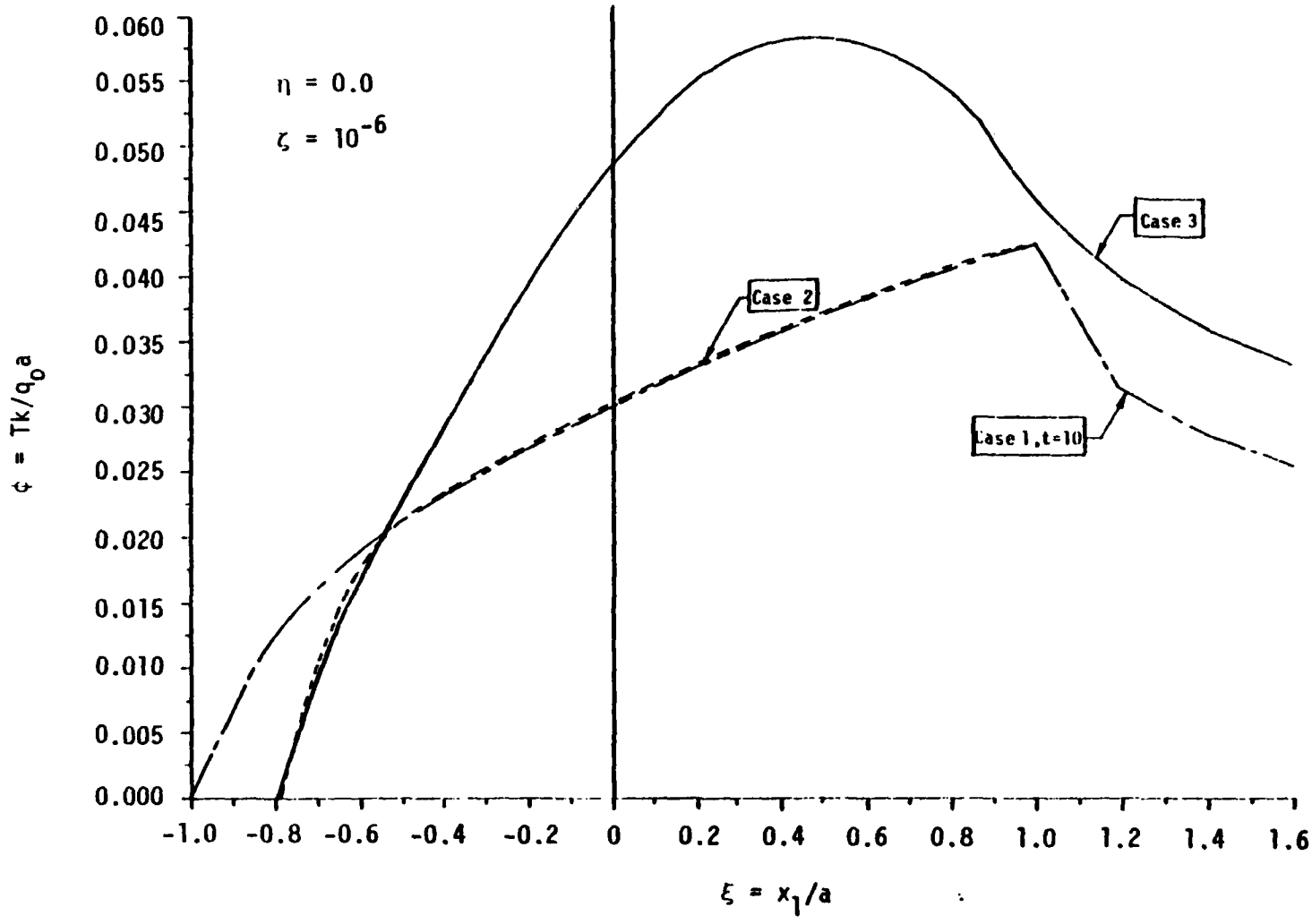

Figure 5.2. Temperature fields for three cases.

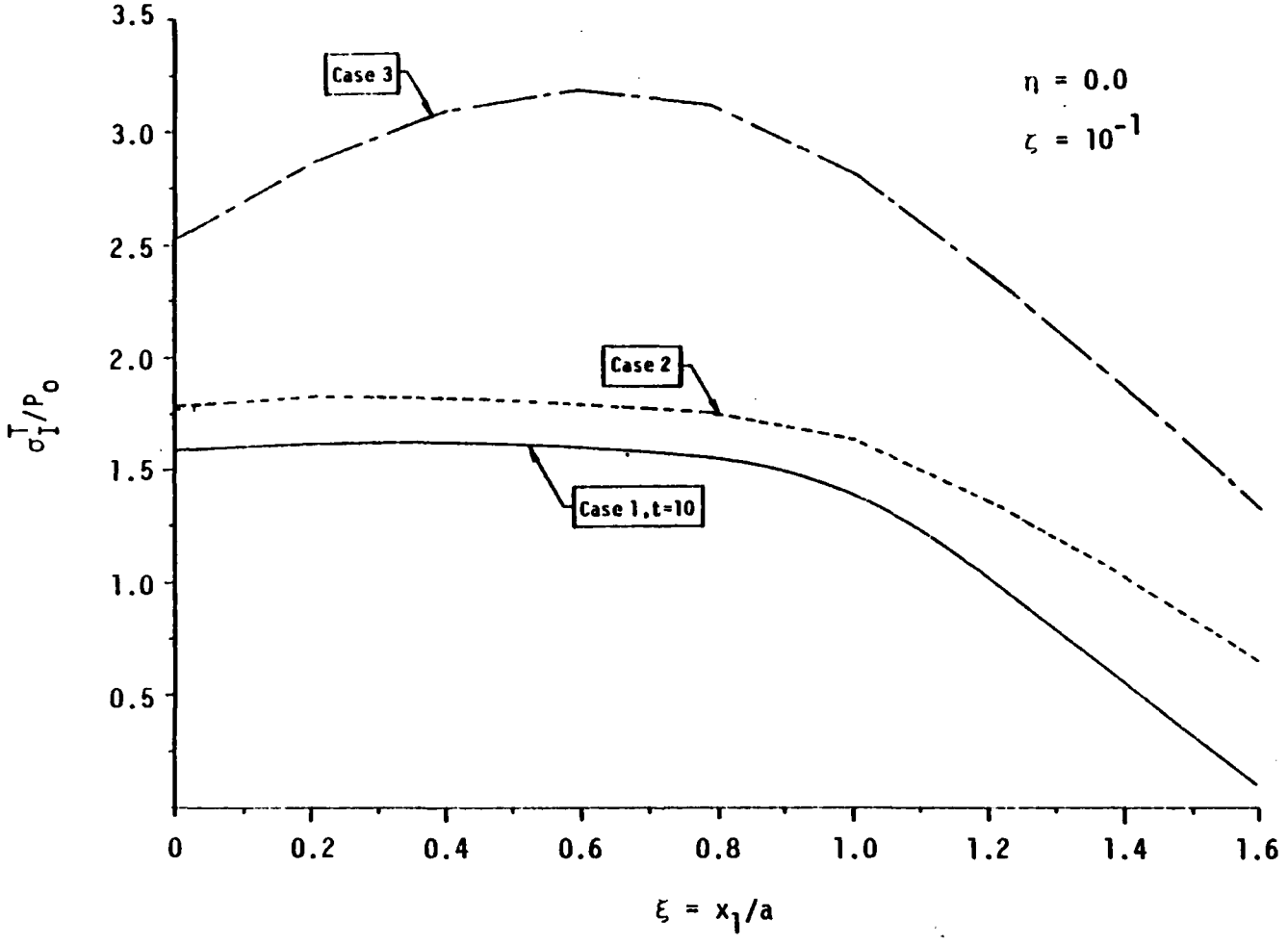

Figure 5.3. Maximum thermal principal stress fields for three cases.

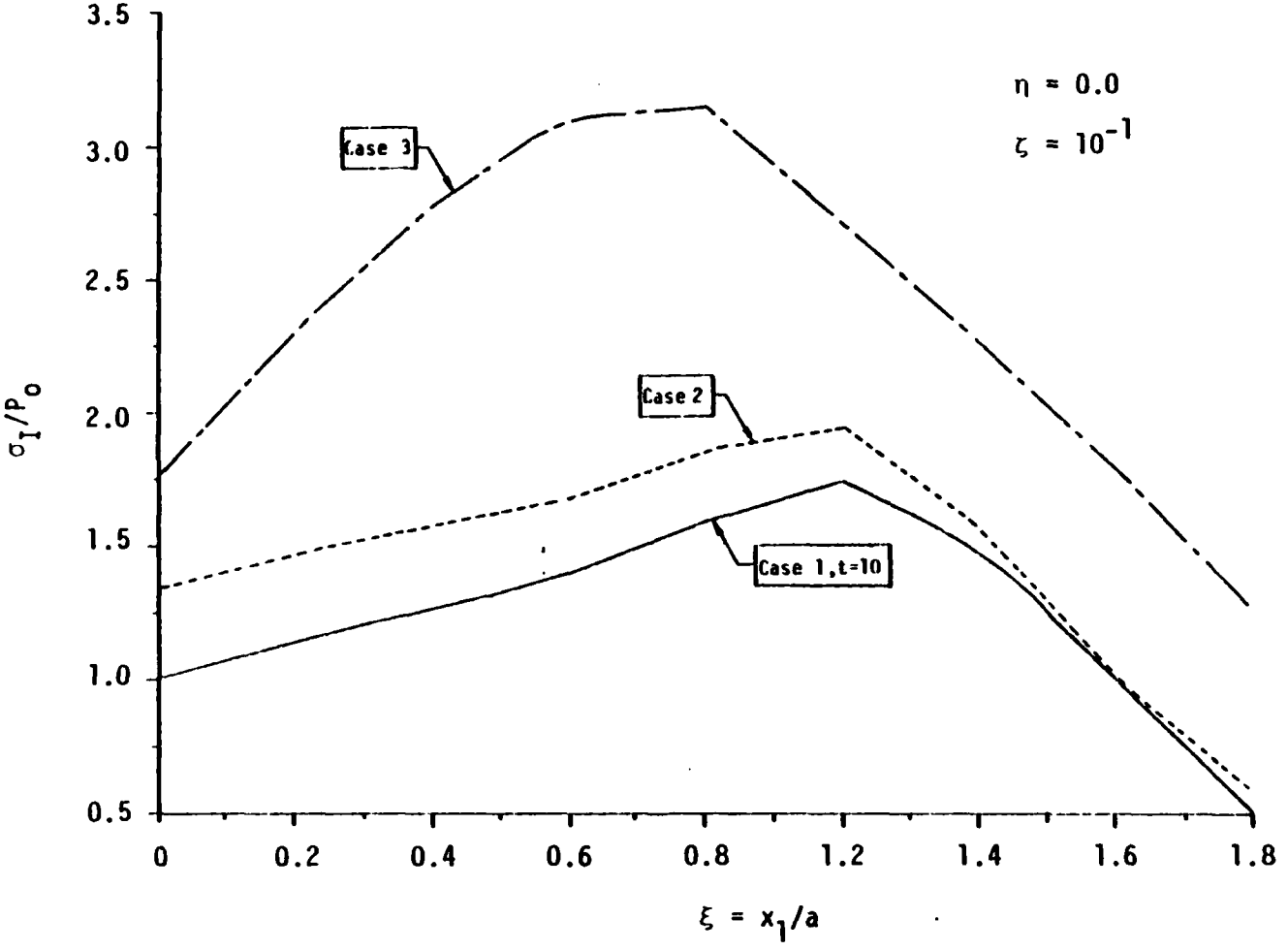

Figure 5.4. Maximum combined thermomechanical principal stress fields for three cases.

sizes are investigated in Figures 5.5 and 5.6, respectively, where ℓ_i's, i = 1, 2, 3, are the half widths of the contact area, which are 0.25 mm (0.01 in.), 0.5 mm (0.02 in.), and 0.125 mm (0.005 in.), respectively. Mention should be made that the nondimensionalization for (x_1,x_2,x_3) and T are slightly different. Here we define (ξ_i,η_i,ζ_i) as $(x_1,x_2,x_3)/\ell_i$ and ϕ_i as $T_i k/q_o \ell_i$. The comparison should therefore be made cautiously. Referring to Figure 5.5 where the constant average pressure P_o and heat flux q_o are used, it can be shown that at the same location higher temperature results from larger asperity size if we compare (ξ_1,ϕ_1) with $(\xi_1/2,2\phi_2)$ and $(2\xi_1,\phi_3/2)$ and take into account the fact that the temperature decreases as the depth increases. In fact, temperature is by all means expected to be higher when the total heat input over the contact region increases. It is clear that higher surface temperature causes higher compressive thermal stresses in the thermal layer and as a result, the tensile stresses at $\zeta_i = 10^{-1}$ from larger asperity size are higher as shown in Figure 5.6. In other words, the thermal fracturing is more likely to happen if the total heat input increase is achieved by the increase of the contact area over which the average pressure is assumed to be constant. This result checks with Figure 2.9 obtained from the two-dimensional analysis.

5.2 Comparison of Two- and Three-Dimensional Analyses

In the two-dimensional analysis, the aspect ratio, t = b/a, of the moving asperity has a length much larger than the width measured in the direction of motion, that is, a moving line asperity is considered.

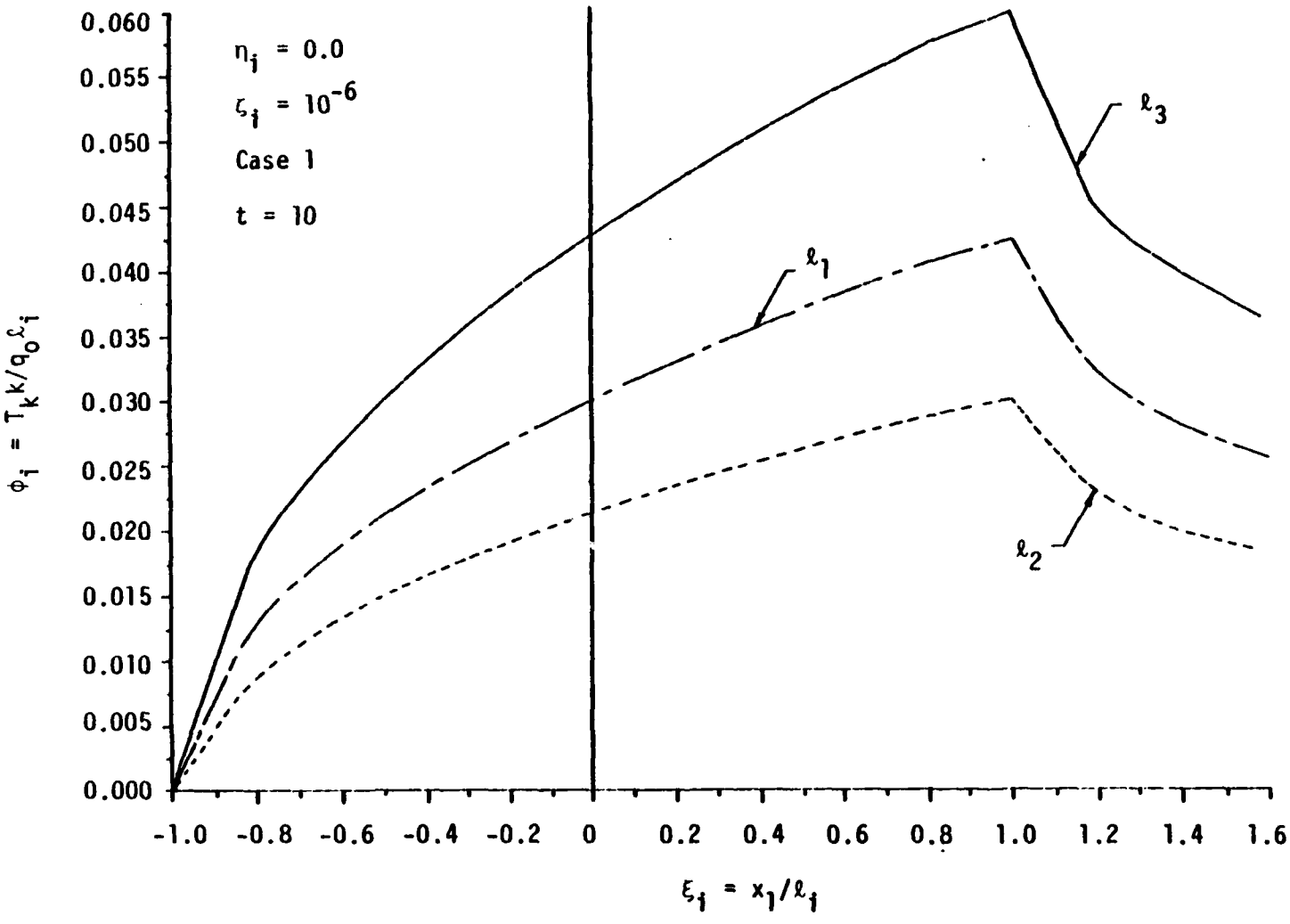

Figure 5.5. Temperature fields from different asperity sizes.

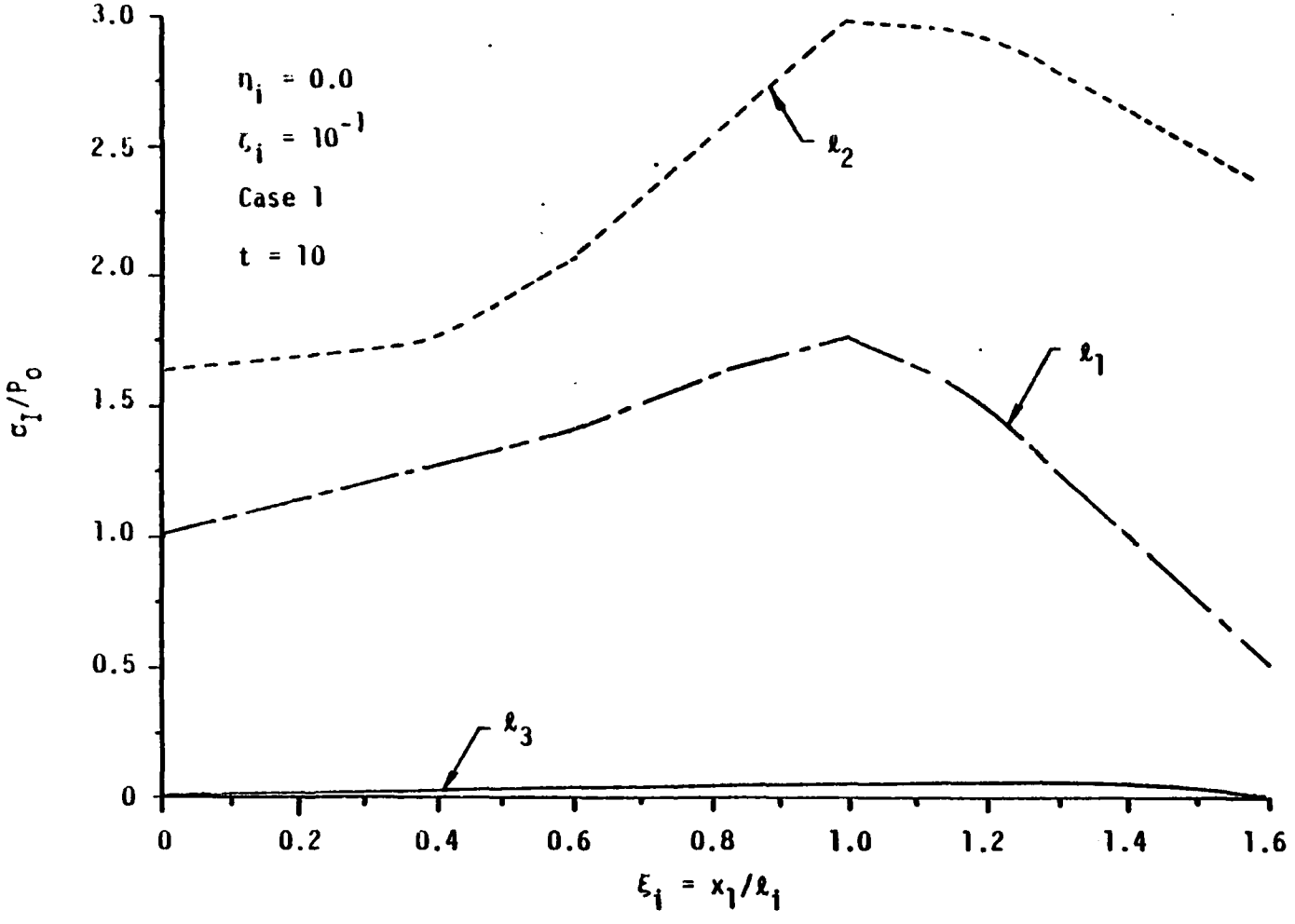

Figure 5.6. Maximum combined thermomechanical principal stress fields from different asperity sizes.

For the mechanical effect portion, the dynamic stress potentials are of the Lamé type. When transformed to the coordinates fixed to the asperity, the stress potentials become harmonic with distorted depth coordinates. The distortion is caused by the subsonic velocity of the moving asperity. Using a unit normal and a unit tangent, the impulse responses in the stress and the displacement fields were determined to be of the Eringen-Suhubi type [19]. The impulse responses were employed as Green's function to compute the displacement and the stress fields for any distribution of pressure and friction force. In the thermal effect, following Ling's assumption [48] for high Peclet number, the heat conduction in the traverse direction is neglected, retaining only the convective term in that direction from the local variation. The temperature and the thermal stress fields are computed from the thermal impulse responses, which were obtained from a unit heat input [22].

In the three-dimensional model of a single moving asperity the potential theory cannot be readily used, that is the three-dimensional formulation cannot be simply extended from the two-dimensional mathematical model. Double Fourier transform methods are therefore applied for deriving the analytical solutions. Due to the complexity of the formulations, they are first left in the transformed space. Numerical integrations are then to be carried out for corresponding inverse transforms.

It is clear that two-dimensional theory provides a much simpler approach which also leads to fairly good numerical results of the mechanical and the temperature fields. This can be seen if we compare

Figures 2.5 and 2.6 with 3.2 and 3.5, respectively. However, even with the analytical difficulty, the three-dimensional modeling is virtually unavoidable as it best describes the geometrical shape of the asperity. Therefore, in that model, different load distributions over a circular or a rectangular area, instead of the unrealistic line asperity, can be analyzed. In addition, taking Case 1, $t = 10$ from the three-dimensional theory and the one with uniform pressure distribution from two-dimensional theory for comparison, thermal stresses have a different order of magnitude as shown in Figures 3.8 and 2.8. This is deduced from the dimensional effect which is of great importance. As we know there is no temperature variation in the η direction in two-dimensional analysis; while in three-dimensions the temperature drops off near the edge of the contact area in the η direction, i.e., $\eta = \pm 10$, illustrated by Figures 5.7 and 5.8 for Case 1, $t = 10$ at depths $\zeta = 10^{-6}$ and 10^{-1}, respectively. Thus far, the cool regions outside the hot spot in the η direction also constrain the thermal layer from expanding. As a result, tensile stresses at $\zeta = 10^{-1}$ is elevated to a higher order of magnitude. Thus the fracture threshold predicted from three-dimensional theory is at a much lower asperity pressure or a lower asperity rubbing speed than that from the two-dimensional theory. It is worth mentioning that three-dimensional theory can be applied to justify two-dimensional theory. Numerically it is shown in Figure 5.9 where the result for Case 1 "moves toward" two-dimensional solution as the aspect ratio increases. Theoretically the Dirac function $\delta(\overline{x}_2)$ will be associated with the transformed boundary functions such as $\overline{R}_i$

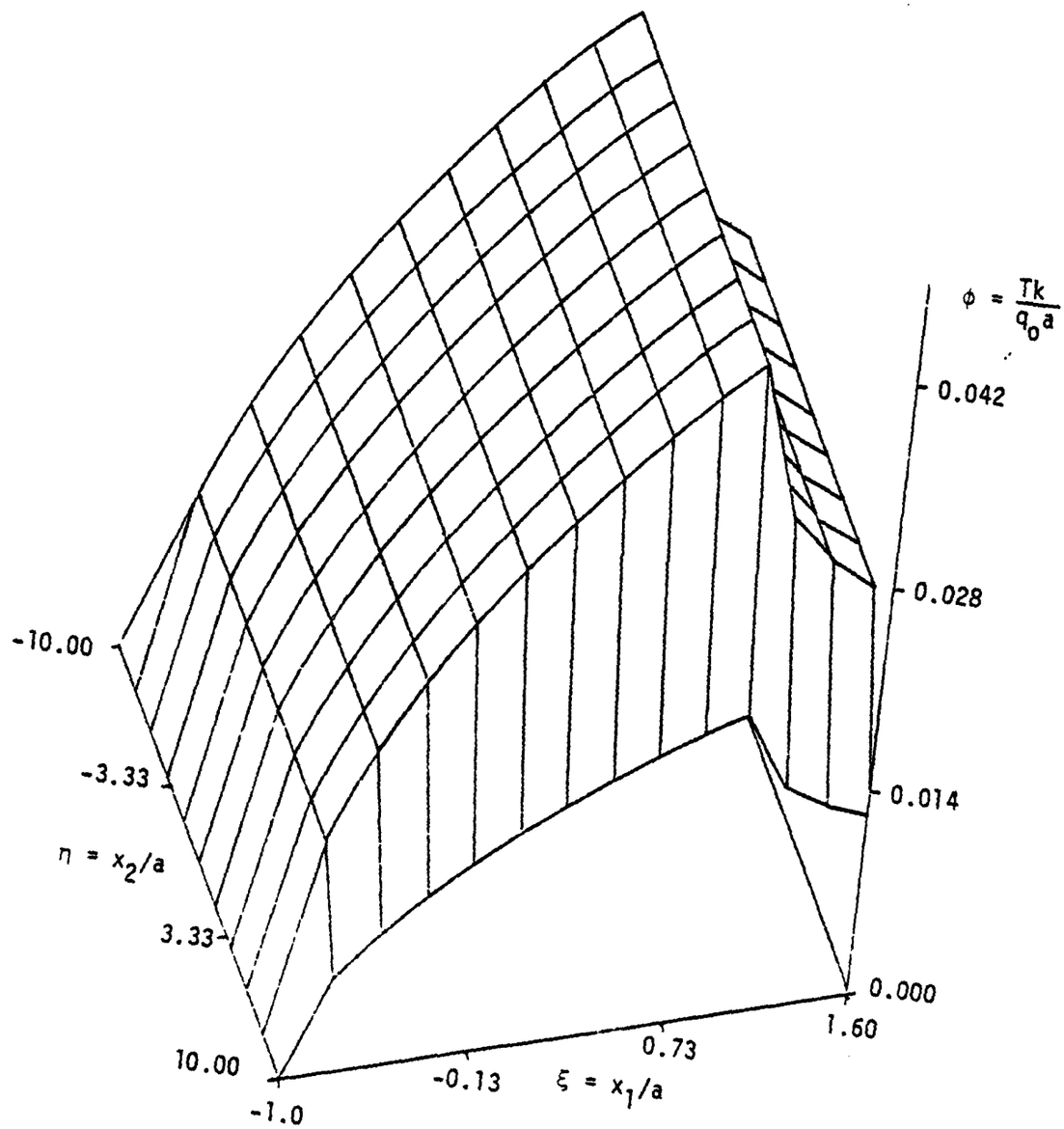

Figure 5.7. Temperature field at $\zeta = 10^{-6}$ for Case 1, t = 10.

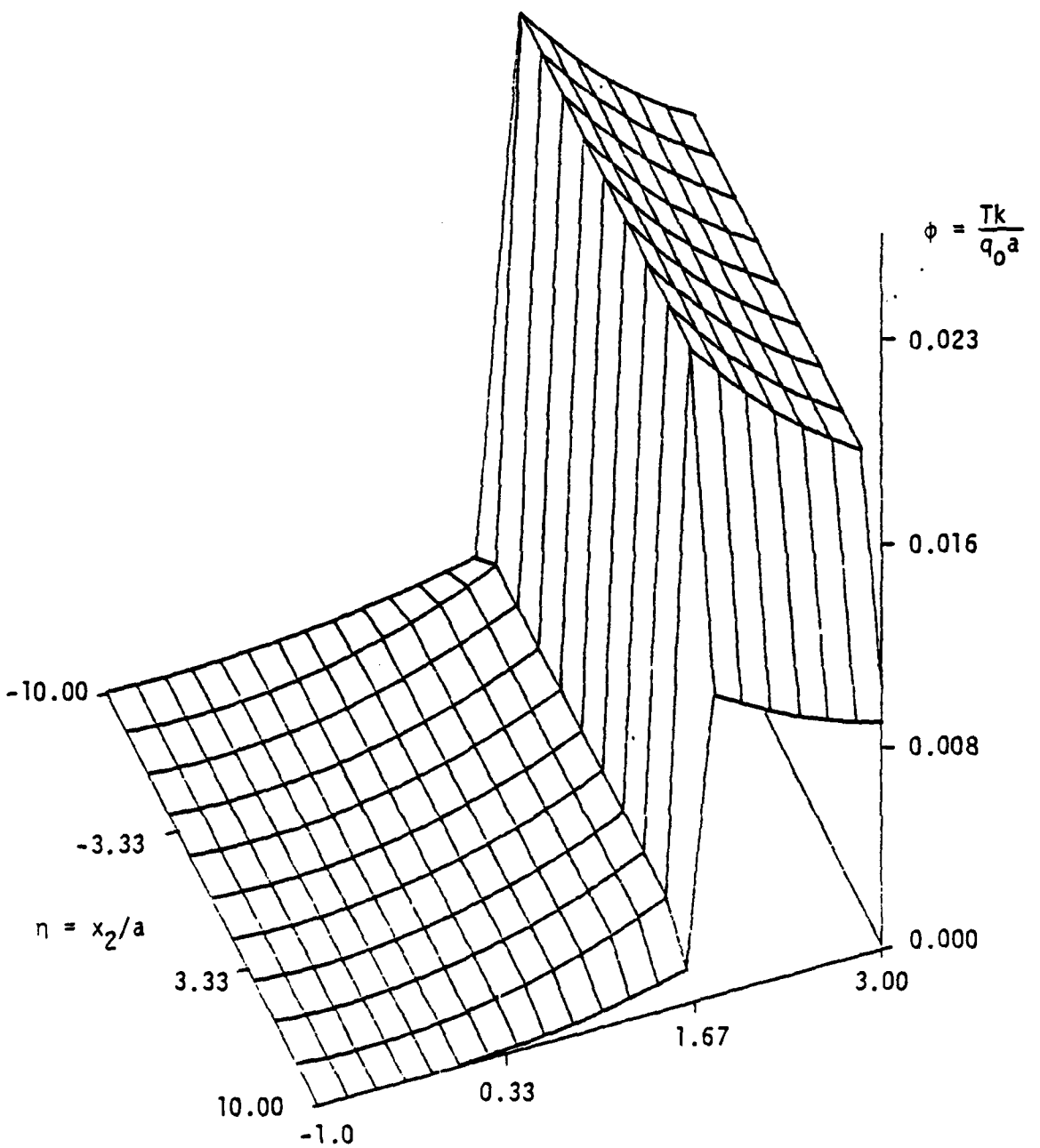

Figure 5.8. Temperature field at $\zeta = 10^{-1}$ for Case 1, t = 10.

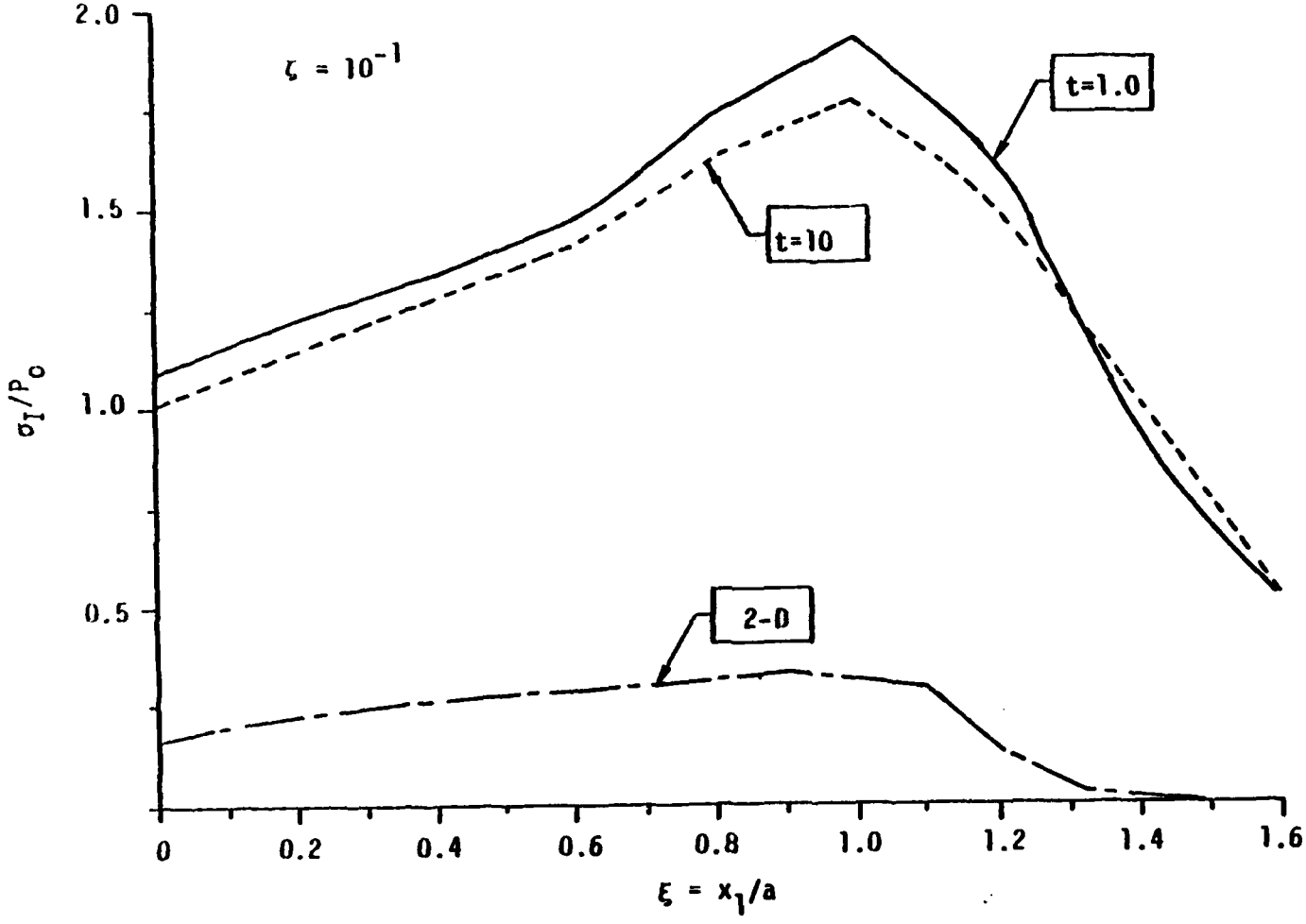

Figure 5.9. Stresses from two- and three-dimensional analyses for Case 1.

in Equation (3.15) or $\bar{P}_1$ in Equation (3.67) if we consider a moving line asperity instead of a moving asperity with a rectangular contact area. Consequently, three-dimensional formulations of double integrals can be easily simplified to single integrals which converge to the two-dimensional solutions.

5.3 Cumulative Effects of Periodic Loads

It is evident that the spacing between asperities and the number of repetitions serve as governing parameters. The cumulative effects on mechanical stresses, temperature distributions, and thermal stresses have been demonstrated with a sequence of three asperities with center distance $\lambda' = 12$ in Figures 4.2, 4.4, and 4.5, respectively. In summary, the mechanical stress distribution duplicates individual effect as in the problem of a single moving asperity. The temperature field however, because of the periodic updating of the initial temperature field at individual asperities, shows a definite cumulative effect, albeit with a reducing increment at individual passing asperities. Since thermal stress distribution is sensitive to the temperature variation, the magnitudes of tensile stresses in the vicinity of the first moving asperity are increased. As a result, the combined stress field, as shown in Figure 4.6, reaches a fracture threshold at a much lower critical average pressure compared with that for a single moving asperity. If the center distance of asperities is increased to 1200 times the characteristic dimension of the contact area, i.e., $\lambda' = 1200$, not only the mechanical stress field from

individual excitation propagating at the sound speed is noncumulative, but also the thermal responses from the preceding asperities have died out. Hence in this case, the mechanical and thermal responses are essentially repeated under energy passage of moving asperities. As for the cumulative effects from the number of repetitions, Figures 5.10 and 5.11 show temperature fields and maximum combined thermomechanical principal stress fields for different number of moving asperities. As expected, the increase of the number of repetitions may result in higher tensile stresses and thus the seal is most likely easier to crack. Nevertheless, the damaging aspect of cumulative effects is not to increase indefinitely. For if we recall the temperature field in Equation (4.20)

$$\bar{T} = \frac{\bar{Q}_N}{k} e^{-\omega x_3}[C_1 \cos(\theta x_3) + C_2 \sin(\theta x_3)]$$

where $\bar{Q}_N$ is associated with a series of the form

$$\sum_{j=1}^{N} e^{i\bar{x}_1 \lambda' (j-1)}$$

which has a close form as

$$e^{i\tau_N} \cdot \sin(\tfrac{1}{2} N\lambda' \bar{x}_1)/\sin(\tfrac{1}{2} \lambda' \bar{x}_1)$$

with τ_N expressed as $1/2\ \lambda'(N - 1)\ \bar{x}_1$. It can be shown that all terms in $\bar{T}$ are bounded and the resultant thermal solutions after the inverse Fourier transform are convergent on the consideration of the Riemann-Lebesgue theorem, as the number of periodic excitation of traversing asperities approaches infinity.

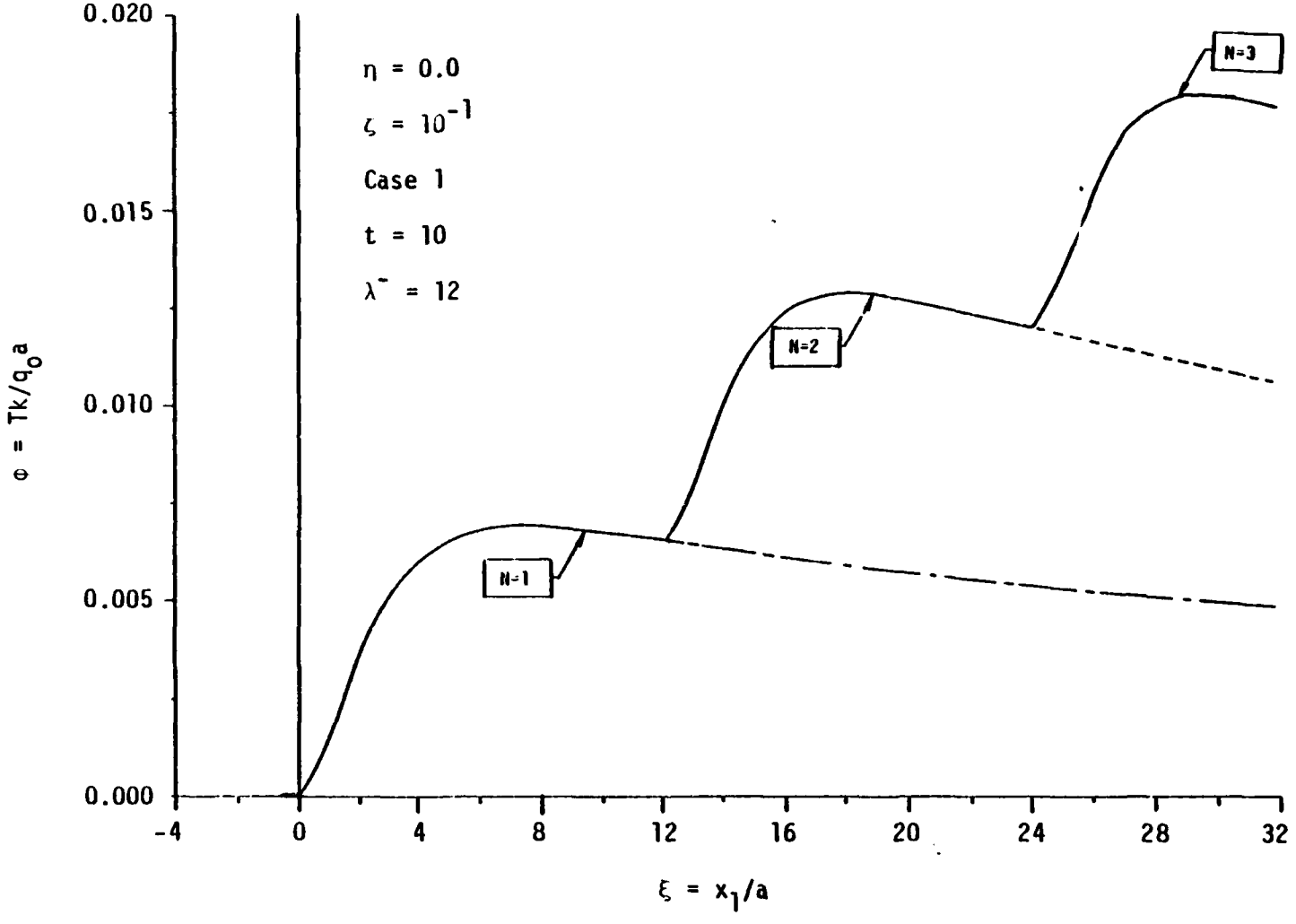

Figure 5.10. Temperature fields due to different number of moving asperities.

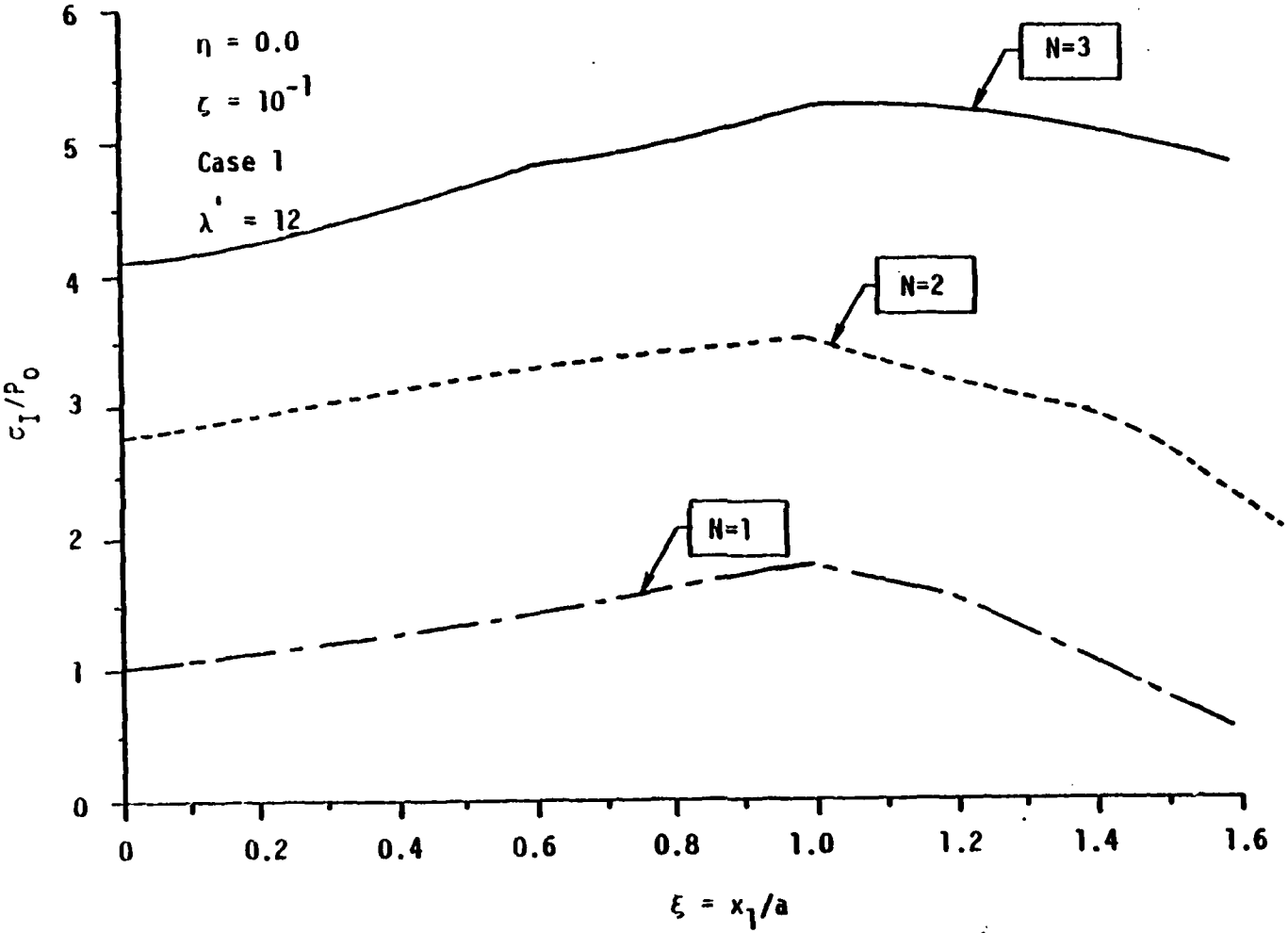

Figure 5.11. Maximum combined thermomechanical principal stress fields due to different number of moving asperities.

Thus far, three models characterizing the heat checking failure have been established. These models contribute general straightforward methods so that we can assess the tendencies of the crack initiation, which is of major concern. The avoidance of thermocracks by controlling some parameters such as E, α, k, V, a, etc. can be optimized. In general, it can be concluded that reducing the size and number of asperities, decreasing the moving velocity, and having uniform pressure distributions, and choosing a seal material with low modulus of elasticity, low coefficient of thermal expansion, high thermal conductivity, and high fracture strength are efficient to alleviate the thermal fracturing problem.

5.4 Justifications and Recommendations

Of concern here are the justifications of the major assumptions, the formulations, and the numerical results. In the analysis, the flash temperature in the neighborhood of the asperities contained on the mating ring is so high that all the frictional heat may be assumed to flow predominately into the primary ring since the temperature difference between the asperities and the primary ring is much higher than that between the asperities and the mating ring. As a result, this yields an upper limit of the solution and gives a conservative estimate of the critical pressure which would result in heat checking.

In practice, the velocity of the moving asperities is much less than that of the Rayleigh waves, and there is no plastic deformation observed in tension tests at temperatures as high as 1960°R (1089 K) for Stellite III. Consequently, the physical conditions of the low

dilatation rate and no thermal shock phenomenon justify the application of the theory of uncoupled quasi-static thermoelasticity. In addition, the linear theory holds since the base material subjected to the asperity friction is essentially elastic from observations of failed specimens.

In order to justify the analytical and the numerical results obtained, several strategies were used. Both the mechanical and the thermal solutions for Case 1, with the aspect ratio $t \to \infty$, from the three-dimensional theory were checked by the solutions from the two-dimensional theory. The general solution and the integral solution of the mechanical stress field for Case 1 from a single moving asperity were checked by Eason's result [21]. He fixed the coordinate system to the semi-infinite solid and used the technique of the triple Fourier transform to analyze the mechanical responses from a moving surface force. As for the temperature field, using the Green's function concept or the Fourier transform technique led to the same result. In the computation of the thermal stress field of a single moving asperity, the approach adopted a semi-inverse scheme by assuming the displacement expression to satisfy the governing equations, the boundary and the regularity conditions. The results were checked by the solutions from periodic excitation with N=1 using the method of the Inverse Differential Operator in conjunction with the Cramer's rule.

The numerical results were also carefully obtained and justified. In general, the numerical evaluations were checked with both Simp and Quanc8 codes for single integrals and with both the double iterative

Gaussian-Laguerre quadratures and the double adaptive Simpson schemes for double integrals (see Appendix II).

The proposed models have been successfully applied to study the brittle failure in the submarine face seals. The material properties are considered to be constant with respect to the temperature in the analysis. This holds since the temperature above the stress-free ambient temperature at the depth of the order of one-twentieth asperity size where the cracking occurs is much lower than that in the thermal layer. However, it may be of practical interest to investigate the multilayer effect. In this case, the material properties may be constant in each layer but varied in different layers. Mention should also be made that the analyses so far are restricted to the homogeneous material. Since it is very hard to perfect the material beneath the surface, it is worthwhile to study the layered media with the hetergeneity induced by the rigid inclusion or the cavity among layers. The principal stress field from combined thermomechanical effects strongly depends on the pressure distributions over the contact areas; while the pressure distributions are much affected by the contact force and the geometries of the asperities. For the mechanical face seal, the total force remains constant during the operation. Therefore, the experimental research to optimize the control of the size of the moving asperities is extremely important.

APPENDIX I

METHODS OF INTEGRAL TRANSFORMS AND GREEN'S FUNCTIONS

If we have a function $f: \mathfrak{R}^n \to \mathbb{C}$, the n-dimensional Fourier transform is defined by

$$\overline{f}(\underset{\sim}{\bar{x}}) = \frac{1}{(\sqrt{2\pi})^n} \int_{\mathfrak{R}^n} \int_{-\infty}^{\infty} f(\underset{\sim}{x}) \cdot \exp[i(\underset{\sim}{\bar{x}} \cdot \underset{\sim}{x})] \, d\underset{\sim}{x}$$

and the appropriate inversion form is

$$f(\underset{\sim}{x}) = \frac{1}{(\sqrt{2\pi})^n} \int_{\mathfrak{R}^n} \int_{-\infty}^{\infty} \overline{f}(\underset{\sim}{\bar{x}}) \exp[-i(\underset{\sim}{\bar{x}} \cdot \underset{\sim}{x})] \, d\underset{\sim}{\bar{x}}$$

where

$$(\underset{\sim}{\bar{x}} \cdot \underset{\sim}{x}) = \bar{x}_1 x_1 + \bar{x}_2 x_2 + \cdots + \bar{x}_n x_n$$

denotes the inner product of the vectors $\underset{\sim}{x}$ and $\underset{\sim}{\bar{x}}$ of $\mathfrak{R}^n$.

In applications to physical problems the following two formulas are often employed with the transform.

$$\overline{D^{\alpha}_{\underset{\sim}{x}} f(\underset{\sim}{x})} = (-i)^{|\alpha|} \, \underset{\sim}{\bar{x}}^{\alpha} \, \overline{f}(\underset{\sim}{\bar{x}}) \, ,$$

$$\overline{\underset{\sim}{x}^{\alpha} f(\underset{\sim}{x})} = (-i)^{|\alpha|} \, D^{\alpha}_{\underset{\sim}{\bar{x}}} \, \overline{f}(\underset{\sim}{\bar{x}})$$

where the notations are explained as follows. For nonnegative integers $\alpha_j (j = 1,2,\ldots,n)$,

$$\alpha = (\alpha_1, \alpha_2, \ldots, \alpha_n)$$

is called a multi-index of n variables, and

$$|\alpha| = \alpha_1 + \alpha_2 + \cdots + \alpha_n$$

is called its length.

When $\underset{\sim}{x} = (x_1, x_2, \ldots, x^n)$ is a point in $\mathfrak{R}^n$, let $\underset{\sim}{x}^\alpha$ be the monomial of degree $|\alpha|$, which is

$$\underset{\sim}{x}^\alpha = x_1^{\alpha_1} x_2^{\alpha_2} \cdots x_n^{\alpha_n}$$

and $D_{\underset{\sim}{x}}^\alpha$ be the differential operator of order $|\alpha|$ with respect to x, which is

$$D_{\underset{\sim}{x}}^\alpha = \left(\frac{\partial}{\partial x_1}\right)^{\alpha_1} \left(\frac{\partial}{\partial x_2}\right)^{\alpha_2} \cdots \left(\frac{\partial}{\partial x_n}\right)^{\alpha_n} .$$

For example, if m is a natural number, and a_α are constants with indices α, then

$$\sum_{|\alpha| \leq m} a_\alpha D^\alpha$$

expresses a partial differential operator of order m with constant coefficients.

Detailed theories and applications of Fourier integral transform have been well established by Snedden [49] and many other authors. The aforementioned formulation serve as the basic tool and are sufficient for the analysis.

The Green's function used to solve the partial differential equations of mathematical physics can be found in several references [50-53]. Of concern here is the use of Green's function in the solution of the general heat conduction equation. For generality the problem is formulated as

$$\nabla^2 T(\underset{\sim}{r},t) + \frac{1}{k} g(\underset{\sim}{r},t) = \frac{1}{\kappa} \frac{\partial T(\underset{\sim}{r},t)}{\partial t} \quad \text{in} \quad R,\ t > 0 \ ,$$

$$k_i \frac{\partial T}{\partial n_i} + h_i T = f_i(\underset{\sim}{r},t) \quad \text{on} \quad S_i,\ t > 0 \ ,$$

$$T(\underset{\sim}{r},t) = F(\underset{\sim}{r}) \quad \text{for} \quad t = 0, \text{ in } R$$

where $\partial/\partial n_i$ denotes differentiation along the outward-drawn normal to the boundary surface S_i, $i = 1,2,\ldots,m$ and m is the number of continuous boundary surfaces of the region R. $g(\underset{\sim}{r},t)$, the internal heat generation, and $f_i(\underset{\sim}{r},t)$, the boundary-condition functon on S_i, vary with position and time. $F(\underset{\sim}{r})$ is the initial condition function.

The corresponding Green's function is the solution of the following auxiliary problem for the same region R:

$$\nabla^2 G + \frac{1}{\kappa} \delta(\underset{\sim}{r} - \underset{\sim}{r}') \ \delta(t - \tau) = \frac{1}{\kappa} \frac{\partial G}{\partial t} \quad \text{in} \quad R,\ t > \tau \ ,$$

$$k_i \frac{\partial G}{\partial n_i} + h_i G = 0 \quad \text{on} \quad S_i,\ t > \tau$$

$$G = 0 \quad \text{if} \quad t < \tau$$

where

$$\delta(\underset{\sim}{r} - \underset{\sim}{r}') = \delta(x_1 - x_1') \ \delta(x_2 - x_2') \ \delta(x_3 - x_3')$$

for (x_1,x_2,x_3) coordinates.

It is noted that this auxiliary problem satisfied by the Green's function has homogeneous boundary conditions and has an impulsive point heat source and zero initial condition. In other words, this solution

represents the temperature distribution in the region R, which is initially at zero temperature and subjected to homogeneous boundary conditions, due to an impulsive heat source of strength unity located at $\underset{\sim}{r}'$ and releasing its heat spontaneously at time τ.

The temperature distribution in terms of the Green's function according to Özisik [54], is

$$T(\underset{\sim}{r},t) = \int_R G\Big|_{\tau=0} F(\underset{\sim}{r}')\, dv' + \frac{\alpha}{k}\int_{\tau=0}^{t} d\tau \int_R Gg(\underset{\sim}{r}',\tau)\, dv'$$

$$+ \kappa \int_{\tau=0}^{t} d\tau \sum_{i=1}^{m} \int_{S_i} G\Big|_{S_i} \frac{1}{k_i} f_i(\underset{\sim}{r},t)\, dS_i$$

where $G\big|_{S_i}$ refers to the Green's function evaluated at the boundary surface.

Most often the heat conduction equation is not in the form presented. Under this circumstance, a different Green's function needs to be determined or some transformation may be useful to reduce the equation to the standard form for which Green's function is known. For example, if we have

$$\frac{\partial T}{\partial t} = \kappa\nabla^2 T - \beta_1 \frac{\partial T}{\partial x_1} - \beta_2 \frac{\partial T}{\partial x_2} - \beta_3 \frac{\partial T}{\partial x_3} + \gamma T + g$$

where κ, β_1, β_2, β_3 and γ are constants. We define a new dependent variable ω as

$$T(\underset{\sim}{r},t) = \omega(\underset{\sim}{r},t)\ \exp\left[\frac{\beta_1}{2\kappa}\,x_1 - \left(\frac{\beta_1^2}{4\kappa} - \gamma\right)t\right]$$

$$\cdot\ \exp\left[\frac{\beta_2}{2\kappa}\,x_2 - \frac{\beta_2^2}{4\kappa}\,t\right]\ \exp\left[\frac{\beta_3}{2\kappa}\,x_3 - \frac{\beta_3}{4\kappa}\,t\right].$$

Under this transformation we have the standard form:

$$\nabla^2\omega(\underset{\sim}{r},t) + \frac{1}{k}\,G(\underset{\sim}{r},t) = \frac{1}{\kappa}\,\frac{\partial\omega(\underset{\sim}{r},t)}{\partial t}$$

where

$$G = \rho c\ \exp\left[-\frac{\beta_1}{2\kappa}\,x_1 + \left(\frac{\beta_1^2}{4\kappa} - \gamma\right)t\right]\exp\left[-\frac{\beta_2}{2\kappa}\,x_2 + \frac{\beta_2^2}{4\kappa}\,t\right]$$

$$\cdot\ \exp\left[-\frac{\beta_3}{2\kappa}\,x_3 + \frac{\beta_3}{4\kappa}\,t\right].$$

APPENDIX II

NUMERICAL INTEGRATION

The numerical methods for evaluating the integral of the form

$$I(f) = \int_a^b f(x)\, dx ,$$

with [a,b] finite, are well established and can be found in most textbooks of numerical analysis [55-59]. In general, the integration methods can be viewed within a simple framework. First, try to find a family of functions, $\{f_n(x), n \geq 1\}$, of which each approximates the integrand f(x) in the following sense

$$\|f - f_n\|_\infty \to 0 \quad \text{as} \quad n \to \infty .$$

The form of each f_n should be chosen such that we can easily evaluate the integral

$$I_n(f) = \int_a^b f_n(x)\, dx$$

which approximates I(f), that is $I(f) \approx I_n(f)$. As for the error, we have

$$E_n(f) = I(f) - I_n(f) = \int_a^b [f(x) - f_n(x)]\, dx$$

and

$$|E_n(f)| \leq \int_a^b |f(x) - f_n(x)|\, dx \leq (b - a)\, \|f - f_n\|_\infty .$$

The typical best-known example is the Newton-Cotes integration formulas which are obtained by a suitable interpolation polynomial $f_n(x)$ on the nodes $x_0, x_1, \ldots, x_n$ to replace the integrand $f(x)$. Consider an equally-spaced partition of the closed interval $[a,b]$ given by

$$x_i = a + i \frac{b - a}{n}, \qquad i = 0,1,\ldots,n .$$

Let f_n be expressed in connection with the Lagrange polynomial as

$$f_n(x) = \sum_{i=0}^{n} f(x_i)\, L_i(x), \qquad L_i(x) = \prod_{\substack{j=0 \\ j \neq i}}^{n} \frac{x - x_j}{x_i - x_j} .$$

If we define

$$I_n(f) = \sum_{i=0}^{n} f(x_i)\, \alpha_i$$

and introduce the new variable t such that $x = a + t(b - a)$, then α_i can be expressed as

$$\alpha_i = (b - a) \int_0^1 \prod_{\substack{j=0 \\ j \neq i}}^{n} \frac{nt - j}{i - j}\, dt$$

which depends on n only. For sufficiently smooth $f(x)$, it can be shown [60] that the approximation error has the form

$$E_n(f) = K_n \left(\frac{b - a}{n}\right)^{P_n + 1} f^{(P_n)}(\xi), \qquad \xi \in (a,b)$$

where P_n and K_n depend only on n but not on the integrand f.

In particular, for $n = 2$, the Newton-Cotes formula becomes the Simpson rule which is

$$\int_a^b f(x)\,dx = \frac{b-a}{6}\left[f(a) + 4f\left(\frac{a+b}{2}\right) + f(b)\right] - \frac{(b-a)^5}{2880} f^{(4)}(\xi) .$$

The corresponding composite rule is obtained as follows

$$\int_a^b f(x)\,dx = \sum_{i=0}^{N-1} \int_{x_i}^{x_{i+1}} f(x)\,dx = \sum_{i=0}^{N-1} h_i \int_0^1 f(x_i + h_i t)\,dt$$

$$= \sum_{i=0}^{N-1} \frac{h_i}{6}\left\{f(x_i) + 4f\left(x_i + \frac{h_i}{2}\right) + f(x_{i+1})\right\} - \sum_{i=0}^{N-1} \frac{h_i^5 f^{(4)}(\zeta_i)}{2880}$$

where $h_i = x_{i+1} - x_i$. For the case of equally-spaced intervals, i.e.,

$$h_i = \frac{b-a}{N} = h ,$$

the above formula becomes

$$\int_a^b f(x)\,dx = \frac{h}{6}\left\{f(a) + 4\sum_{k=0}^{N-1} f\left(a + (k+\tfrac{1}{2})h\right) + 2\sum_{k=1}^{N-1} (a+kh) + f(b)\right\}$$

$$- \frac{(b-a)^5}{2880\,N^4} f^{(4)}(\eta) , \qquad \eta \in (a,b) .$$

Another powerful integration method is the Gaussian quadrature behind which the idea is to find an integration formula

$$I_n(f) = \sum_{j=1}^{n} A_j f(x_j) \approx \int_a^b \omega(x)\, f(x)\,dx$$

where $\omega(x)$ is a given non-negative weight function on the interval (a,b), which may be infinite; and assumes the following properties:

1. $\int_a^b |x|^n \omega(x)\, dx$ is integrable and finite for all $n \geq 0$.

2. If $\int_a^b \omega(x)\, g(x)\, dx = 0$ for some continuous non-negative function $g(x)$, then $g(x) \equiv 0$ on (a,b).

A_j, x_j can be determined by the method of undetermined coefficients which asks for perfect accuracy when $f(x)$ is one of the power functions $1,x,x^2,\ldots,x^{2n-1}$. This provides $2n$ conditions for the determined $2n$ unknowns A_j and x_j. In fact,

$$A_j = \int_a^b \omega(x)\, L_j(x)\, dx$$

where $L_j(x)$ is the Lagrange polynomial. The arguments $x_1,\ldots,x_n$ are the zeros of nth degree orthogonal polynomials $\phi_n(x)$ on (a,b) with respect to the weight function, i.e.,

$$\int_a^b \omega(x)\, \phi_n(x)\, \phi_m(x)\, dx = 0 \quad \text{for} \quad n \neq m .$$

The error expression can be shown to have the form [61]

$$E_n(f) = \frac{\gamma_n}{A_n^2 (2n)!} f^{(2n)}(\eta) , \qquad \eta \in (a,b) .$$

Gaussian-Laguerre quadrature is one particular type of Gaussian quadrature with $\omega(x) = e^{-x}$. It takes the form

$$\int_0^\infty e^{-x} f(x)\, dx = \sum_{i=1}^{n} A_i f(x_i) + \frac{(n!)^2}{(2n)!} f^{(2n)}(\eta)$$

the arguments x_i being the zeros of the nth Laguerre polynomial

$$P_n(x) = e^x \frac{d^n}{dx^n} (e^{-x} x^n)$$

and the coefficients A_i being

$$A_i = \frac{(n!)^2}{x_i [P_n'(x_i)]^2} .$$

The numbers x_i and A_i are available in Tables [62].

It is known that an iterative scheme or an adaptive scheme should be employed in conjunction with the composite rule of integration. In an iterative scheme, successive approximations to the integral are computed until it has met the required accuracy. For instance, the algorithm can be set as follows.

Let $I_{2^k N}(f)$ denote the approximation solution based on the composite rule with $2^k N$ equal-width subintervals. For $k = 0,1,2,\ldots$, if

$$\left| I_{2^{k+1} N}(f) - I_{2^k N}(f) \right|$$

is sufficiently small, then we exit with $I_{2^{k+1} N}(f)$ as the result.

The iterative scheme can be quite inefficient, since the accuracy may be satisfactory on many subintervals where the refinement becomes unnecessary. Based on this idea, an adaptive scheme, which refines only where necessary, has been well established [63-69]. The integration codes Simp and Quanc8 associated with the Simpson rule and 8 panel Newton-Cotes formula, respectively, are examples of such a scheme.

Singular integrals, whether for singular integrands or for infinite range of integration, are encountered in previous chapters. Since strategies to handle such singularities are too varied and numerous, only some of them which have been applied successfully are delineated in the following.

1. Apparent (or removable) singularities may exist at some values of the integration variable. Limiting values should be found with the help of L'Hospital's rule if necessary.

2. A change of variable may exchange a difficult singularity for a less critical one, or it may remove the singularity completely. For instance, if $f(x) \in C[0,1]$, the change of variable $t^n = x$ transforms the integral

$$\int_0^1 x^{-\frac{1}{n}} f(x)\, dx \ , \ n \geq 2 \ ,$$

into

$$n \int_0^1 f(t^n)\, t^{n-2}\, dt \ ,$$

which is a proper integral. Note that a change of variable is one of the most effective methods to evaluate an integral with an infinite limit since it can transform the infinite region into a finite region. For example, if $y = e^{-x}$, then

$$\int_0^\infty f(x)\, dx = \int_0^1 \frac{f(-\ln y)}{y}\, dy \ .$$

3. Reduce the infinite integral $\int_0^\infty f(x)\,dx$ to a finite integral $\int_0^k f(x)\,dx$ and estimate the truncation error due to $\int_k^\infty f(x)\,dx$ if possible.

4. It has been suggested by Squire [70] that the infinite integral can be transformed to

$$\int_0^\infty f(x)\,dx = s\int_0^1 [f(st) + t^{-2} f(s/t)]\,dt\ .$$

For the double integral of the form

$$\int_0^\infty \int_0^\infty f(x,y)\,dx\,dy\ ,$$

both the inner and outer integrals can be evaluated by using Gaussian-Laguerre quadrature based on an iterative scheme. Alternatively, the integral above can be first transformed into the integral with finite intervals by the technique of change of variable. Then the application of any of the adaptive quadrature schemes of two dimensions can lead to respectable results.

SELECTED REFERENCES

1. Parker, R. C. and Marshall, P. R., "The Measurement of the Temperature of Sliding Surfaces with Particular Reference to Railway Blocks," Proc. Inst. Mech. Eng., 159, 1948, pp. 209-229.

2. Wetenkamp, H. R. and Kipp, R. M., "Hot Spot Heating by Composition Shoes," J. Eng. Ind., 98, May 1976, 453.

3. Johnson, M. R., Welch, R. E., and Young, K. S., "Analysis of Thermal Stresses and Residual Stress Changes in Railroad Wheels Caused by Severe Drag Braking," J. Eng. Ind., 99, Feb. 1977, 18.

4. Carpenter, G. F., "The Cause of Thermal Fatigue Cracking in Metro-liner Wheels," Final Report to DOT, Rep. No. FRA-ORD-77/17, U.S. Steel Corporation Res. Lab., Monroeville, Pa. 15146, March 1977.

5. Dow, T. A., "Thermoelastic Effects in Brakes," Wear, 59, 1980, pp. 213-221.

6. Archard, J. F., "The Temperature of Rubbing Surfaces," Wear, Vol. 2, 6, 1959, pp. 438-455.

7. Burton, R. A., "Thermomechanical Effects in Sliding Wear," Workshop on Frictionally Induced Thermal Deformation and Wear, Annapolis, MD, June 19-20, 1979.

8. Naumann, F. K. and Spies, F., "Grinding Cracks," pp. 228-233, "Crack Due to Frictional Heating," pp. 337-340, Source Book in Failure Analysis, ASM, 1974.

9. Burton, R. A., "Friction and Wear," Chap. 2, Tribology, ed.: A. Z. Saeri, McGraw-Hill, 1980, pp. 17-38.

10. Sibley, L. B. and Allen, C. M., ASME Paper 61-Lub-15, 1961.

11. Burton, R. A., Nerlikor, V., and Kilaparti, S. R., "Thermoelastic Instability in a Seal-Like Configuration," Wear, 24, 1973, pp. 177-188.

12. Banerjee, B. N. and Burton, R. A., "Experimental Studies of Thermoelastic Effects in Hydrodynamically Lubricated Face Seals," J. Lubr. Technol., 101, 1979, pp. 275-282.

13. Netzel, J. P., "Surface Disturbance in Mechanical Face Seals from Thermoelastic Instability," Lubr. Eng., 37, 1981, pp. 272-278.

14. Burton, R. A., "Thermal Deformation in Frictionally Heated Contact," Wear, 59, 1980, pp. 1-20.

15. Barber, J. R., "Thermoelastic Instabilities in the Sliding of Conforming Solids," Proc. Roy. Soc. A.312, 1969, pp. 381-394.

16. Kennedy, F. E., Grim, J. N., and Glovsky, R. P., "Factors Influencing Thermomechanical Failure of Face Seals," II, Interium Report No. 2 (ONR Contract No. N00014-81-K-0090), Jan. 1983, Thayer School of Engineering, Darmouth College, Hanover, NH.

17. Cole, J. and Huth, J., "Stresses Produced in a Half Plane by Moving Loads," J. Appl. Mech., 25, 1958, pp. 433-436.

18. Sneddon, I. N., "Stress Produced by a Pulse of Pressure Moving Along the Surface of a Semi-Infinite Solid," Rendiconti Circolo Matematico di Palermo, Vol. 2, January-April, 1952, pp. 57-62.

19. Eringen, A. C. and Suhubi, E. S., "Moving Line Load on the Surface of a Half-Space," Elastodynamics, Vol. II, Academic Press, New York, pp. 574-578.

20. Ling, F. F. and Mow, V. C., "Surface Displacement of a Convective Elastic Half-Space Under an Arbitrarily Distributed Fast-Moving Heat Source," J. Basic Eng., September 1965, pp. 729-734.

21. Eason, G., "The Stresses Produced in a Semi-Infinite Solid by a Moving Surface Force," Int. J. Engrg. Sci., Vol. 2, pp. 581-609.

22. Mow, V. C. and Cheng, H. S., "Thermal Stresses in an Elastic Half-Space Associated with an Arbitrarily Distributed Moving Heat Source," Z. Angrew. Math Phys., 18, 1967, pp. 500-507.

23. Ling, F. F. and Yang, C. C., "Temperature Distribution in a Semi-Infinite Solid Under a Fast-Moving Arbitrarily Heat Source," Int. J. Heat Mass Transfer, Vol. 14, pp. 199-206.

24. Kennedy, F. E., "Surface Temperatures in Sliding Systems--A Finite Element Analysis," ASME J. of Lub. Tech., 103, 1981, pp. 90-96.

25. Kennedy, F. E. and Karpe, S. L., "Thermocracking of a Mechanical Face Seal," Wear, 79, 1982, pp. 21-36.

26. Marscher, W. D., "A Phenomenological Model of Abradable Wear in High Performance Turbomachinery," Wear, Vol. 59, 1980, pp. 191-211.

27. Marscher, W. D., "Thermal Versus Mechanical Effects in High Speed Sliding," Wear, Vol. 79, 1982, pp. 129-143.

28. Burton, R. A. and Nerlikar, V., "Large Disturbance Solutions for Initially Flat Frictionally Heated Thermoelastically Deformed Surfaces," J. Lub. Tech., July 1975, pp. 539-545.

29. Kilaparti, S. R. and Burton, R. A., "A Moving Hot-Spot Configuration for a Seal-Like Geometry with Frictional Heating Expansion and Wear," ASLE Paper No. 75-LC-2B-2, Oct. 1975.

30. Tseng, M.-L. and Burton, R. A., "Thermal Stress in a Two-Dimensional (Plane Stress) Half-Space for a Moving Heat Input," Wear, Vol. 79, 1982, pp. 1-9.

31. Nowacki, W., Thermoelasticity (English trans.), Pergamon Press, 1962.

32. Kovalenko, A. D., Thermoelasticity, Basic Theory and Applications, (English trans.), Wolters-Noordhoff Publishing Groningen, 1969.

33. Fung, Y. C., Foundation of Solid Mechanics, Prentice-Hall, Inc., 1965.

34. Gatewood, B. E., Thermal Stresses, McGraw-Hill, 1957.

35. Melan, E. and Parkus, H., Wärmespannungen, Springer, 1953.

36. Nowinski, J. L., Theory of Thermoelasticity with Application, Noordhoff International Publishing, 1978.

37. Duhamel, J.M.G., "Second Mémoires sur les Phénomènes Thermomécaniques," Jour. de l'Ecole Polytechnique, V. 15, Cahier 25, 1837, pp. 1-57.

38. Boley, B. A. and Weiner, J. H., Theory of Thermal Stress, Wiley, 1960.

39. Duhamel, J.M.G., "Mémoire sur le calcul de Actions Moleculaires Developpeés par les Changements de Temperature dans le corps solids," Memoires...par diveis savan ts, V. 5, 1838, pp. 440-498.

40. Parkus, H., Instationäre Wärmeshannungen (Russian trans.), Springer-Verlag, Wien, 1959.

41. Danilovskaya, V. I., "Thermal Stresses in an Elastic Half-Space Arising After a Sudden Heating of Its Boundary," Prikl. Mat. Mekh., Vol. 14, May-June 1950, pp. 316-318.

42. Danilovskaya, V. I., "On a Dynamical Problem of Thermoelasticity," Prikl. Mat. Mekh., Vol. 16, No. 3, May-June, 1952, pp. 341-344.

43. Kingery, W. D., "Factors Affecting Thermal Stress Resistance of Ceramic Materials," J. American Ceramic Soc., Vol. 38, 1955, pp. 3-15.

44. Griffith, A. A., "The Phenomena of Rupture and Flow in Solids," Phil. Trans. Roy. Soc., London, A221, pp. 163-198, 1921.

45. Griffith, A. A., "Theory of Rupture," Proc. First International Congress Applied Mechanics, Delft, pp. 55-63, 1924.

46. McClintock, F. A. and Argon, A. S., Mechanical Behavior of Materials, Addison-Wesley, Chap. 7, pp. 276-278.

47. Carslaw, H. S. and Jaeger, J. C., Conduction of Heat in Solids, 2nd Ed., Clarendon Press, Oxford, 1959.

48. Ling, F. F., "A Quasi-Iterative Method for Computing Interface Temperature Distributions," Z. Angew. Math. Phys., X, 1959, pp. 461-474.

49. Sneddon, I. N., Fourier Transforms, McGraw-Hill, New York, 1951.

50. Sneddon, I. N., Partial Differential Equations, McGraw-Hill, New York, 1957.

51. Dettman, J. W., Mathematical Methods in Physics and Engineering, McGraw-Hill, New York, 1962.

52. Courant, R. and Hilbert, D., Methods of Mathematical Physics, Interscience Publishers, New York, 1953.

53. Özisik, M. N., Boundary Value Problems of Heat Conduction, International Textbook Company, Scranton, PA., 1968.

54. Özisik, M. N., Heat Conduction, Wiley-Interscience, 1980.

55. Stoer, J. and Bulirsch, R., Introduction to Numerical Analysis, Springer-Verlag, New York, 1980.

56. Dahlquist, G. and Björck, A., Numerical Methods, Englewood Cliffs, NJ: Prentice-Hall, 1974.

57. Stiefel, E., An Introduction to Numerical Mathematics, London, Academic Press, 1963.

58. Householder, A. S., Principals of Numerical Analysis, New York, McGraw-Hill, 1953.

59. Isaccson, E. and Keller, H. B., Analysis of Numerical Analysis, New York, Wiley, 1966.

60. Steffensen, J. F., Interpolation (1927), 2nd edition, New York, Chelsea, 1950.

61. Atkinson, K. E., An Introduction to Numerical Analysis, Wiley, 1978.

62. Stroud, A. H. and Secrest, D. H., Gaussian Quadrature Formulas, Prentice-Hall, Englewood Cliffs, NJ, 1966.

63. Robinson, I. G., "Adaptive Gaussian Integration," Austral. Comput. J.3, 1971, pp. 126-129.

64. Rice, J. R., "An Educational Adaptive Quadrature Algorithm," SIGNUM Newsletter 8, No. 2, 1973, pp. 27-41.

65. Amble, O., "An Autoadaptive Method for Numerical Integration," Norske Vid. Selsk. Forh. (Trondheim) 42, 1969, pp. 43-50.

66. Hillstrom, K. E., "Comparison of Several Adaptive Newton-Cotes Quadrature Routines in Evaluating Definite Integrals with Peaked Integrands," ANL-7511, Argonne Nat. Lab., November 1968.

67. Hillstrom, K. E., "Comparison of Several Adaptive Newton-Cotes Quadrature Routines in Evaluating Definite Integrals with Peaked Integrands, II," CACM 13, 1970, pp. 362-365.

68. McKeeman, W. M., "Certification of Algorithm 145 Adaptive Numerical Integration by Simpson's Rule," CACM 6, 1963, pp. 167-168.

69. Shampine, L. F. and Allen, R. C., Jr., Numerical Computing: An Introduction, W. B. Saunders Company.

70. Squire, W., Integration for Engineers and Scientists, Amer. Elsevier, New York, 1970.

71. Ju, F. D. and Huang, J. H., "Heat Checking in the Contact Zone of a Bearing Seal (A Two-Dimensional Model of a Single Moving Asperity)," Wear, Vol. 79, pp. 107-118, 1982.

72. McClintock, F. A. and Walsh, J. B., Proc. Fourth U.S. Congress of Applied Mechanics, Berkeley, pp. 1015-1021, 1962-63.

73. Nemat-Nasser, S. and Horii, H., "Compression Induced Nonplanar Crack Extension with Application to Splitting, Exfoliation, and Rockburst," Journal of Geophysical Research, Vol. 87, No. B8, pp. 6805-6821, Aug. 10, 1982.

END

FILMED

2-85

DTIC